OSPAR COMMISSION

Trends in Deposition of Heavy Metals to the OSPAR Maritime Area in the period 1990-2019

OSPAR

QUALITY STATUS REPORT 2023

2022

OSPAR's Quality Status Report 2023

OSPAR Convention

The Convention for the Protection of the Marine Environment of the North-East Atlantic (the “OSPAR Convention”) was opened for signature at the Ministerial Meeting of the former Oslo and Paris Commissions in Paris on 22 September 1992. The Convention entered into force on 25 March 1998. The Contracting Parties are Belgium, Denmark, the European Union, Finland, France, Germany, Iceland, Ireland, Luxembourg, the Netherlands, Norway, Portugal, Spain, Sweden, Switzerland and the United Kingdom.

Convention OSPAR

La Convention pour la protection du milieu marin de l'Atlantique du Nord-Est, dite Convention OSPAR, a été ouverte à la signature à la réunion ministérielle des anciennes Commissions d'Oslo et de Paris, à Paris le 22 septembre 1992. La Convention est entrée en vigueur le 25 mars 1998. Les Parties contractantes sont l'Allemagne, la Belgique, le Danemark, l’Espagne, la Finlande, la France, l’Irlande, l’Islande, le Luxembourg, la Norvège, les Pays-Bas, le Portugal, le Royaume-Uni de Grande Bretagne et d’Irlande du Nord, la Suède, la Suisse et l’Union européenne.

MSC-E

MCS-E

Meteorological Synthesizing Centre - East

EMEP/MSC-E Technical Report 1/2022

Trends in Deposition of Heavy Metals to the OSPAR Maritime Area in the period 1990-2019

Ilia Ilyin, Oleg Travnikov, Olga Rozovskaya, Irina Strizhkina

Contents

Executive summary

Model assessment of atmospheric inputs of cadmium (Cd), lead (Pb), and mercury (Hg) to the OSPAR maritime area was carried out by the Meteorological Synthesizing Centre East (MSC-E) of EMEP for the period 1990-2019. The results of the assessment comprise time-series of annual anthropogenic emissions of Pb, Cd and Hg from the OSPAR Contracting Parties and modelled total annual atmospheric deposition to 5 regions of the OSPAR maritime area. Besides, contributions of the OSPAR Contracting Parties to total annual deposition of Cd, Pb, and Hg in 1995, 2005 and 2015 were estimated. The modelling results were evaluated against measurements of the OSPAR Comprehensive Atmospheric Monitoring Programme (CAMP). The modelled atmospheric deposition to the OSPAR maritime regions were compared with the previous model estimates performed by MSC-E for the period 1990-2006 [*OSPAR*, 2009].

Emissions of Pb, Cd and Hg in the OSPAR Contracting Parties declined over the considered period by 96%, 73%, and 83%, respectively. The most significant reduction occurred in the first third of the period. The reduction of emissions led to considerable decrease of deposition to the OSPAR maritime area in the period from 1990 to 2019. The largest decline was found for the Greater North Sea (Region II), where the deposition decreased by 87%, 80% and 45% for Pb, Cd and Hg, respectively. The lowest reduction was estimated for the Arctic Waters (Region I) and the Wider Atlantic (Region V), where deposition decline amounted to about 55 – 60% for Pb, about 35 – 40% for Cd, and below 25% for Hg. The decline of deposition to the OSPAR regions is lower than the emission reduction because of the effect of secondary and global sources.

The largest contribution of the OSPAR Contracting Parties to deposition of heavy metals is estimated for the Greater North Sea (Region II), while the lowest ones for the Arctic Waters (Region I) and the Wider Atlantic (Region V). The major contributors to the Regions I, II, III are the United Kingdom, France and Germany, whereas the Regions IV and V are mostly affected by Spain, Portugal, France and the United Kingdom.

Modelled Pb and Cd air concentrations and wet deposition agree with the observed values within a factor of two at most of the monitoring stations. However, the model tends to somewhat underestimate wet deposition fluxes. Most of the modelled and observed Hg wet deposition fluxes agree within ±40%. At most of the stations with a long monitoring period the modelling results agree with observations demonstrating declining trends over the considered period.

Presented estimates of heavy metal deposition to the OSPAR maritime area generally agree with the results of the previous assessment covering the period 1990-2006. The modelling results were revised due to re-calculation of national emissions by the EMEP countries, updates of meteorological and other input data as well as the refinement of the model parameterisations. The new model estimates demonstrate 10-30% lower deposition fluxes and somewhat higher pollution reduction rates for most of the OSPAR regions.

Récapitulatif

Une évaluation par modèle des apports atmosphériques de cadmium (Cd), de plomb (Pb) et de mercure (Hg) dans la zone maritime OSPAR a été réalisée par le Centre de synthèse météorologique Est (MSC-E) de l'EMEP pour la période 1990-2019. Les résultats de l'évaluation comprennent les séries chronologiques des émissions anthropiques annuelles de Pb, Cd et Hg des Parties contractantes d'OSPAR et les dépôts atmosphériques annuels totaux modélisés dans 5 régions de la zone maritime OSPAR. En outre, les contributions des Parties contractantes d'OSPAR au dépôt annuel total de Cd, Pb et Hg en 1995, 2005 et 2015 ont été estimées. Les résultats de la modélisation ont été évalués par rapport aux mesures du Programme exhaustif de surveillance de l'atmosphère (CAMP) d'OSPAR. Les retombées atmosphériques modélisées dans les régions maritimes d'OSPAR ont été comparées aux estimations précédentes du modèle réalisées par le MSC-E pour la période 1990-2006 [OSPAR, 2009].

Les émissions de Pb, Cd et Hg des Parties contractantes d'OSPAR ont diminué au cours de la période évaluée de 96%, 73% et 83%, respectivement. La réduction la plus significative a eu lieu dans le premier tiers de la période. La réduction des émissions a entraîné une diminution considérable des dépôts dans la zone maritime OSPAR entre 1990 et 2019. La baisse la plus importante a été constatée dans la mer du Nord au sens large (Région II), où les dépôts ont diminué de 87%, 80% et 45% pour le Pb, le Cd et le Hg, respectivement. La réduction la plus faible a été estimée pour les eaux arctiques (Région I) et l'Atlantique au large (Région V), où la diminution des dépôts s'est élevée à environ 55-60 % pour le plomb, environ 35-40 % pour le cadmium et moins de 25 % pour le mercure. La diminution des dépôts dans les régions d'OSPAR est inférieure à la réduction des émissions en raison de l'effet des sources secondaires et mondiales.

La plus grande contribution des Parties contractantes d'OSPAR au dépôt de métaux lourds est estimée pour la mer du Nord au sens large (Région II), tandis que les plus faibles sont estimées pour les eaux arctiques (Région I) et l'Atlantique au large (Région V). Les principaux contributeurs aux Régions I, II et III sont le Royaume-Uni, la France et l'Allemagne, tandis que les Régions IV et V sont principalement affectées par l'Espagne, le Portugal, la France et le Royaume-Uni.

Les concentrations atmosphériques de Pb et Cd et les dépôts humides modélisés concordent avec les valeurs observées à un facteur de deux près dans la plupart des stations de surveillance. Cependant, le modèle a tendance à sous-estimer les flux de dépôts humides. La plupart des flux de dépôts humides de Hg modélisés et observés concordent à ±40%. Dans la plupart des stations ayant une longue période de surveillance, les résultats de la modélisation sont en accord avec les observations qui montrent des tendances à la baisse sur la période évaluée.

Les estimations présentées des dépôts de métaux lourds dans la zone maritime OSPAR concordent généralement avec les résultats de l'évaluation précédente couvrant la période 1990-2006. Les résultats de la modélisation ont été révisés en raison d'un nouveau calcul des émissions nationales par les pays de l'EMEP, de la mise à jour des données météorologiques et autres données ainsi que de l'affinement des paramétrages du modèle. Les nouvelles estimations du modèle montrent des flux de dépôt inférieurs de 10 à 30% et des taux de réduction de la pollution légèrement plus élevés pour la plupart des régions d'OSPAR.

1. Introduction

Heavy metals and their compounds are toxic pollutants, which can harmfully impact human health and ecosystems. These substances are dangerous at low exposure levels and have acute and chronic effects on human health. In particular, they are multi-organ toxicants and adversely affect neurological, cardiovascular, renal, gastrointestinal, hematological and reproductive systems. In the environment, heavy metals are toxic to plants, animals and microorganisms. In particular, they can bioaccumulate in food webs and cause harm to marine life. Heavy metals enter the marine environment through various routes including direct discharges, riverine inputs and atmospheric deposition. The atmospheric pathways remain important providing from one fifth to two thirds of total heavy metal input to the marine environment [*OSPAR*, 2017], despite progress made under the 1998 Aarhus Protocol (and its 2012 amendment) of the UN ECE Convention on Long-Range Transboundary Air Pollution [*UNECE*, 2012]. Importance of the atmospheric route varies significantly over the marine regions and in time.

This report is focused on model assessment of atmospheric inputs of selected heavy metals, including cadmium (Cd), lead (Pb) and mercury (Hg), to the maritime area of the Convention for the Protection of the Marine Environment of the North-East Atlantic (OSPAR). The assessment was performed by the Meteorological Synthesizing Centre – East (MSC-E) of the Co-operative Programme for Monitoring and Evaluation of the Long Range Transmission of Air Pollutants in Europe (EMEP) at the request of the OSPAR Commission and includes evaluation of long-term trends of Cd, Pb, and Hg deposition to the North-East Atlantic Ocean (OSPAR maritime area) for the period 1990-2019 as well as the source-receptor relationships of heavy metal deposition for selected years of the period.

The data products of the assessment include (Annex A):

- Annual anthropogenic emissions of three heavy metals (Cd, Pb, Hg) from the OSPAR Contracting Parties for the period 1990-2019.
- Modelled time-series of total annual atmospheric deposition of the selected heavy metals to 5 regions of the OSPAR maritime area (Arctic Waters, Greater North Sea, Celtic Seas, Bay of Biscay and Wider Atlantic) for the period from 1990 to 2019.
- Contributions of the OSPAR Contracting Parties to total annual deposition of Cd, Pb, and Hg to the 5 regions of the OSPAR maritime area for selected years (1995, 2005, 2015).

In addition, the modelling results were evaluated against monitoring data from the OSPAR Comprehensive Atmospheric Monitoring Programme (CAMP) for available years of the period. The modelled time-series of total annual atmospheric deposition to the OSPAR maritime regions were also compared with previous estimates performed for the period 1990-2006 [*OSPAR*, 2009].

The report presents main results of the assessment. An overview of the assessment approach is given in Chapter 2. Long-term changes of anthropogenic emissions of the considered heavy metals to the atmosphere in the OSPAR Contracting Parties are characterized in Chapter 3 as well as emissions data on a global scale used for modelling effect of distant emissions sources on the OSPAR region. Description of time series of heavy metal deposition to the OSPAR maritime is given in Chapter 4. Evaluation of the modelling results against observed air concentrations and wet deposition is given in

Chapter 5 and Annex C. Chapter 6 includes comparison of the current results with previous estimates of heavy metal atmospheric input to the marine environment from the OSPAR Assessment 2009. Main conclusions of the study are formulated in Chapter 7. Numerical data products of the assessment in the form of tables are presented in Annex B.

2. Assessment Approach

The chapter outlines the assessment approach including information on the modelling system, processing of the output data products and the procedure of evaluation of the modelling results against observations.

2.1. Model setup

The model assessment was performed using the Global EMEP Multi-media Modelling System (GLEMOS), version v2.2.1. Description of the current stable version of the model is available at the MSC-E website (http://msceast.org/index.php/j-stuff/glemos).

Model simulations of Pb, Cd and Hg deposition to the OSPAR maritime area and source-receptor relationships were carried out on both regional (EMEP domain, https://www.ceip.at/the-emep-grid) and global scales. Anthropogenic emission data for modelling of the pollutants for the period 1990-2019 were prepared based on the EMEP emissions reporting (Chapter 3).

Data on wind re-suspension of particle-bound heavy metals (Pb and Cd) from soil and seawater were generated using the dust pre-processor [*Gusev et al*., 2006; 2007]. Data on background topsoil concentrations of heavy metals is derived from the results of the FOREGS programme [*Salminen*, 2005]. In order to take into account long-term accumulation over a long-term period, spatially distributed enrichment factors for concentrations in soils were utilized. It is assumed that the enrichment factor is proportional to the accumulated deposition. The enrichment of sea-salt aerosol with Pb and Cd was calculated based on [*Richardson et al*., 2001].

Prescribed fluxes of natural and secondary Hg^0 re-emissions from soil and seawater were generated depending on Hg concentration in soil, soil temperature, and solar radiation for emissions from land and proportional to the primary production of organic carbon in seawater for emissions from the ocean [*Travnikov and Ilyin,* 2009]. Additionally, prompt re-emission of Hg from snow is taken into account using an empirical parametrization based on the observational data [*Kirk et al.*, 2006; *Johnson et al.*, 2008; *Ferrari et al*., 2008].

Meteorological information for model simulations for the period from 1990 to 2018 was generated from the ERA-Interim re-analysis data of the European Centre for Medium Range Weather Forecasts [*ECMWF*, 2020]. Operational analysis data of ECMWF were used for 2019. Original meteorological data were processed by meteorological pre-processor based on the Weather Research and Forecast modelling system (WRF) [*Skamarock et al*., 2008]. Atmospheric concentrations of chemical reactants (O_3, OH, SO_2, NO_3 and Br), which are required for description of Hg chemistry, were derived from the MOZART and p-TOMCAT models [*Emmons et al*., 2010; *Yang et al*., 2005; 2010].

Boundary conditions for the regional scale simulations of all considered pollutants were obtained from the GLEMOS model runs on a global scale. Initial conditions were generated with one-month spin-up model runs for regional simulations and a three-year spin-up run for the global-scale Hg modelling.

2.2. Data processing

OSPAR maritime area is presented by five regions: Region I - Arctic Waters; Region II - Greater North Sea; Region III - the Celtic Seas; Region IV - Bay of Biscay and Iberian Coast and Region V - Wider Atlantic. Regions II, III and IV are fully covered by the EMEP grid (Fig. 1). However, only part of the Regions I and V is covered by the EMEP grid. In order to prepare deposition data for the entire OSPAR area global scale modelling with coarse spatial resolution (3°x3°) was performed. Merging of the modelling results based on global-scale and regional-scale calculations in Regions I and V results in inconsistency at the western and northern borders of the EMEP grid. In order to avoid the inconsistency, the regional grid was extended to cover the OSPAR regions I and V entirely. Global-scale results were interpolated to the extended grid with finer spatial resolution. These interpolated data were used to fill in parts of the OSPAR regions, which are not covered by the EMEP grid. To smooth the border between the interpolated global-scale and regional-scale calculations five westernmost grid cells of the EMEP grid were assumed to be "transitional", where deposition flux was calculated as weighted mean between interpolated global deposition and regional-scale deposition. The weight is proportional to the distance from the western border of the EMEP grid along latitude. The resulting spatial distribution of deposition flux was further used to calculate long-term trends of deposition and to establish source-receptor relationships for each OSPAR region.

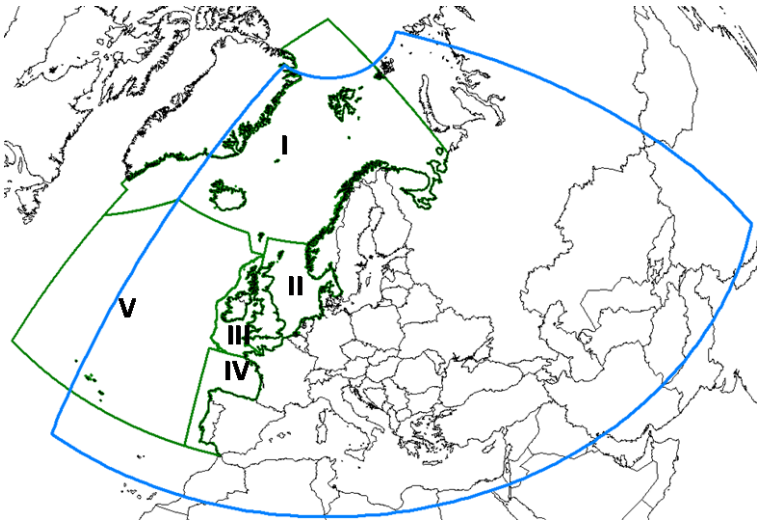

Figure 1. *Border of the EMEP domain (blue line) and OSPAR maritime area (green line) with indication of the OSPAR regions (I - V).*

In order to characterize long-term changes of heavy metal pollution levels the bi-exponential approximation of trends was applied [*Colette et al*., 2016]. The changes of heavy metal pollution levels in the period from 1990 to 2019 are typically non-linear with faster decline in nineties and slower change after nineties. The bi-exponential approach assumes that long-term changes are approximated by "fast" exponent well describing the reduction in the beginning of the period, and "slow" exponent explaining the decline after the nineties (1):

$$C(t) = a_1 \cdot \exp\left(-\frac{t}{\tau_1}\right) + a_2 \cdot \exp\left(-\frac{t}{\tau_2}\right) \quad (1)$$

Here $C(t)$ is approximated deposition or concentration trend at time t, τ_1 and τ_2 are characteristic times and a_1 and a_2 are coefficients.

This approach was applied to characterize trends of deposition to the OSPAR regions, and to modelled and observed air concentrations and wet deposition at monitoring stations. Long-term changes are characterized by total change for the period (2) and mean relative annual rate of change (3):

$$R_{tot} = \frac{(C_{beg} - C_{end})}{C_{beg}} = 1 - \frac{C_{end}}{C_{beg}} \quad (2)$$

$$R_{av} = 1 - \left(\frac{C_{end}}{C_{beg}}\right)^{\frac{1}{N-1}} \quad (3)$$

Average rate of change is geometric mean of the annual changes between two neighbouring years. C_{beg} and C_{end} are the trend values of the first and the final years of the considered period and N is number of considered years.

2.3. Comparison of modelling results with observations

Statistical indicators used for comparison of modelled and observed values includes mean relative bias (MRB), Pearson's coefficient of correlation (R_c), calculated by formulas (4) and (5), respectively:

$$MRB = \frac{(\bar{M} - \bar{O})}{\bar{O}} \cdot 100\% \quad (4)$$

$$R_c = \frac{\sum_{i=1}^{N}(M_i - \bar{M}) \cdot (O_i - \bar{O})}{\sqrt{\sum_{i=1}^{N}(M_i - \bar{M})^2 \cdot \sum_{1}^{N}(O_i - \bar{O})^2}} \quad (5)$$

In (4) and (5) modelled values are denoted as M and observed values as O. Besides, faction of stations where discrepancy between modelled and observed values lies within a factor of 2 (F2) was determined. Finally, in order to characterize long-term changes of modelled and observed air concentrations or deposition fluxes at monitoring stations mean relative rate of change (3) was used. The change was calculated for stations where measurements for at least half of the considered period were available.

Prior to the comparison, the outliers in raw measurement data were identified and filtered out. In order to identify the outliers in time series of each year the standard deviation method was applied [e.g., *Bain and Engelhardt,* 1992]. The method defines the outlier as a value falling outside the range of <M>±(3*SD), where <M> is the mean value, and SD is the standard deviation. This method was applied for concentrations in air and in precipitation.

Due to gaps caused by missing or incorrect measurements or filtering out of outliers the time series of each year are often incomplete. Annual mean measured concentrations or annual sums of wet deposition were not used in the analysis if their completeness was below 50%. Besides, for comparability of measured wet deposition fluxes at different stations and different years observed

wet deposition fluxes were adjusted to the full-year period. Each accumulated annual value was converted to mean daily flux via dividing by actual number of days when measurements were available. Then daily flux was multiplied by a number of days in a year (365 or 366). Implicitly it means that for the missing period of a year the same average concentration in precipitation and the same average daily precipitation sums are assumed [*Ilyin et al*., 2020].

Comparison of modelled and observed air concentrations and wet deposition was carried out for stations of Comprehensive Atmospheric Monitoring Programme (CAMP) (Fig. 2). The results of the comparison presented as time series diagrams for the period from 1990 to 2019 period are summarized in Annex C. There are several stations where modelled values markedly (by an order of magnitude) underestimate the observed values. These are wet deposition fluxes for stations BE4, GB92, GB93 and DK5. Wet deposition fluxes observed at these stations are not included into the statistical analysis. Data on Hg in air measured at station BE13 are unrealistically low and are also not used in the analysis. Nevertheless, the diagrams showing comparison of modelled and observed levels are presented in Annex C for all stations.

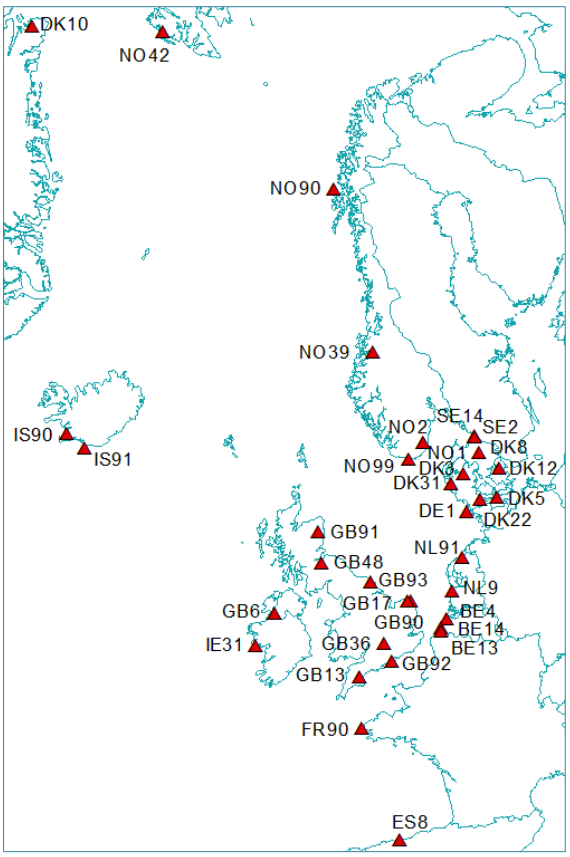

Figure 2. *Location of stations of Comprehensive Atmospheric Monitoring Programme (CAMP).*

3. Emission Data

The chapter is focused on emission data used for modelling of heavy metals on regional and global scales. Emissions of Pb, Cd and Hg and their long-term changes in the OSPAR Contracting Parties are overviewed. Available global-scale emission data for Hg and development Pb and Cd global emissions estimates are described.

3.1. EMEP regional emissions

Total annual emissions of heavy metals are officially reported by EMEP countries to the UN ECE Secretariat. These data are available from the EMEP Centre on Emission Inventories and Projections (CEIP) (http://www.ceip.at/). Time-series of annual heavy metal emissions for the years 1990-2018 (submission 2020) and 2019 (submission 2021) were reported by 33 EMEP countries (65%), including all OSPAR Contracting Parties. For other EMEP countries that provided data for the part of the period (20% of the countries) or did not submit their emission data (15% of the countries) expert estimates of emissions were used elaborated on the basis of methodology developed by CEIP [*Tista et al.*, 2019].

Spatial distribution of heavy metal emissions in the EMEP domain was constructed by CEIP for 2018 and 2019. For other years (1990-2017) the spatial pattern for 2018 was applied for the model simulations, taking into account the sectoral composition for each country. The spatial distribution in every EMEP country is available for each of the 13 GNFR emission sectors used in modelling (A_PublicPower; B_Industry; C_OtherStatComb; D_Fugitive; E_Solvents; F_RoadTransport; G_Shipping; H_Aviation; I_Offroad; J_Waste; L_AgriOther and M_Other) for 2018. For each sector a ratio between total sector emissions in 2018 and the emission in every year of the period 1990-2017 was determined. The spatial distribution of sector emissions in 2018 was multiplied by the calculated ratios to produce spatial distributions of sector emissions for other years. Therefore, total sector emissions differ from year to year, whereas the spatial patterns of sector emissions remain the same for the period from 1990 to 2018.

Long-term changes of Pb, Cd and Hg anthropogenic emissions in the OSPAR Contracting Parties in the period 1990-2019 are shown in Figs. 3-5. Total annual atmospheric emissions of all the OSPAR countries have decreased by 96% for Pb, 73% for Cd and 83% for Hg from 1990 to 2019. In 2019 total emissions of Pb, Cd and Hg made up 543, 36 and 23 t/y, respectively. The largest contributions to total annual heavy metal emissions were made by Germany, Spain and the United Kingdom. Numerical data on heavy metal emissions in the mentioned above countries along with total emissions from the EMEP area are presented in Tables B.2-B.4. (Annex B).

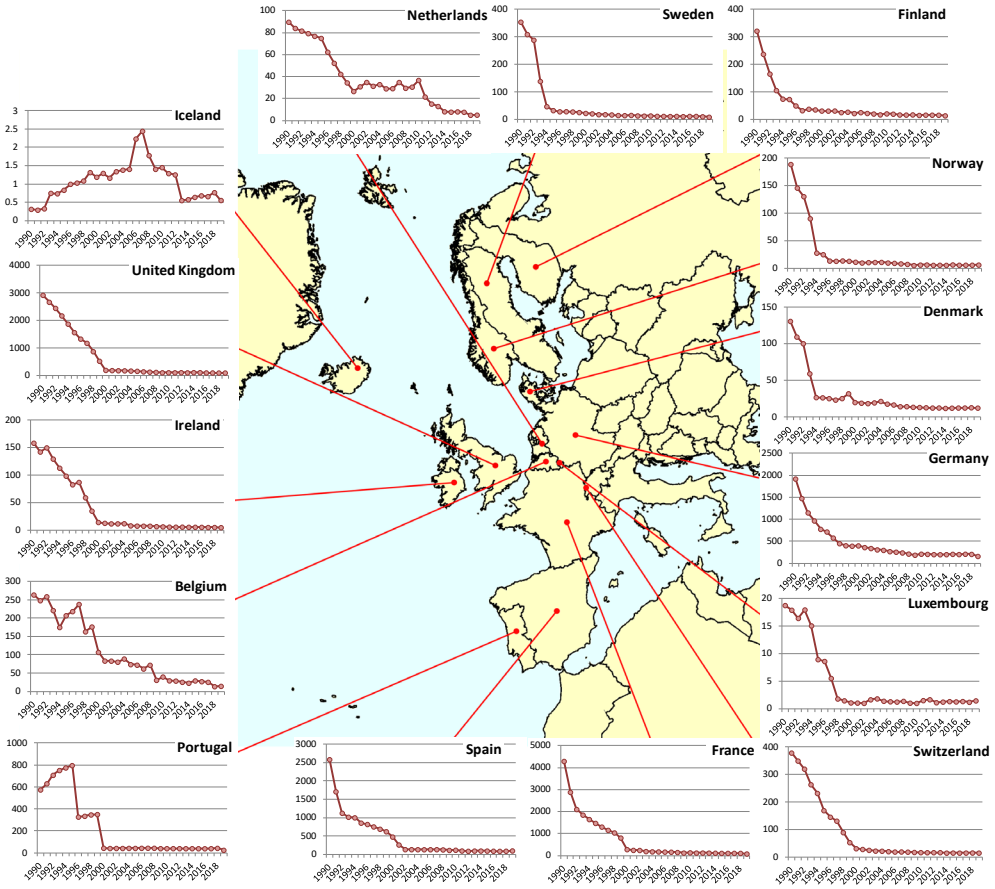

Figure 3. *Time series of Pb emissions from the OSPAR Contracting Parties. Units: t/y.*

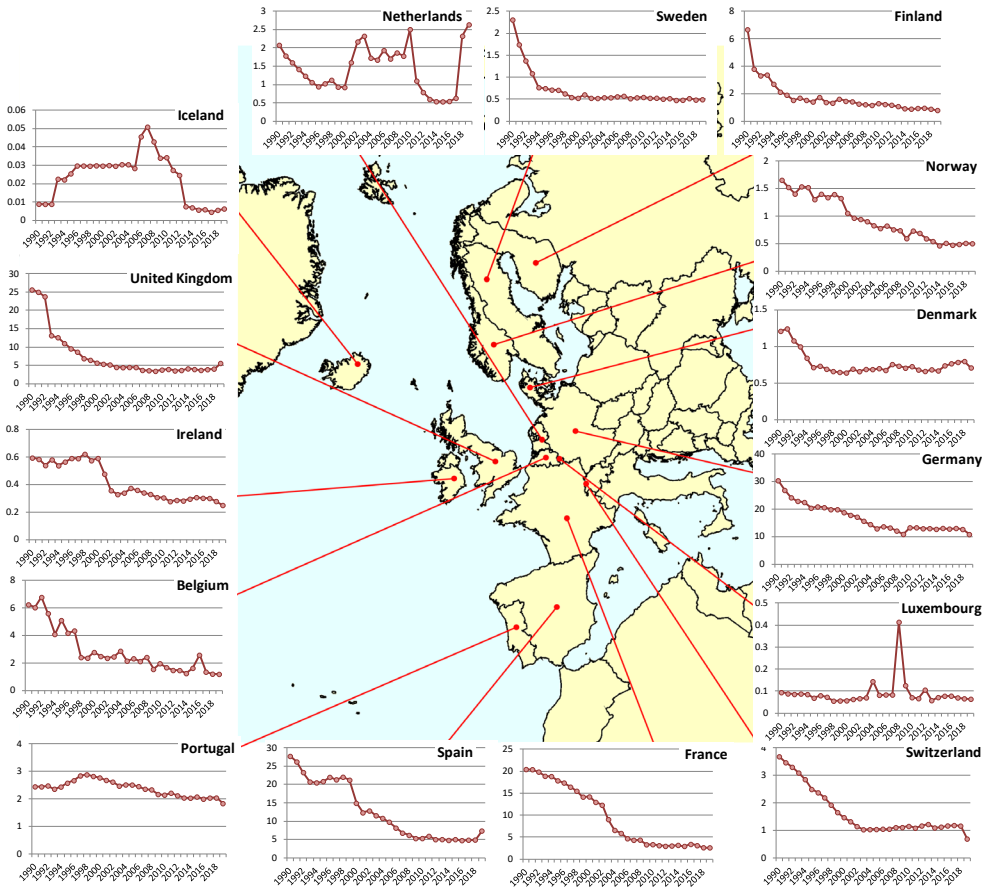

Figure 4. *Time series of Cd emissions from the OSPAR Contracting Parties. Units: t/y.*

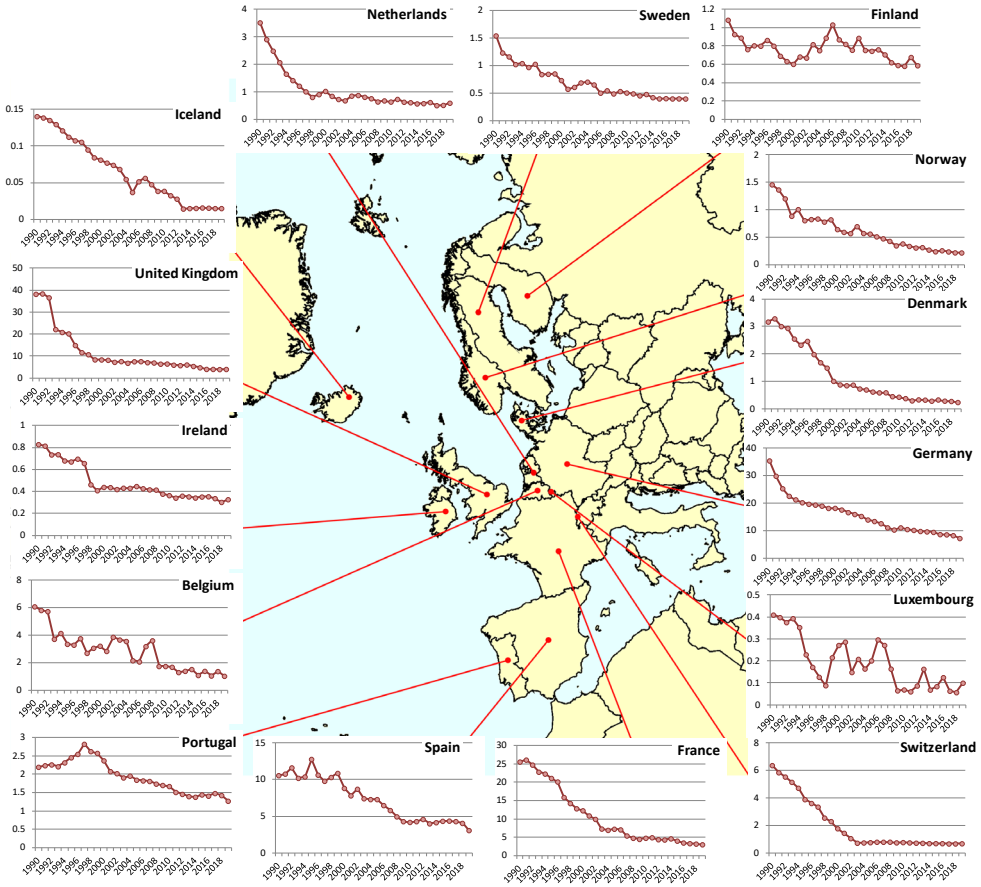

Figure. 5. *Time series of Hg emissions from the OSPAR Contracting Parties. Units: t/y.*

Among the OSPAR countries the level of uncertainty in official data on HM emissions was reported by Belgium, Denmark, Finland, France, Sweden, Switzerland and the United Kingdom. Uncertainties in the reported data on HM emissions for 2019 expressed as percentage relative to mean value of emissions are given in Table 1. In most of the Contracting Parties the uncertainties make up tens of per cents with minimum of 25% for Pb emissions in Sweden. The highest uncertainties reaching almost 500% are reported by Denmark.

Table 1. *Uncertainties (%) of officially reported total values of national emission data on Pb, Cd and Hg of the OSPAR Contracting Parties in 2019.*

	Belgium	Denmark	Finland	France	Sweden	Switzerland	UK
Pb	86	492	33	121	25	50-100	70
Cd	107	365	35	40	35	50-100	-30 to +50
Hg	42	120	39	34	72	50-100	-30 to +50

Along with gridded emission data additional emission parameters are required. They include seasonal variations, distribution of emissions heights and chemical speciation of Hg emissions. Required vertical and temporal disaggregation of the emissions was generated using emission pre-processing tool, developed by MSC-E for the GLEMOS modelling system. More detailed

information on the emission pre-processing procedure is presented in the heavy metal Status Report [*Ilyin et al*., 2018].

3.2. Global emissions

In order to simulate deposition to parts of OSPAR Regions I and V located outside of the EMEP grid as well as to produce boundary concentrations of Pb, Cd and Hg for the EMEP domain global-scale calculations of atmospheric transport have been performed. Gridded Pb, Cd and Hg emission data over the global scale have been prepared by MSC-E.

The only available emission data on Pb are related to 1989 [*Pacyna et al,* 1995]. This dataset can hardly be used because it does not present long-term changes for the considered thirty-year period. Since lead presented in the atmosphere in particulate form, it was assumed that spatial distribution of Pb emission is similar to that of particulate matter. For each EMEP country and each considered year the ratio of officially reported national total Pb emission to PM2.5 emission was established. Then median value of the ratio was determined for each year. Since the USA and Canada also reported their national emission data, the ratios for North America were calculated following the same approach (Fig. 6). As seen from the figure, the ratio for the EMEP countries in 1990 – 2000 is much higher than the ratio after 2000. It is explained by significant contribution of lead emissions from combustion of leaded gasoline in the beginning of the considered period. After phasing out of leaded gasoline in Europe the ratio of Pb to PM2.5 emissions almost stabilized.

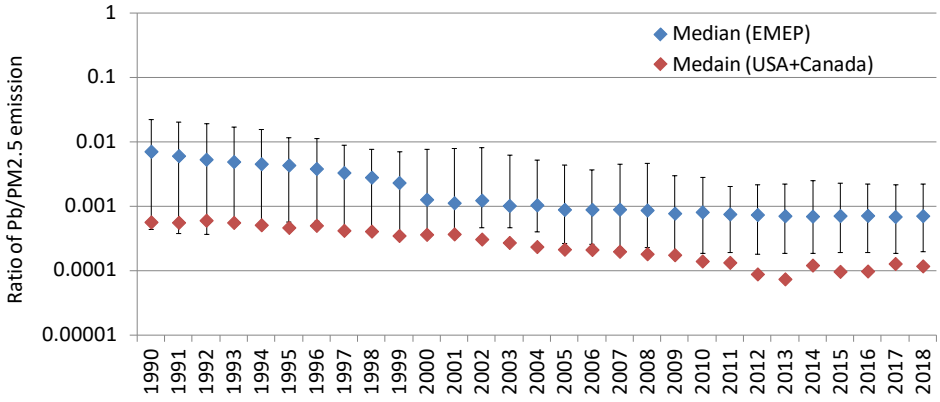

Figure 6. *Median value of Pb/PM2.5 national total emission ratio for the EMEP countries and North America. Whiskers for the EMEP countries denote range of the ratios between 10th and 90th percentiles.*

Global-scale gridded data of PM2.5 emissions have been available in the EDGAR database [*Crippa et al*., 2018; *EDGAR*, 2021] for the period from 1990 to 2015. For the remaining years (2016-2019) it was assumed that PM2.5 emissions had not changed since 2015. The ratio of Pb/PM2.5 emissions calculated for Europe was applied for the whole world, except for North America where Pb/PM2.5 ratio for the USA and Canada was used. Finally, emissions in the EMEP domain were substituted by gridded emission data for modelling based on CEIP data.

Final spatial distributions of Pb emissions over the globe in 1990 and 2019 used in the modelling are shown in Fig. 7. Significant decline of Pb emissions in Europe, Central Asia and North America is explained by sharp decline in nineties due to phasing out of leaded gasoline and further continuous

emission reduction in other sectors. Decline of Pb emissions is also noted for China. Analysis of temporal changes of heavy metal emissions in China from 1949 to 2012 was carried out by [*Tian et al.,* 2015]. According to [*Tian et al.,* 2015], increase of the Chinese Pb emissions from 1990 to 2000 is followed by sharp two-fold reduction due to transition to unleaded gasoline. Although after 2000 Pb emissions have been increasing, the overall decline of emissions in China between 1990 and 2012 made up around 20%.

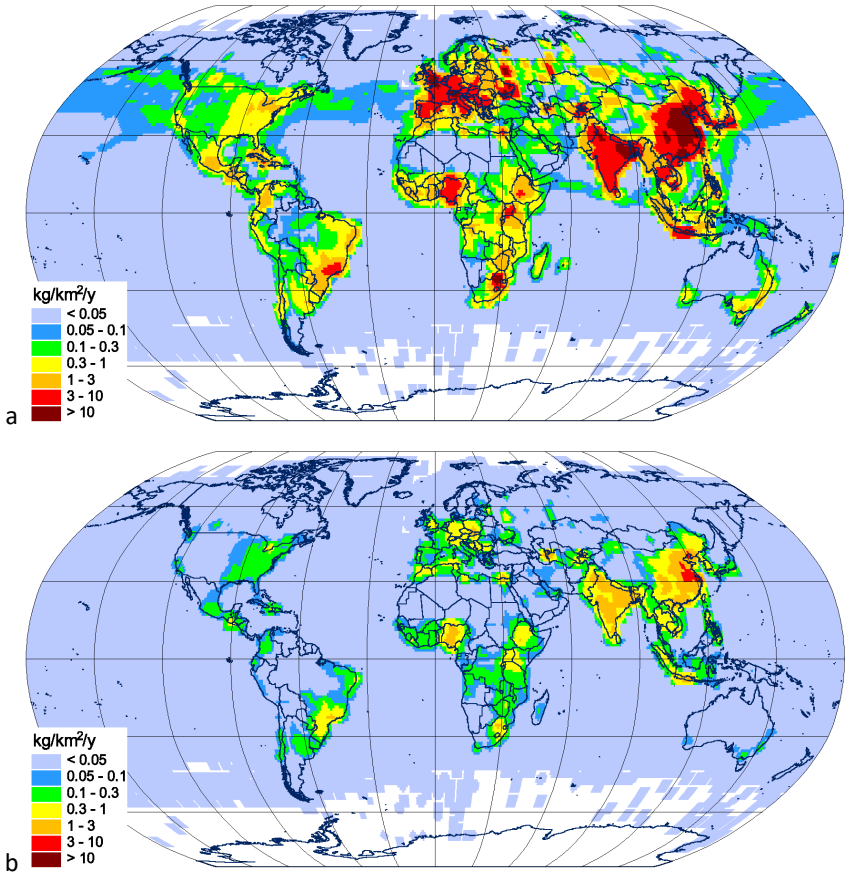

Figure 7. *Global distribution of anthropogenic emissions of Pb in 1990 (a) and 2019 (b).*

Global-scale gridded emissions of Cd are not available. *Zhu et al*. [2020] published maps of emissions of a number of trace elements, including Cd, in 2012 with spatial resolution 0.5°x0.5°. However, the access to the numerical data was not found. In order to produce spatial distribution of Cd emissions over the globe, it was assumed that spatial distributions of Cd and Hg are similar. Gridded global Hg emissions for 1990-2019 available for modelling purposes are described below. Long-term trend of Cd emissions was obtained based on [*Zhu et al.,* 2020]. The authors presented time series of Cd and Hg emissions for 1995 – 2012 (Fig. 8a), and total emissions of Cd and Hg in six sub-regions of the world: Asia, South America, North America, Europe, Africa and Oceania (Fig. 8b). Assuming constant ratios between Cd and Hg emissions in each region, and the same temporal changes of Cd and Hg emissions as for the entire globe, spatial distribution for modelling purposes was reproduced for period from 1995 to 2012. Ratios of Cd to Hg emissions for 1990-1994 were assumed to be equal to those in 1995, and for 2013-2019 - equal to those in 2012. Emissions in the EMEP domain were substituted by gridded regional emission data.

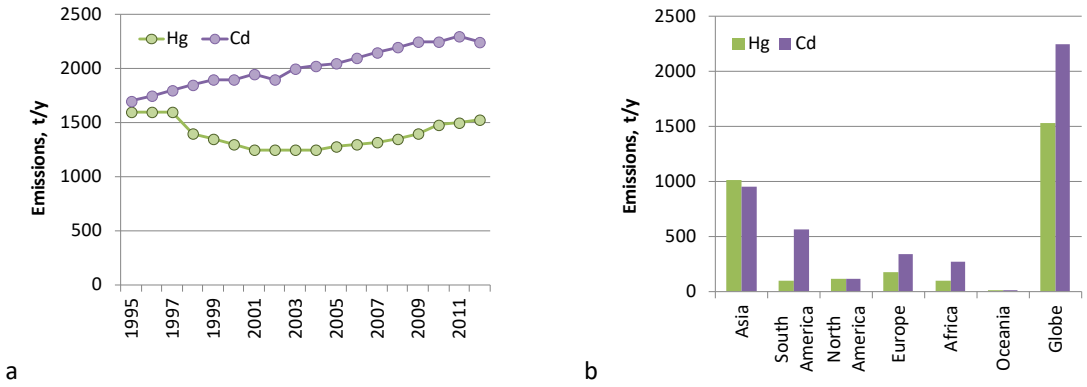

Figure 8. *Time series of global Cd and Hg emissions (a) and Cd and Hg emissions of sub-regions of the world in 2012 (b) according to [Zhu et al, 2020].*

Spatial distributions of Cd emissions in 1990 and 2019 used in the modelling are shown in Fig. 9. As seen, marked reduction of Cd emissions took place in Europe, Central Asia and North America. Some increase of Cd emissions is noted for China. Emission estimates in China made by [*Tian et al.,* 2015] support this tendency, but the rate of the increase seems to be much higher (about 3.3-fold). Increase of Cd emissions in South America and some counties of Africa is likely artificial and explained by the increase of Hg emissions from artisanal small-scale gold mining. Since it is assumed that spatial distribution of Cd emissions is similar to that of Hg, the increase of Hg regional emission leads to the corresponding increase of Cd emissions. Nevertheless, these regions of South America and Africa are located far from the OSPAR maritime area and the influence of their emissions is expected to be minor on Cd deposition to the OSPAR regions.

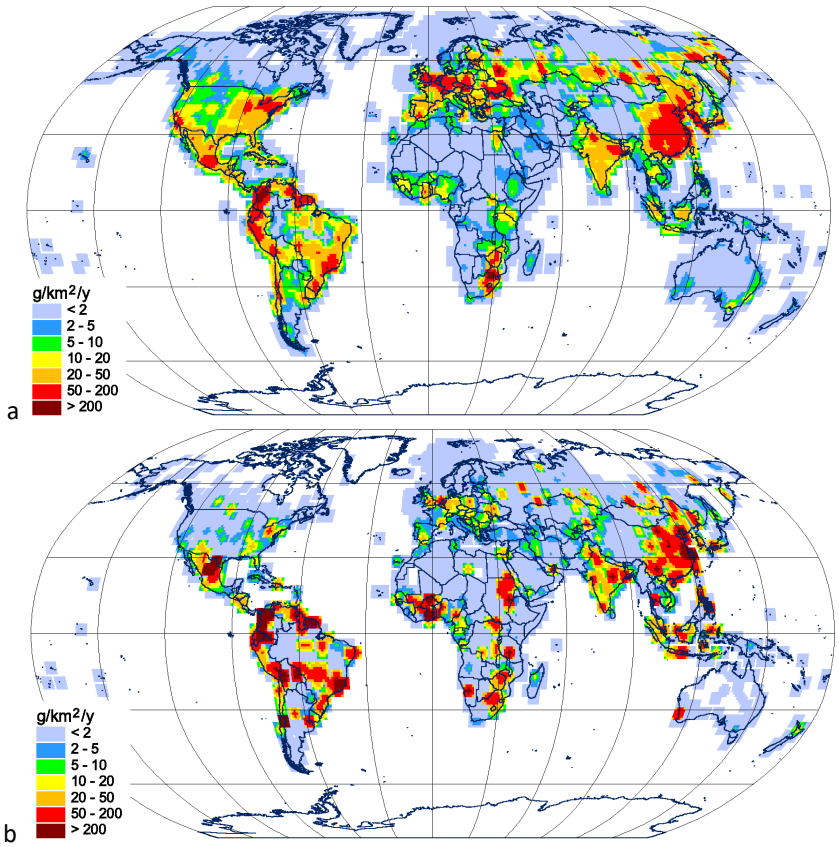

Figure. 9. *Global distribution of anthropogenic emissions of Cd in 1990 (a) and 2019 (b).*

There are a few global emissions inventories for Hg published over the past decade. However, none of them provide reliable and consistent estimates of Hg anthropogenic emissions for the entire time period 1990-2019. Besides, there are significant deviations between the inventories in terms of total estimates of Hg emissions in various regions (see discussion in *Travnikov et al*., 2021). Therefore, a global dataset of long-term Hg anthropogenic emissions was compiled as combination of two emissions inventories: the global Hg emissions inventory for 2010 prepared as a part of the UNEP Global Mercury Assessment 2013 (*GMA*, 2013) [*AMAP/UNEP*, 2013] and the harmonized dataset of Hg historical emissions for 1990, 1995, 2000 and 2005 [*AMAP*, 2010; 2011]. Mercury emissions were kept unchangeable after 2010 in all regions of the globe except for Europe and Central Asia (the EMEP region). Long-term Hg emissions in the EMEP region were taken from the regional EMEP emissions data (Section 3.1).

The GMA 2013 inventory estimates global Hg emissions in 2010 at 1960 tonnes and comprises emissions from combustion of fossil fuels (mainly coal) in power plants, industrial and residential boilers, metal production (ferrous and non-ferrous), cement production, product use, cremation, and artisanal and small-scale gold mining (ASGM). The largest emissions of mercury to the global atmosphere in 2010 are associated with ASGM (727 tonnes) and stationary combustion of fossil fuels (484 tonnes, including 474 tonnes from coal combustion). Other major emission sectors include non-ferrous metal production (303 tonnes) and cement production (173 tonnes). Figure 10 presents the global distribution of anthropogenic emissions of Hg in 2010 in comparison with the emissions pattern in 1990. Areas with elevated mercury emissions correspond to highly industrialized regions (China, India, Europe, the eastern part of the United States) and areas of artisanal and small-scale gold mining (East and Southeast Asia, South America, Sub-Saharan Africa).

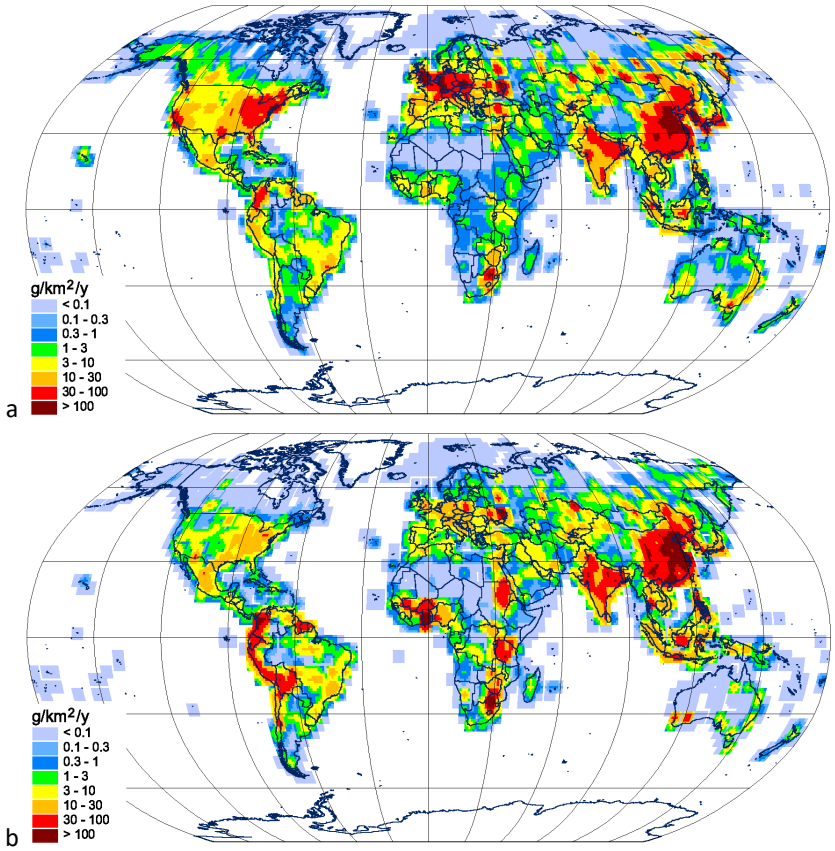

Figure. 10. *Global distribution of anthropogenic emissions of Hg in 1990 (a) and 2010 (b).*

4. Deposition of heavy metals to the OSPAR Maritime Area

The chapter presents the analysis of heavy metal atmospheric deposition to the OSPAR maritime area. It includes information on spatial distribution and long-term changes of Cd, Pb, and Hg deposition for the period 1990-2019 as well as contributions of emissions from the OSPAR Contracting Parties to total deposition to the OSPAR regions. Information on long-term deposition time series and source-receptor relationships is also presented in Tables B.5-B.7 (Annex B).

4.1. Lead

Spatial distribution of Pb deposition was characterized by higher fluxes in the North Sea (Region II), and lower fluxes in the Arctic Waters (Region I) and the southern part of the Wider Atlantic (Region V) (Fig. 11). For example, Pb deposition flux in 1995 exceeded 1 kg/km^2/y over most part of the North Sea, whereas in the northern part of the Arctic Waters Region the flux ranged from 0.05 to 0.1 kg/km^2/y (Fig. 11a). Somewhat higher deposition flux (0.1-0.3 kg/km^2/y) was noted for the southern part of the Wider Atlantic Region. Relatively low deposition in the northern and southern parts of the OSPAR maritime area was explained by two factors. First of all, the mentioned regions were located far from main anthropogenic sources. Besides, they were characterized by relatively low annual precipitation sums. In the years close to the end of the considered period deposition flux in the North Sea Region and over the Wider Atlantic become comparable.

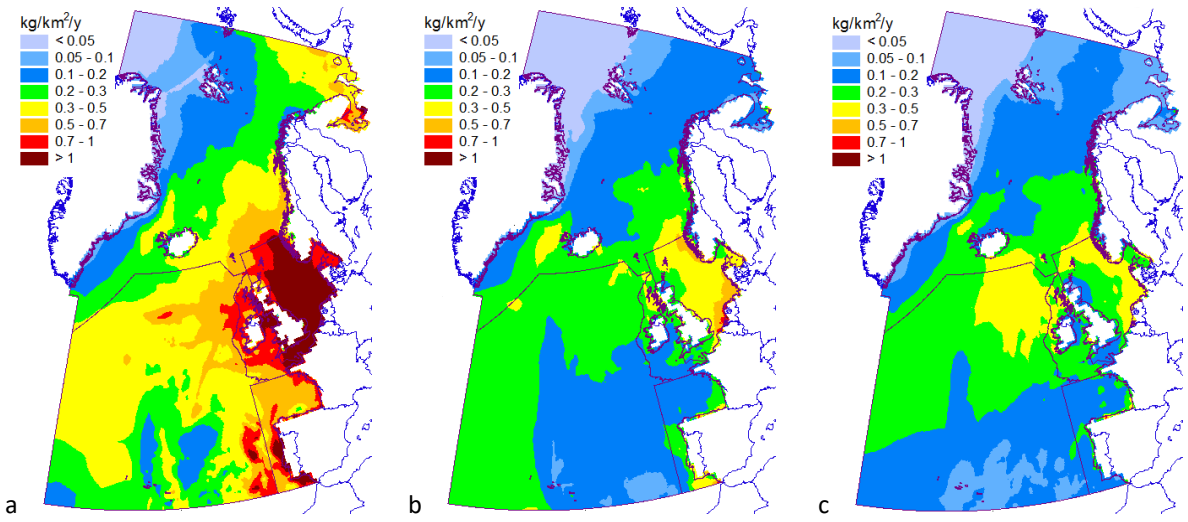

Figure. 11. *Spatial distribution of annual Pb deposition flux to the OSPAR maritime area in 1995 (a), 2005 (b) and 2015 (c). Purple lines depict borders of the OSPAR regions.*

Since 1990 deposition of Pb declined markedly in all OSPAR regions. However, the character of the reduction varied in different regions (Fig. 12). The highest (almost 90%) reduction between 1990 and 2019 took place in the Greater North Sea (Region II) followed by the around 80% decline in the Celtic Seas (Region III). In these regions the highest reduction rate was obtained for the first part of the considered period (1990-2001), while after 2000 the rate of deposition change decreased. The Regions II and III were surrounded by the countries characterized by relatively high emissions in

nineties (e.g., the United Kingdom, Germany, France, Belgium etc.). Emissions in these countries declined markedly due to phasing out leaded gasoline that resulted to the strong decrease of Pb deposition to Regions II and III. The Arctic Waters (Region I) and (Wider Atlantic (Region V) were the most remote from main anthropogenic emission sources. Therefore, the overall decline of deposition in these regions was smaller (about 55%-60%).

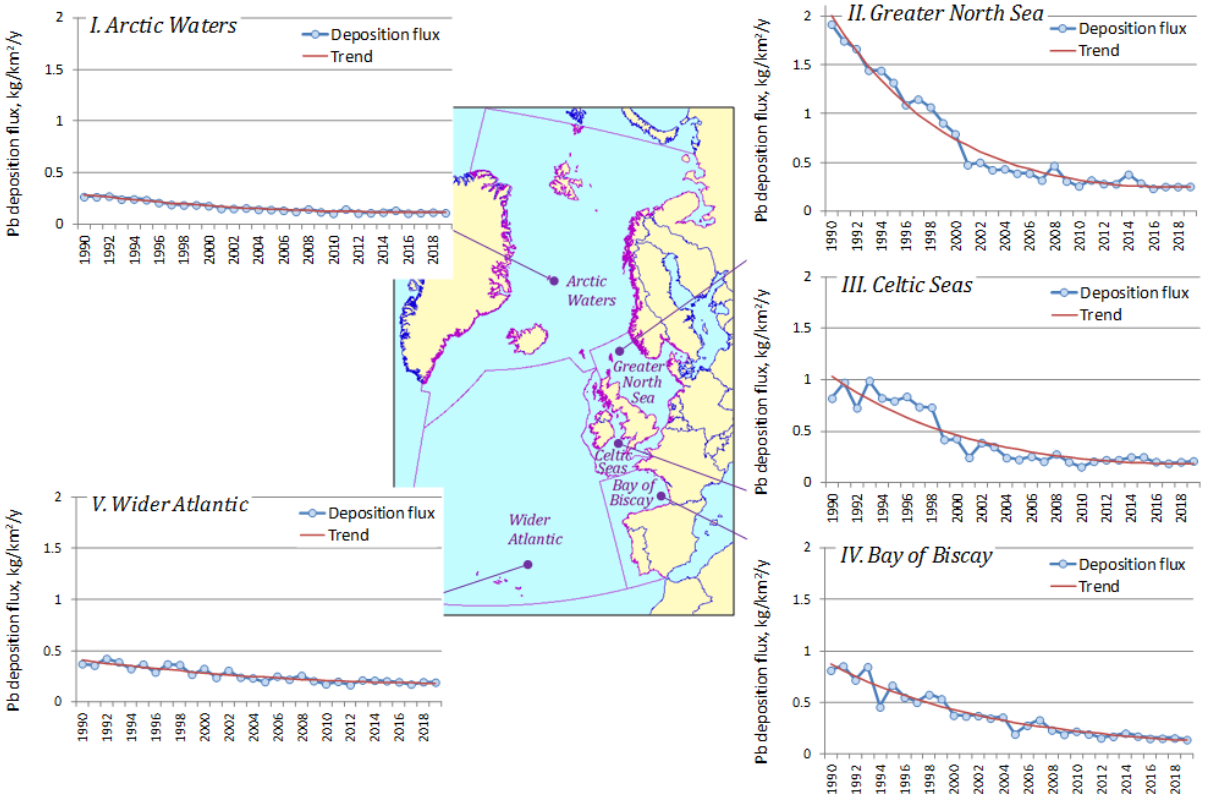

Figure 12. *Time series of average annual Pb deposition flux to five regions of the OSPAR maritime area in the period 1990-2019. Blue line is model estimate, red line is trend approximation.*

Source-receptor calculations have been carried out for 1995, 2005 and 2015. Contributions of all EMEP countries, wind re-suspension and non-EMEP sources were calculated for each of the OSPAR regions. Due to substantial reduction of anthropogenic emissions in the EMEP countries, including OSPAR Contracting Parties, the relative contribution of anthropogenic sources to deposition to the OSPAR decreased between 1995 and 2015 (Annex B). However, it should be kept in mind that the model parameterization of wind re-suspension contained significant uncertainties. Besides, waters of the OSPAR regions were remote from the main anthropogenic sources, especially those of the Arctic Waters (Region I) and Wider Atlantic (Region V).

In absolute terms of contribution the deposition from almost all OSPAR Contracting Parties decreased between 1995 and 2005. Between 2005 and 2015 the deposition decreased or almost stabilized. However, since the rate of decline of national emissions differed among the countries, the change of relative contribution of a particulate country to deposition in the OSPAR regions varied markedly among the countries. For example, the main countries-contributors of Pb deposition to the

Arctic Waters (Region I) were the United Kingdom, France and Germany. The contribution of the British sources to the Arctic Waters (Region I) declined from 8% in 1995 to about 1% in 2015, whereas the contribution of German sources decreased insignificantly remaining at about 1% (Fig. 13). It is explained by the fact that Pb emissions in the United Kingdom declined by almost 15-fold, while the decrease of national German emissions was about 3.5-fold.

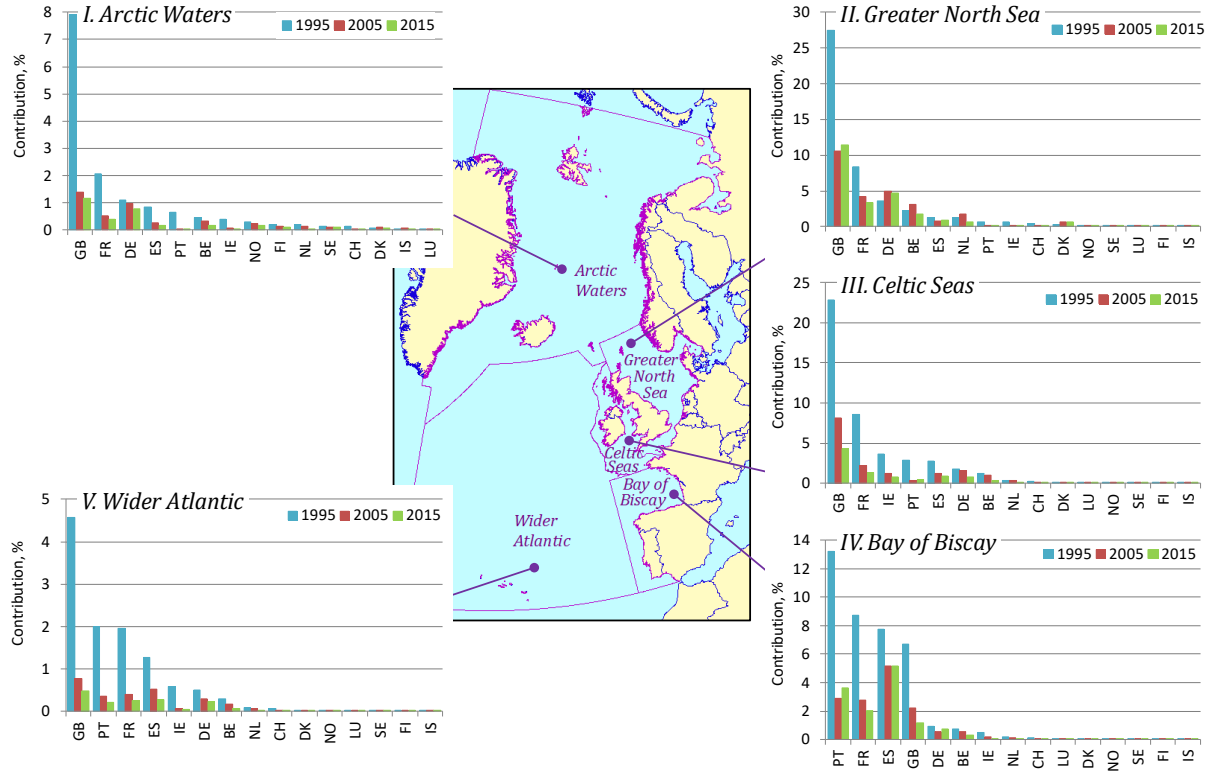

Figure 13. *Contribution of the OSPAR Contracting Parties to Pb deposition to 5 regions of the OSPAR maritime area in 1995, 2005 and 2015. Codes of the countries are given in Annex B. Numerical values are presented in Table B.8*

The Greater North Sea (Region II) is characterized by the highest relative impact of the OSPAR countries compared to other regions. In 1995 the emission sources of the United Kingdom were predominant in Region II, contributing about 27% to anthropogenic deposition. In 2005 and 2015 the contribution of the British sources was lower (about 10%), nevertheless remaining the highest among the OSPAR Contracting Parties. Other significant contributors were France and Germany. Similar situation was noted for the Celtic Seas (Region III). The major contributor to deposition was the United Kingdom, which contribution to total deposition declined from 23% in 1995 to 4% in 2015. Other important contributors were France, Germany and Spain.

The main contributors to deposition in Bay of Biscay (Region IV) were Spain, Portugal, France and the United Kingdom. The changes in the contributions of these countries between 1995, 2005 and 2015 we explained by different rates of changes of national emissions. In 1995 the main contributor to deposition was emission sources of Portugal (13%). In nineties emissions of the OSPAR countries had been declining at higher rate than wind re-suspension. Hence, their contribution to total deposition

decreased significantly between 1999 and 2005. Further decline (from 2005 to 2015) of national emissions slowed down, that resulted to lower reduction of the contribution from sources of France and the United Kingdom, and even some increase of the contribution from German and Portuguese emission sources.

Similar to the Arctic Waters, (Wider Atlantic (Region V) was remote from the main anthropogenic sources and thus the Pb deposition levels were dominated by secondary sources, in particular, re-suspension of marine aerosol particles from sea surface. The contribution of the anthropogenic emissions of the OSPAR Contracting Parties was quite low (few percents). The main contributor in all years (1995, 2005 and 2015) was the United Kingdom. Other key contributors were France, Portugal and Spain.

4.2. Cadmium

The highest Cd deposition flux was obtained for Grater North Sea (Region II) due to close location of significant anthropogenic sources and relatively high annual precipitation sums. In 1995 the Cd flux in the North Sea exceeded 30 g/km^2/y, and by 2015 it declined to 10-20 g/km^2/y (Fig. 14). Lower deposition flux took place over the Celtic Seas (Region III) and the Bay of Biscay (Region IV). In 1995 deposition flux in these regions varied within limits of 10-20 g/km^2/y, while in 2005 and 2015 it was 5-10 g/km^2/y over most part of these regions. Deposition fluxes in the Arctic Waters (Region I) and Wider Atlantic (Region V) exhibited distinct gradient from land mass to remote water area. In 1995 the deposition in the southern part of Region I and the eastern part of Region V varied from 10 to 20 g/km^2/y, while in the south-west of Region V the flux was 3-5 g/km^2/y, and in the high Arctic – below 3 g/km^2/y. Deposition in the eastern part of region V in 2005 were lower than those in 2015 due to higher precipitation sums in 2015 compared to 2005.

Deposition of Cd to the OSPAR regions reduced by about 34 – 80% (1.5 – 5 fold) in the period from 1990 to 2019 (Fig. 15). The highest reduction was noted for the Greater North Sea (Region II). This region was surrounded by countries characterized by significant emissions in 1990, e.g. the United Kingdom, Germany, Belgium, Denmark and the Netherlands. Therefore, the reduction of emissions in these countries had the strongest impact on the deposition change on the Greater North Sea. Lower reduction in other regions was explained by their relative remoteness from main emission sources and higher relative influence of re-suspension. The lowest reduction of Cd deposition taken place in the Arctic Waters (Region I) and Wider Atlantic (Region V) equaled to 40% and 34%, respectively. Unlike Pb, the rate of Cd deposition decline was more uniform in time.

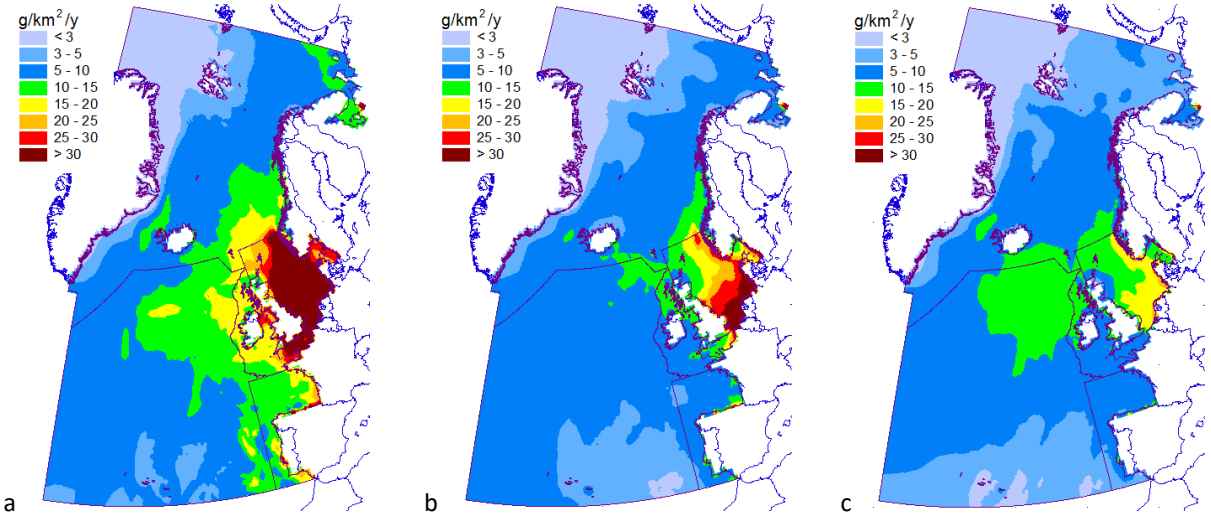

Figure 14. *Spatial distribution of annual Cd deposition flux to the OSPAR maritime area in 1995 (a), 2005 (b) and 2015 (c). Purple lines depict borders of the OSPAR regions.*

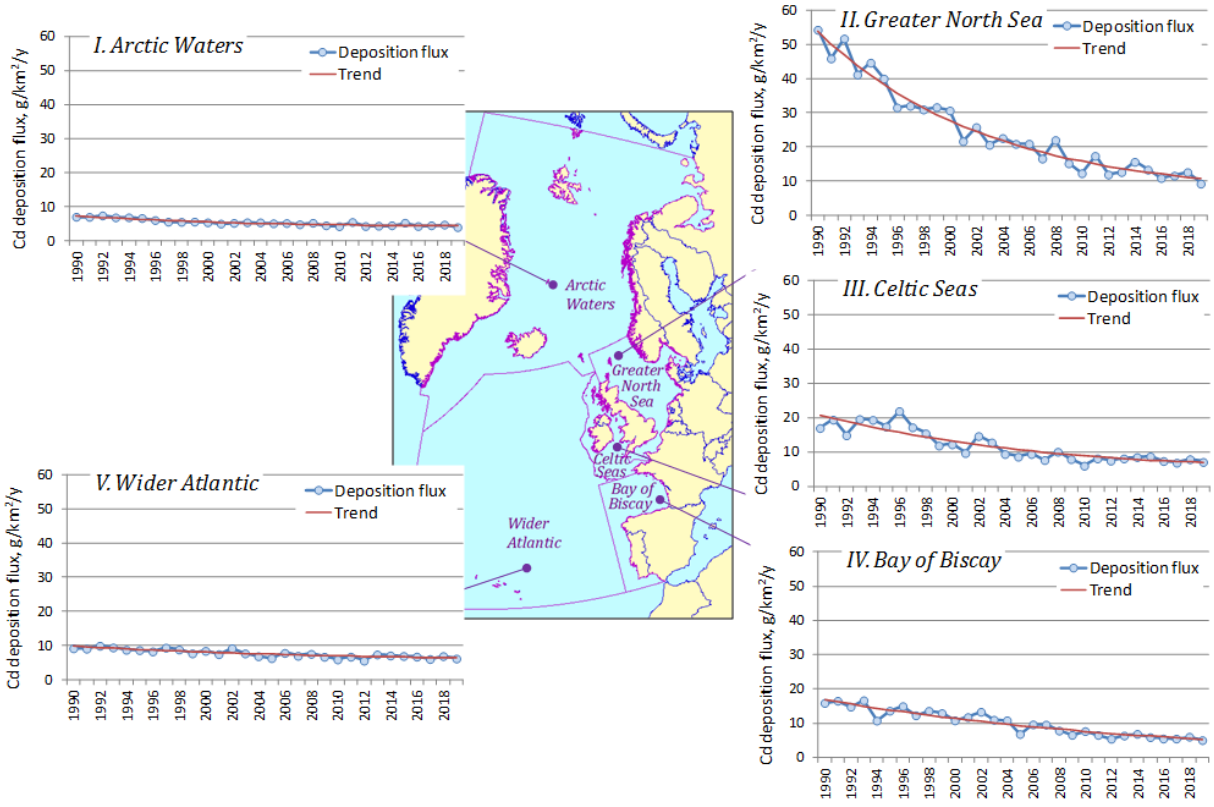

Figure 15. *Time series of average annual Cd deposition flux to five regions of the OSPAR maritime area in the period 1990-2019. Blue line is model estimate, red line is trend approximation.*

Contributions of emission sources of OSPAR Contracting Parties to Cd anthropogenic deposition to the OSPAR maritime area varied largely in time and between particular OSPAR regions (Fig. 16). The Arctic Waters (Region I) and Wider Atlantic (Region V) were remote from major anthropogenic

emission sources, including those of the OSPAR countries. The main contribution to deposition was made by secondary emission sources, such as re-suspension from sea surface. Among the OSPAR Contracting Parties the main contributors to deposition to Region I were the United Kingdom, France, Germany, Norway and Spain. The main contributors to deposition to Region V were Spain, Portugal, the United Kingdom, France and Germany.

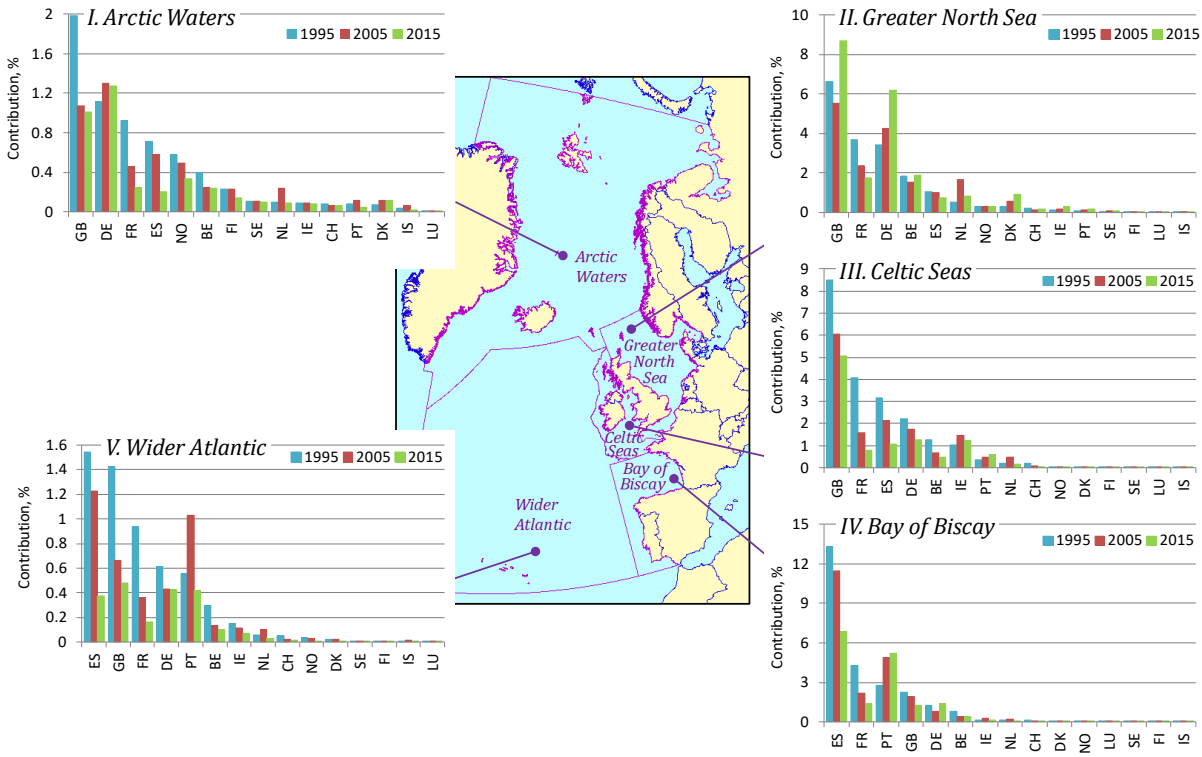

Figure 16. *Contribution of the OSPAR Contracting Parties to Cd deposition to 5 regions of the OSPAR maritime area in 1995, 2005 and 2015. Codes of the countries are given in Annex B. Numerical values are presented in Table B.9*

The largest contribution of the OSPAR countries to Cd deposition was noted for the Greater North Sea (Region II). Sources of the United Kingdom, France and Germany were the main contributors to Cd deposition in the Region II. The contribution of the United Kingdom was the highest in all considered years ranging from about 6% to 9%. Decline of Cd emissions in France from 1995 to 2015 was stronger than that of Germany. Therefore, the contribution of the French sources declined, while the contribution of German sources increased between 1995 and 2015.

The major contributor to Cd deposition to the Celtic Seas (Region III) was the United Kingdom which input declined from 8% in 1995 to 5% in 2015. Other main countries-emitters were France, Spain and Germany. Contributions of all these countries declined between 1995 and 2015 due to significant reduction of national emissions and much lower changes of wind re-suspension contributing to total deposition.

Spain was the predominant contributor to Cd deposition to (Bay of Biscay (Region IV). In 1995 the sources of Spain were responsible for 13% of total deposition, and this share declined to about 7% in

2015. Portugal was characterized by more moderate reduction of Cd emissions over the considered periods. Therefore, its contribution increased from 3% in 1995 to almost 5% in 2015.

4.3. Mercury

Mercury differs from Pb and Cd by long atmospheric life time due to large proportion of the elemental gaseous form (Hg^0) and intensive chemical transformations in the atmosphere. It results in longer atmospheric transport of Hg from emission sources and significant deposition fluxes in remote regions, where intensive oxidation of Hg^0 occurs. In particular, relatively large Hg deposition (15-20 $g/km^2/y$) was estimated in the Arctic Waters region (Fig. 17) due to Hg chemical transformations from the elemental to oxidized forms in springtime during the atmospheric Hg depletion events (AMDEs) [*Steffen et al*., 2008]. However, significant part of Hg deposited to snow and ice surface was photo-reduced and re-emitted to the atmosphere [*Moore et al.,* 2014; *Wang et al.,* 2019]. The deposition over the Arctic Ocean somewhat increased between 1995 and 2005 due to inter-annual variation of meteorological conditions. The following decrease of Hg deposition between 2005 and 2015 was caused by leveled global Hg emissions and gradual decrease of Hg emissions in Europe and North America. Relatively high Hg deposition was also predicted over the North Sea in 1995 due to direct effect of Hg emissions from the neighboring countries and over the coastal waters of Norway because of increased precipitation amount in this area. The lowest deposition fluxes occurred over the high Arctic and the southern part of the Wider Atlantic region.

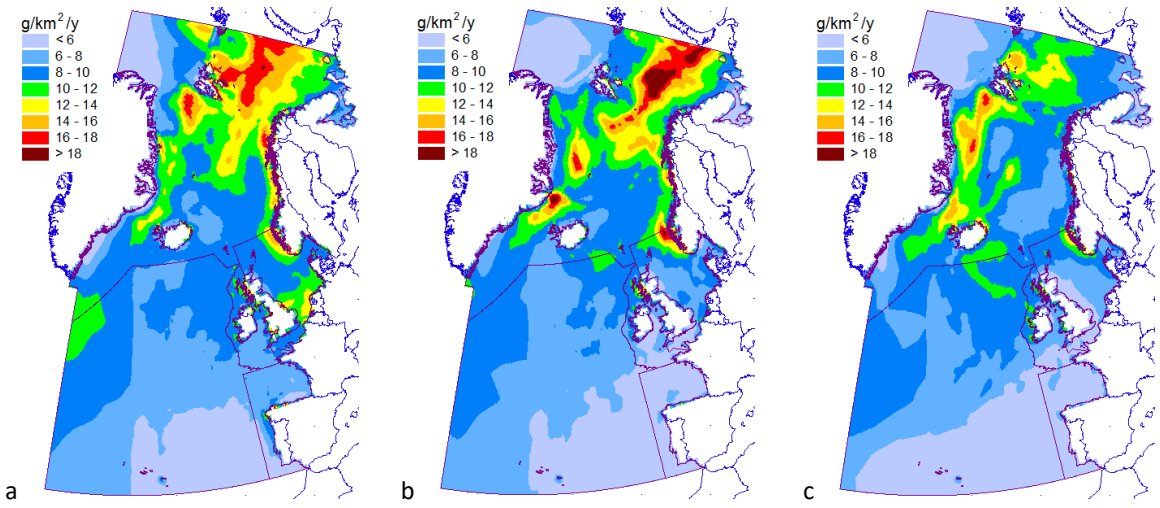

Figure 17. *Spatial distribution of annual Hg deposition flux to the OSPAR maritime area in 1995 (a), 2005 (b) and 2015 (c). Purple lines depict borders of the OSPAR regions.*

Long-term changes of Hg average deposition to all 5 regions of the OSPAR maritime area are shown in Fig. 18. Deposition reduction was more pronounced in the marginal seas (Greater North Sea, Celtic Seas, Bay of Biscay) due to stronger influence of the European emissions. Average deposition to the Greater North Sea decreased by 45% between 1990 and 2019, whereas deposition to the Celtic Seas and the Bay of Biscay decreased by 34% and 27%, respectively. The changes in the first two regions were more pronounced in the first part of the period (1990-2000) and then slow down in the second part (2000-2019). The decrease was largely caused by emissions reduction in the neighboring OSPAR

countries, as it will be shown below, but damped down by slowly changed global anthropogenic and secondary emissions. The long-range atmospheric transport from global anthropogenic and secondary sources even stronger affected remote regions, the Arctic Waters and the Wider Atlantic, where deposition decrease over the whole period did not exceed 25%.

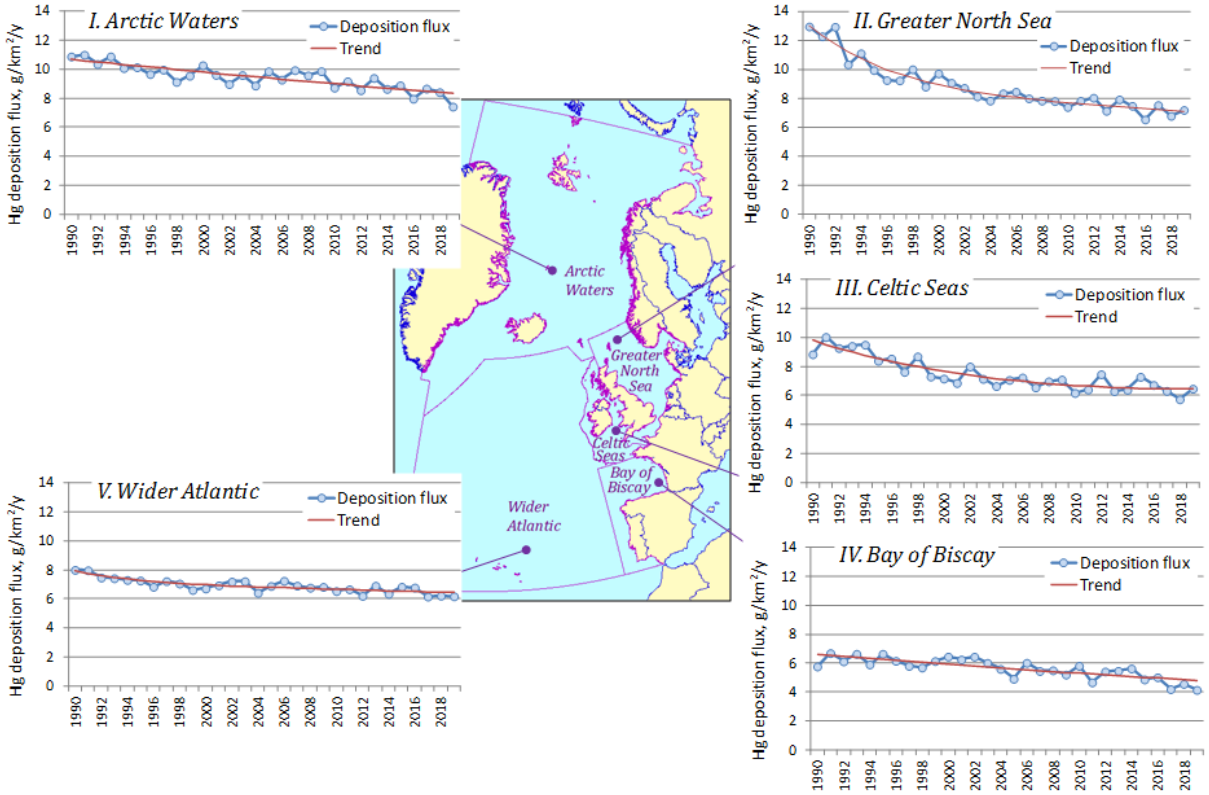

Figure 18. *Time series of average annual Hg deposition flux to five regions of the OSPAR maritime area in the period 1990-2019. Blue line is model estimate, red line is trend approximation.*

Mercury deposition to the OSPAR maritime regions is comprised of contributions of anthropogenic emissions from European countries including the OSPAR Contracting Parties, emissions from sources located in other regions of the globe and natural/secondary emissions from land and the ocean. The global anthropogenic and secondary emissions dominate over the remote regions due to relatively low contemporary Hg emissions in Europe. Relative contribution of the OSPAR Contracting Parties to Hg deposition to the OSPAR maritime area is illustrated in Fig. 19.

The effect of the OSPAR countries on Hg atmospheric input was the greatest for the Greater North Sea and followed by that for the Celtic Seas and the Bay of Biscay. The Greater North Sea was largely influenced by the Great Britain (10-22%), Germany (4-6%) and France (2-6%). The contributions of these countries decreased by a factor of 2-3 from 1995 to 2015 due to reduction of national Hg emissions. The major contributors of Hg deposition to the Celtic Seas were the Great Britain (4-16%), France (1-4%), and Spain (1-2%). Relative contribution of the Great Britain decreased between 1995 and 2015 by a factor of 4 because of strong reduction of national emissions and insignificant contributions of other countries. The Bay of Biscay was dominated by contributions of Spain (6-11%),

France (2-5%), the Great Britain (2-4%), and Portugal (2.5-3%). Contributions of these countries decreased by a factor 2-3 except for that of Portugal, which did not changed considerably due to insignificant change of national emissions.

Relative contributions of the OSPAR countries to Hg atmospheric deposition to the Arctic Waters and the Wider Atlantic did not exceed a few percents due to remoteness of these regions from emission sources and strong influence of global atmospheric transport. The most significant contributors to both regions were the Great Britain, Germany, Spain, and France. Besides, the Arctic Waters were also affected by Norway, whereas Portugal contributed to Hg deposition the Wider Atlantic. Contributions of almost all these countries decreased by a factor of 2-3 between 1995 and 2015 in accordance with reductions of their national emissions.

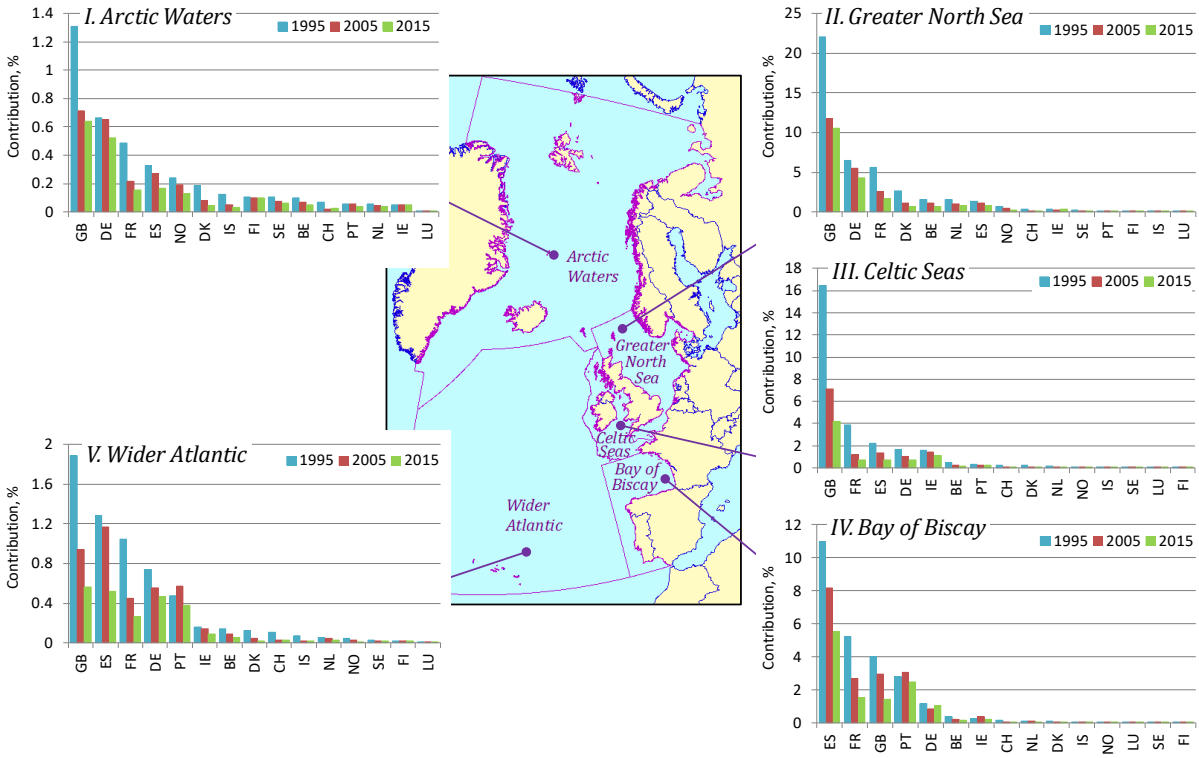

Figure 19. *Contribution of the OSPAR Contracting Parties to Hg total deposition to 5 regions of the OSPAR maritime area in 1995, 2005 and 2015. Numerical values are presented in Table B.10*

5. Evaluation of Modelling Results

Modelled air concentrations and wet deposition fluxes were compared with the available measurement data from Comprehensive Atmospheric Monitoring Programme (CAMP). Stations of the CAMP network are located in OSPAR Contracting Parties on or nearby the sea coast of the OSPAR maritime area. Data from these stations are available in the EMEP data base EBAS (http://ebas.nilu.no/). This section characterizes the model performance and analyses discrepancies between modelled and observed concentrations in air and wet deposition fluxes as well as their long-term changes. Besides, sources of uncertainties associated with the modelling are overviewed.

5.1. Lead

The model performance differs significantly for particular stations and even for particular years. For example, at the German station DE1 (Westerland) the model reasonably well reproduces both magnitude and the long-term variability of Pb concentrations in air and wet deposition fluxes (Fig. 20). For majority of years the discrepancy between modelled and observed air concentrations or wet deposition lies within ±30% limits.

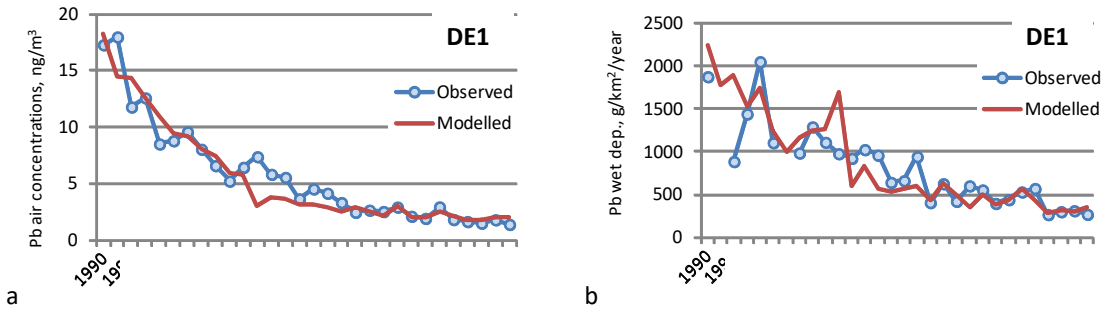

a b

Figure 20. *Modelled and observed annual mean concentrations of Pb in air (a) and annual wet deposition flux (b) in the period 1990-2019 at station DE1 (Westerland, Germany).*

Relative bias applied to each station over the entire considered period varies between -50% to +100% for most of stations (Fig. 21a,c). Therefore, on average the model reproduces the observed air concentrations and wet deposition fluxes within a factor of two. General overestimation of the observed Pb concentrations in air is noted for some British stations and the Norwegian station NO99 (Lista). Underestimation of the observed air concentrations was found for the remote Danish station DK10 (Nord) located in Greenland. The temporal correlation coefficient was calculated only for the stations with at least five years of observations. At most stations the coefficient exceeds 0.5 (Fig. 21b,d). Combination of low bias (MRB) and high temporal correlation coefficient (e.g., DE1, DK31, GB17, NL91 etc.) means that the model successfully reproduced both magnitude and long-term changes of the observed air concentrations.

Negative relative biases for most of stations confirm the tendency of general underestimation of the observed wet deposition fluxes (Fig. 21c). Nevertheless, the mean modelled and observed fluxes agree within a factor of two. Besides, at a number of stations high bias is accompanied with significant correlation, e.g., NO1 (Birkenes, Norway), DK8 (Anholt, Denmark).

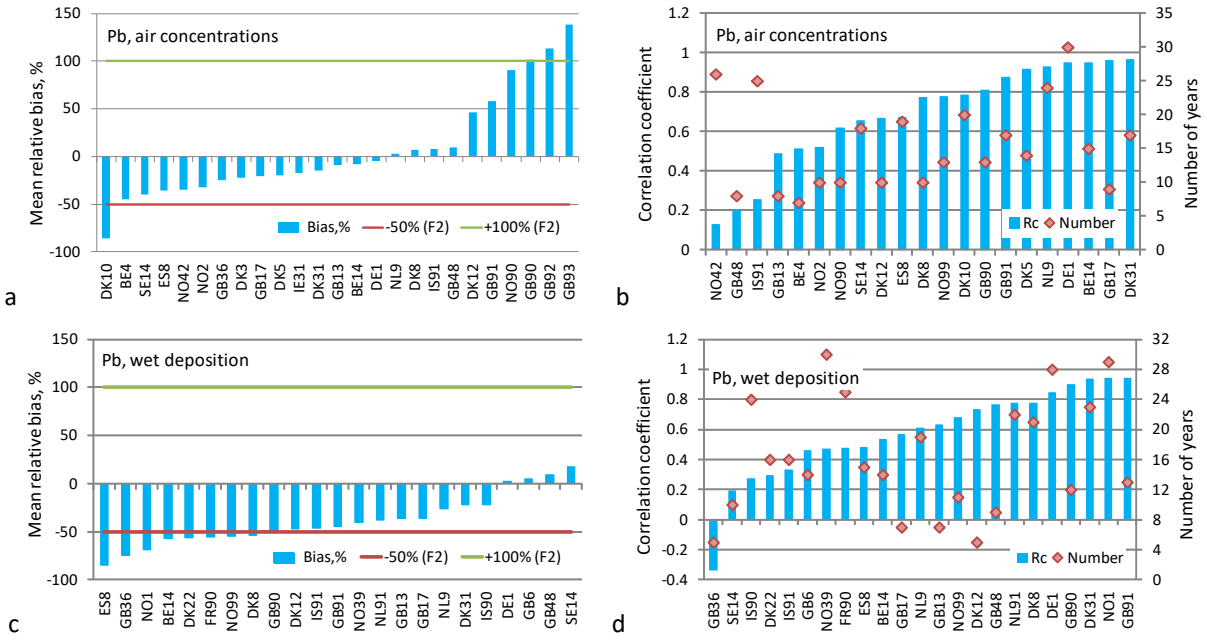

Figure 21. *Mean relative bias (a, c) and temporal correlation coefficient (b, d) for annual mean concentrations in air and annual sums of wet deposition of Pb for 1990-2019. Green and red lines in diagrams (a) and (c) depict limits of a factor of two.*

At some stations, e.g. GB91 (Banchory) overestimation of the observed concentrations in air takes place in the beginning of the considered period (Fig. 22). Analysis of sources contributing to modelled Pb air concentrations at these stations demonstrates that even if only anthropogenic emissions are considered, the model still overestimates the observed concentrations by factors of 1.5–3. At the same time the model underestimates wet deposition fluxes at these stations (Fig. 22b). In years closer to the end of the considered period the discrepancies between modelled and observed Pb levels becomes lower.

At a number of stations the observed concentrations in air (e.g., IS91) or wet deposition fluxes (e.g., FR90) exhibit high inter-annual variability (Fig. 23). These sharp inter-annual changes do not correlate with variations of anthropogenic, secondary emissions or meteorological conditions and may be caused by uncertainties in measurements. However, evaluation of these uncertainties requires additional consideration.

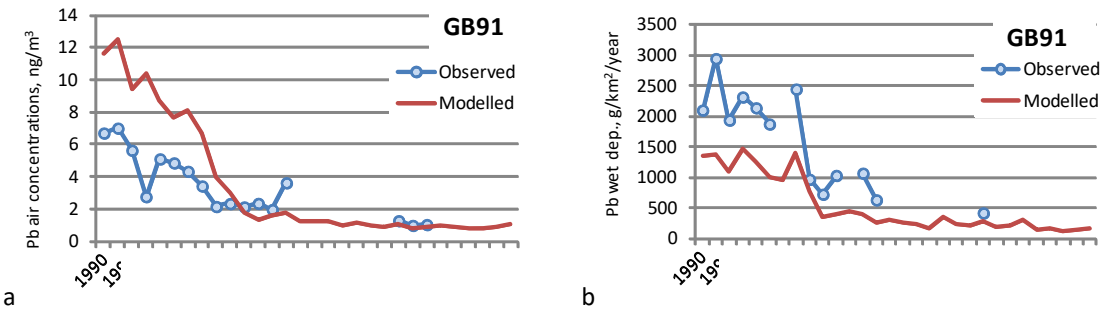

Figure 22. *Modelled and observed annual mean Pb concentrations in air (a) and annual sum of wet deposition flux (b) in the period 1990-2019 at station GB91 (Banchory, the United Kingdom).*

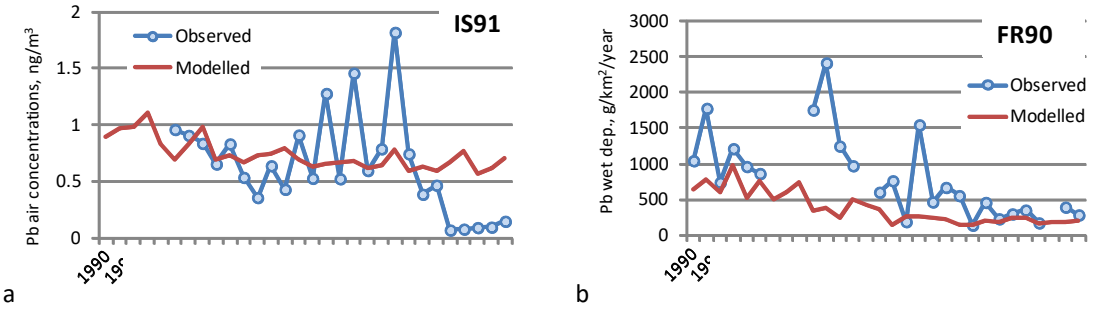

Figure 23. *Modelled and observed annual mean Pb concentrations in air at station IS91 (Storhofdi, Iceland) (a) and annual sum of wet deposition flux at station FR90 (Porspoder, France) (b) in the period 1990-2019.*

Long-term relative changes of Pb pollution levels were compared for ten stations measuring air concentrations and twelve stations where wet deposition fluxes were observed. At most of the stations modelled and observed changes are comparable (Fig. 24). At stations GB91 (air), NL9 and NO39 (wet deposition) the model predicts stronger rate of long-term decline compared to the observations. At stations IS91, NO42, SE14 the reduction of modelled air concentrations is lower than that of observed values.

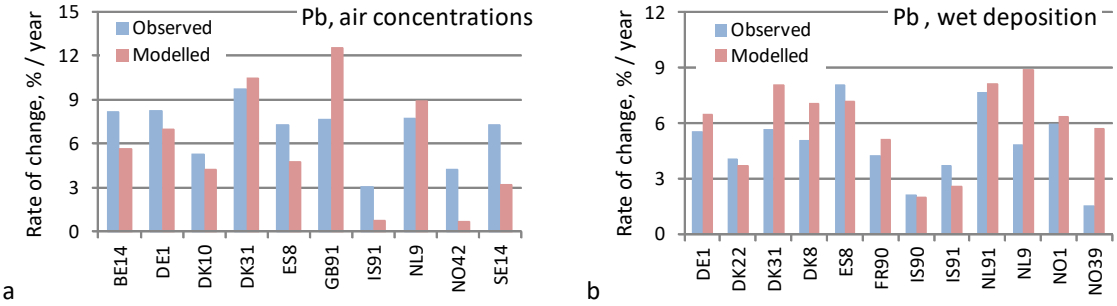

Figure 24. *Mean rate of annual relative change of modelled and observed Pb concentrations in air (a) and wet deposition fluxes (b).*

5.2. Cadmium

Mean relative bias was calculated for Cd air concentrations and wet deposition fluxes for each year of the period from 1990 to 2019. The model performance varies substantially for particular stations. For example, the model reproduced trend of annual mean air concentrations at station NO2 with the bias (MRB) ranging from -30% to 20% (Fig. 25a). Another example is long-term changes of Cd wet deposition flux at station NL91with MRB varying within ±50% in most of years (Fig. 25b).

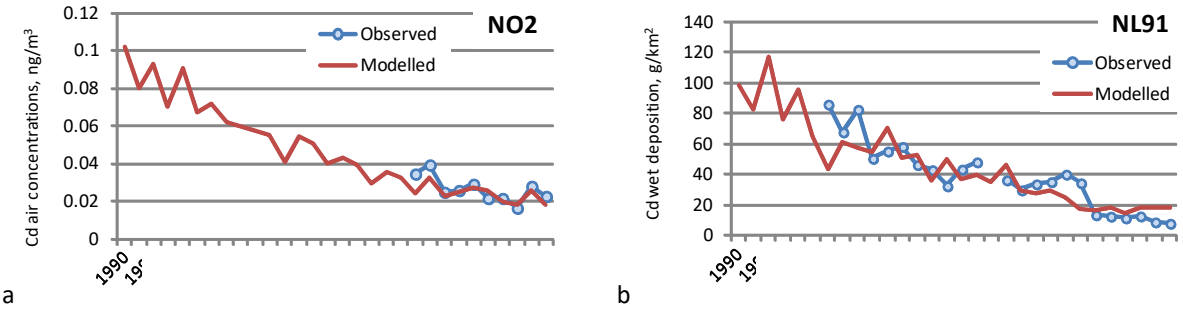

a b

Figure 25. *Modelled and observed annual mean concentrations of Cd in air at station NO2 (Birkenes II, Norway) (a) and annual sum of wet deposition flux at station NL91 (De Zlik, the Netherlands) (b) in the period 1990-2019.*

Combined information on MRB for the entire period, the temporal correlation coefficient and comparison of rates of pollution level change allow evaluating the model performance for each station. On average, some overestimation of the observed concentrations in air and underestimation of wet deposition fluxes take place (Fig. 26a,c). However, at most of the stations the agreement is within a factor of two.

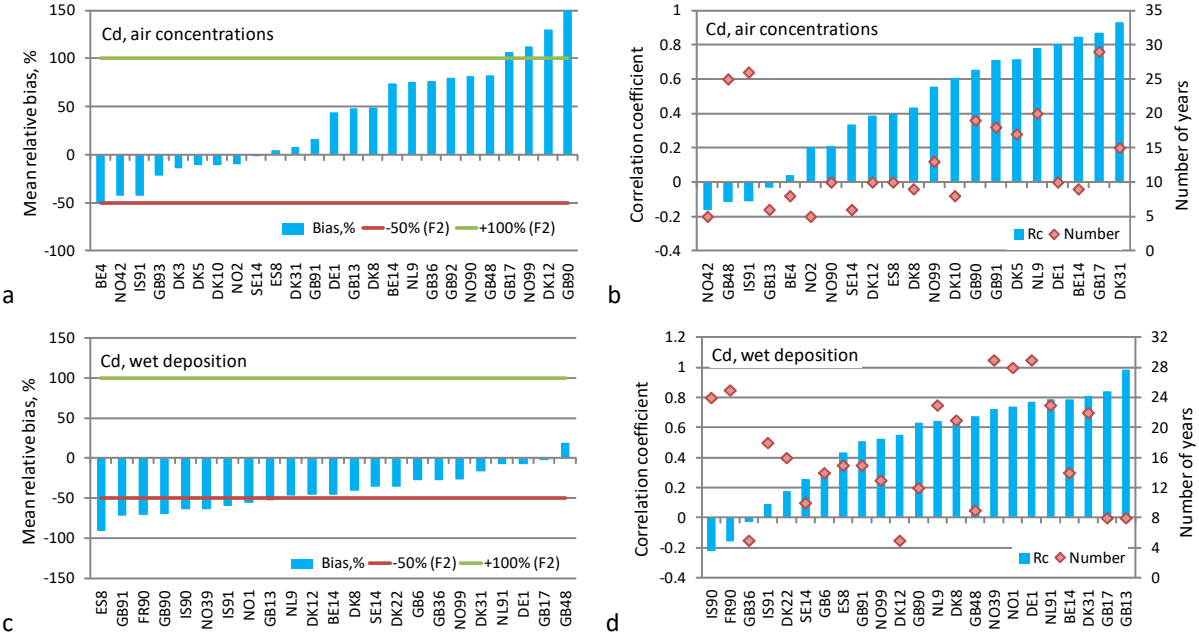

a b c d

Figure 26. *Mean Relative Bias (a, c) and temporal correlation coefficient (b, d) for annual mean concentrations in air and annual sums of wet deposition of Cd for 1990-2019. Green and red lines in diagrams (a) and (c) mean factor of two limits.*

The temporal correlation coefficients for air concentrations and wet deposition fluxes are higher than 0.5 at about one half of the stations. It is important to mention that the Pearson's correlation coefficient is very sensitive to outliers, and low correlations are often noted for short time series. For some stations with relatively long periods of observations low correlations are explained by very high inter-annual variability of the observed level. Examples are wet deposition fluxes at stations FR90, IS90, GB91 etc. (Annex C).

Similar to Pb, at some stations (e.g., GB90) overestimation of air concentrations and underestimation of wet deposition fluxes occurs, especially, in the beginning of the considered period (Fig. 27). The overestimation of the modelled air concentrations can be caused by overprediction of wind re-suspension. However, even in this case measured wet deposition remains underestimated by the model. It could be explained by a number of factors including of parametrization of wet scavenging, contamination of measurement samples and uncertainties of emission estimates.

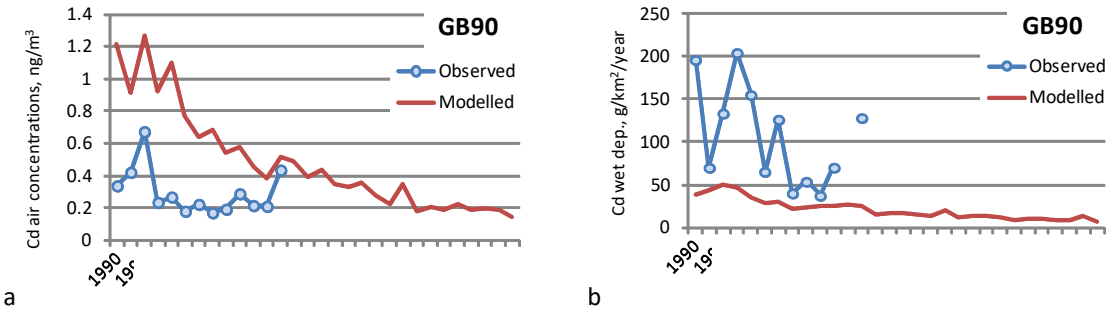

Figure 27. *Modelled and observed annual mean concentrations of Cd in air (a) and annual sum of wet deposition flux (b) in the period 1990-2019 at station GB90 (East Ruston, the United Kingdom).*

There are eight stations measuring Cd in air and thirteen stations measuring wet deposition with long enough (15 year or more) time series used for calculation of the mean rates of long-term pollution reduction (Fig. 28). For stations BE14, DE1 and GB91, the modelled and observed rates of long-term reduction are comparable. The stations NO42 and IS91 are located far from main emission sources, and modelled concentrations at these stations do not exhibit any long-term tendency. However, the observed concentrations at these stations demonstrate high inter-annual variability, especially in the first half of the considered period that results in 3% mean annual decline. Observed concentrations at station ES8 have been declining until 2010, and since this year increasing trend occurs, while the modelled concentrations have been reducing through the whole period. Difference in trend directions after 2010 led to different mean annual rates of concentration decline. The reduction rates of modelled and observed long-term change are similar at most of the stations measuring wet deposition fluxes. Large differences in the rates are typically noted for stations with high inter-annual variability of observed Cd fluxes (e.g., FR90, IS90).

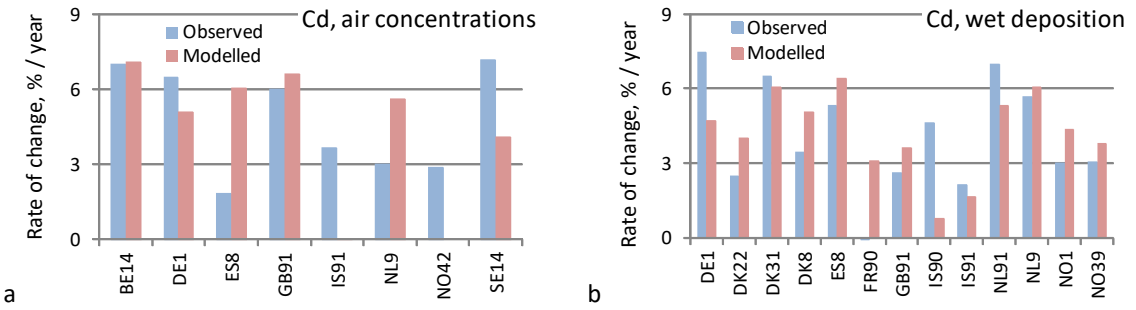

Figure 28. *Mean rate of annual relative change of modelled and observed Cd concentrations in air (a) and wet deposition fluxes (b).*

5.3. Mercury

Figure 29 demonstrates examples of modelled and measured Hg concentrations in air and wet deposition fluxes. High concentrations in air of Hg are noted in 1990 - 1993 at station SE2 (Rörvik, Sweden) which were underestimated by the model by 20-40%, while after 2000 the bias is typically within ±7%. The bias for wet deposition flux at station NL91 (De Zilk, the Netherlands) is within ±30% with exception of 1996 and 2004.

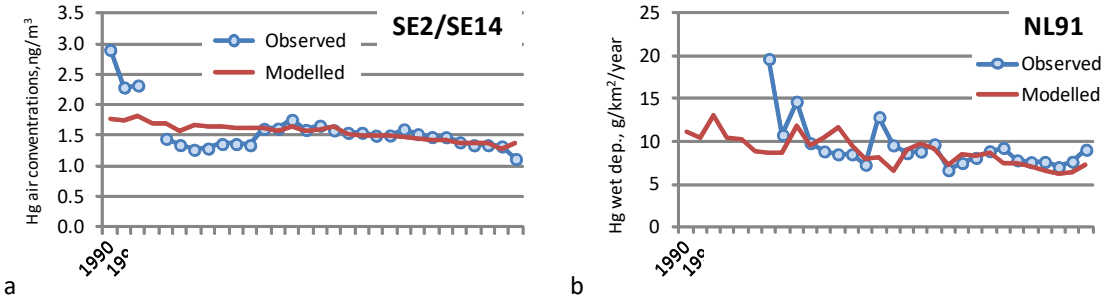

Figure 29. *Modelled and observed annual mean concentrations of Hg in air at station SE2/SE14 (Rörvik/Råö, Sweden) (a) and annual sum of wet deposition flux at station NL91 (De Zilk, the Netherlands) (b) in the period 1990-2019.*

There is a number of stations where period of available measurements is relatively short. However, the temporal changes were reproduced by the model quite well. For example, modelled wet deposition fluxes at station GB17 (Heigham Holmes, the United Kingdom) match the observed fluxes with bias that is below 30% for the period 2011-2019 (Fig. 30a). Another example is Norwegian station NO1 (Birkenes), where the model also reproduced inter-annual variability of the observed Hg wet deposition flux in the period from 2004 to 2019 (Fig. 30b). The observed fluxes in the first several years of the period were underestimated but between 2011 and 2018 the bias between modelled and observed concentrations is smaller than 20%.

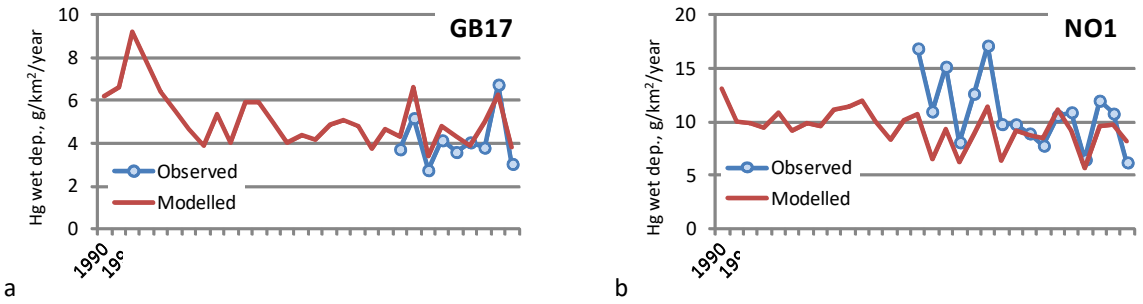

a b

Figure 30. *Modelled and observed annual sum of wet deposition flux of Hg at station GB17 (Heigham Holmes, the United Kingdom) (a) and NO1 (Birkenes, Norway) (b) in the period 1990-2019.*

Long-term time series are also available for Hg concentrations in air at station NO42 (Zeppelin, Norway) and Hg wet deposition flux at station DE1 (Westerland, Germany). Long-term changes of modelled Hg air concentrations at NO42 generally follow the observed Hg levels, except for 1997 and 1999 (Fig. 31a). However, the bias between modelled and observed concentrations tends to increase towards the end of the considered period. Measured Hg deposition fluxes at DE1 are available for two parts of the considered period: from 1993 to 2001 and from 2000 to 2019 (Fig. 31b). The model performance for these two parts differs. The first part is characterized by low mean bias (about 4%) and lack of correlation, while for the second part the correlation is high, but the model overestimates the observations almost two-fold.

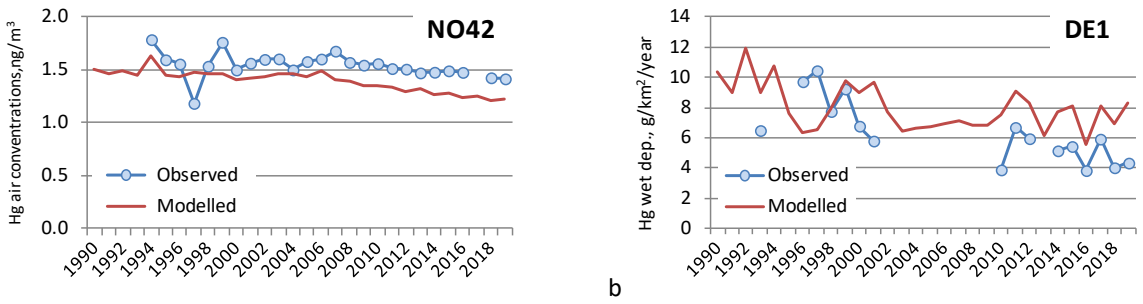

a b

Figure 31. *Modelled and observed annual mean concentrations of Hg in air at station NO42 (Zeppelin, Norway) (a) and annual sum of wet deposition flux at station DE1 (Westerland, Germany) (b) in the period from 1990 to 2019.*

Mean relative bias between modelled and observed air concentrations calculated for the whole period varies from -15% to almost 20%. The bias of wet deposition fluxes ranges from -50% (ES8) to 90% (GB48) but for the majority of stations it lies within ±40%. Considerable mean underestimation of Hg wet deposition at the Spanish station ES8 comes from high temporal variability of the observed fluxes (Annex C). In 2009-2011 the bias does not exceed -20%, while in other years it reaches -70%. At the British station GB48 the model overpredicts the observed fluxes by factor 1.4 – 3.3 throughout the considered period. Nevertheless, mean relative bias for all the stations corresponds to deviations within a factor of two. The coefficient of correlation between modelled and observed values is above 0.5 for about half of stations measuring Hg air concentrations or wet deposition (Fig. 32 b,d).

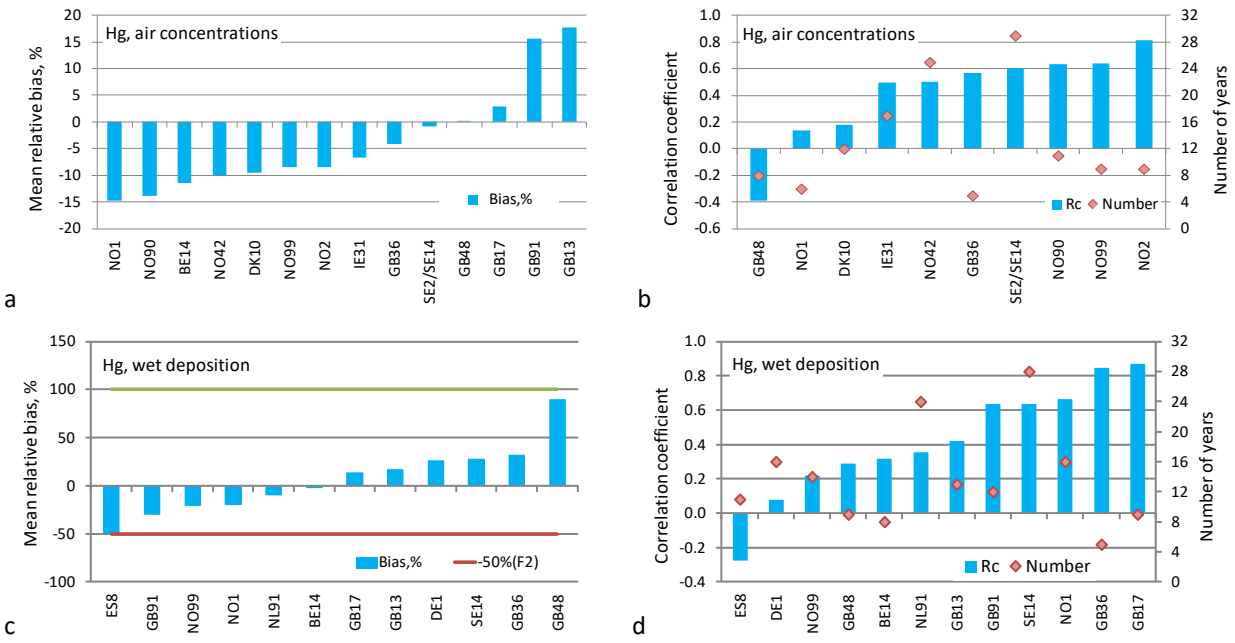

Figure 32. *Mean Relative Bias (a, c) and temporal correlation coefficient (b, d) for annual mean concentrations in air and annual sums of wet deposition of Hg for 1990-2019. Green and red lines in diagram (c) mean factor of two limits.*

Number of stations measuring Hg levels is lower, and their time series are shorter compared to those for Cd and Pb. There are only three stations measuring Hg concentration in air and two stations measuring wet deposition fluxes with long enough time series for calculation of the mean reduction rate (Fig. 33). The limited number of available stations is not sufficient for statistical characterizing agreement between the modelled and observed rates of long-term changes of the Hg pollution levels. The remote station NO42 (Zeppelin, Spitsbergen, Norway) is located far from the main regional anthropogenic sources. Hg levels at this station are mainly governed by global Hg emission sources. Both the model and observations demonstrate low (< 1% per year) rate of long-term decline of Hg concentrations in air. Similar rates of annual changes (about 1% per year) are noted for the Irish station IE31 (Mace Head). The higher rate of long-term reduction of observed air concentrations in comparison with modelled concentrations at stations SE2/SE14 is caused by high Hg concentrations (2.3-2.9 ng/m^3) at the very beginning (1990-1992) of the period .

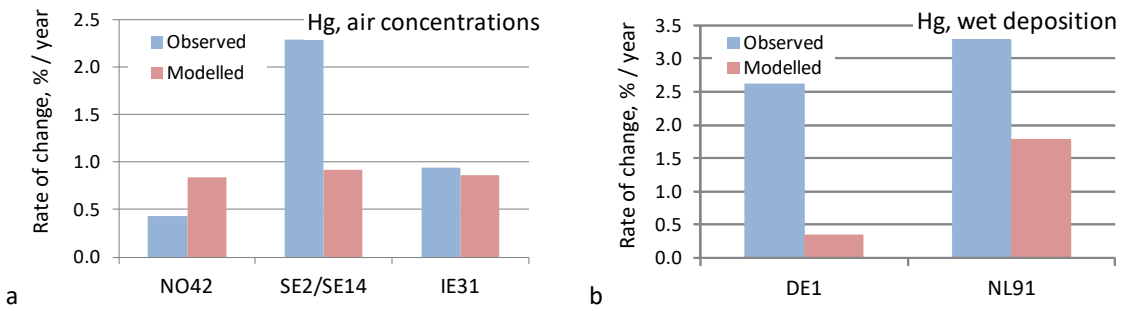

Figure 33. *Mean rate of annual relative change of modelled and observed Hg concentrations in air (a) and wet deposition fluxes (b).*

Similarly, a single high annual observation of Hg wet deposition (20 ng/km^2/y) in the first year of the time-series is responsible for discrepancies between measured and simulated reduction rates of wet deposition at station NL91 (Fig. 29b). The model reasonably well reproduces observed Hg wet deposition levels at station DE1 (Westerland, Germany) at the beginning of the period but tends to overestimate measurement values at the end. It leads to large underestimation of the mean reduction rate.

5.4. Uncertainties

Comparison of the modelled air concentrations and wet deposition fluxes of Pb, Cd and Hg with available measurements from the CAMP programme revealed a number of discrepancies. The factors responsible for the discrepancies can be divided into three groups: 1) uncertainties of anthropogenic emission data and estimates of secondary emissions; 2) uncertainties of the model parameterisations and other input data for modelling (e.g. meteorological fields, land cover distribution, etc.) and 3) uncertainties of measurement data.

According to officially reported information (Chapter 3), uncertainties of national total emissions of Pb, Cd and Hg may reach tens or even hundreds percents. For instance, uncertainties of Danish Pb and Cd emissions estimates make up about 500% and 365%, respectively. These uncertainties can favour over- or underprediction of the observed concentrations and wet deposition by the model. Moreover, uncertainties of other parameters related to emissions (e.g. spatial distribution, seasonal variation, and emission heights, chemical speciation of Hg emissions), which are not or partly reported by the countries, can also contribute to the overall uncertainty of the modelling results.

Model calculations entirely based on anthropogenic emissions of heavy metals lead to substantial underestimation of the observed concentrations in air and wet deposition at almost all EMEP stations. Therefore, secondary emissions, such as natural/legacy emission of Hg and wind re-suspension of Pb and Cd are important component of heavy metal releases to the atmosphere favouring generally better reproduction of the pollution levels by the model. However, estimates of secondary emissions also a subject to high uncertainties.

Uncertainties of the model parameterizations and input data is another possible source of discrepancies between the modelling results and observations. Parameterizations of many physical and chemical processes used in GLEMOS were developed and verified for the EMEP operational modelling of heavy metals [*Travnikov and Ilyin*, 2005] and updated in further versions of the model [**Error! Hyperlink reference not valid.**., 2009, **Error! Hyperlink reference not valid.**, 2011, **Error! Hyperlink reference not valid.**, *Ilyin et al*. 2018; *Gusev et al.*, 2019]. The model parameterizations were verified in a number of intercomparison campaigns [*Gusev et al*., 2000; *Ryaboshapko et al.,* 2001, 2005] and the thorough model review under supervision of the EMEP Task Force of Measurements and Modelling (TFMM) [*ECE/EB.AIR/GE.1/2006/4*]. It was concluded that the results of model were in satisfactory agreement with the available measurements and discrepancies did not exceed on average a factor of two. In addition, the GELMOS modelling system was extensively evaluated in a number of numerical experiments and multi-model studies within the Task Force on Hemispheric Transport of Air Pollution (TF HTAP). The model performance in simulation of Hg

pollution on a global scale was also tested in the multi-model assessments within the Global Mercury Observation System (GMOS) project [*Travnikov et al.*, 2017] and the Global Mercury Assessment 2018 [*AMAP/UN Environment*, 2019].

Uncertainties of measurement data can also affect the interpretation of the model evaluation results. Currently quality of Pb and Cd monitoring data at the EMEP stations (including those reporting to the CAMP programme) is examined via laboratory intercomparison tests. This activity is carried out annually and coordinated by CCC. The tests show that for most of the EMEP laboratories the deviation from theoretical value is below 25% for low concentration samples [*CCC*, 2021]. However, it is important to mention that laboratory intercomparison provides only analytical component of the uncertainties of measurement data. Other sources of the uncertainties (sampling, storing, shipping etc.) remain unaccounted. Laboratory intercomparison tests do not include analysis of quality of Hg measurements. The most recent field intercomparison of Hg measurements in air and precipitation took place in 2004 [*Aas*, 2006]. It was shown that concentrations of Hg in air measured by various monitoring groups are comparable, while for concentrations in precipitation the deviation from the assigned (expected) value is within ±40%.

6. Comparison with previous studies

Modelled atmospheric inputs to the regions of the OSPAR maritime area presented in this study are compared with the previous results reported in [*OSPAR*, 2009]. Since previous estimates of Pb, Cd and Hg deposition to the OSPAR regions cover the period from 1990 to 2006, the comparison was made for this range of years.

The difference between the modelled deposition to the OSPAR maritime area reported in [*OSPAR*, 2009] and obtained in the current study are caused by a number of factors. First of all, national emission data are regularly re-calculated. Besides, transition of the EMEP operational modelling to the new EMEP grid (ECE/EB.AIR/113/Add.1) was accompanied by changes in the model parameterizations and input data. It led to replacement of previous version of operational MSCE-HM model by the new Global EMEP Multi-media Modelling System (GLEMOS) [*Travnikov et al.*, 2009; *Travnikov and Jonson*, 2011]. The main updates are as follows:

- Meteorological preprocessor used for generation of gridded input meteorological data has changed from MM5 [*Grell et al*., 1995] to WRF [*Skamarock et al*., 2008];
- Use of up-to-date land-cover dataset based on the MODIS global satellite observations [*Strahler* et al., 1999];
- Revision of the model processing of anthropogenic emissions data (seasonal variation, vertical distribution and chemical speciation) [*Ilyin et al*., 2018];
- Update of the model parameterization of wind re-suspension of Pb and Cd from soils [*Ilyin et al.*, 2017];
- Refinement of Hg atmospheric chemistry scheme [*Shatalov et al.*, 2013; *Ilyin et al*., 2018; *Gusev et al.*, 2019].

Two statistical parameters were selected for comparison of the modelling results obtained in the previous assessment [*OSPAR*, 2009] and this study. The first parameter is deposition flux to each of five OSPAR regions averaged for 1990-2006. This parameter indicates whether the currently calculated deposition is generally higher or lower than that obtained previously. Another parameter is the mean rate of relative deposition change (percents per year). The aim of this parameter is to compare rates of deposition changes calculated in the previous and current studies.

Compared to the previous study, mean deposition in the considered period decreased in most of the OSPAR regions by 10 – 30% (Fig. 34 a,c,e). The main factors responsible for these changes are re-calculations of anthropogenic emissions by the EMEP countries and changes in annual sums of precipitation due to updates of meteorological pre-processor. In the Arctic waters (Region I) the changes of Pb and Cd deposition are the lowest. This region is remote from the main sources and its northern part is characterized by relatively low precipitation sums. In contrast to Pb and Cd, deposition of Hg to the Region I increased by about 45% compared to the previous study. The main reason for this is improvements of Hg atmospheric chemistry scheme, in particular, the parameterization of Hg oxidation during the atmospheric depletion events in the Arctic.

Rate of Pb and Cd deposition change obtained in this study is 10 – 80% higher compared to the previous study (Fig. 34b,d). It means that the current study assumes sharper decrease of deposition than that in [*OSPAR*, 2009]. The possible reasons of this faster decline are recalculations of long-term emission changes by the countries and update of the wind re-suspension scheme. Besides, the important anthropogenic contributor to Pb and Cd deposition to the OSPAR regions is emission from non-OSPAR countries. Comparison of emission trends used in this and previous studies reveals that sum of non-OSPAR emissions in the current study decreases faster by a factor of 1.3 than that used in previous study. In case of mercury the mean rates of deposition change in this and previous studies are comparable (Fig. 34f).

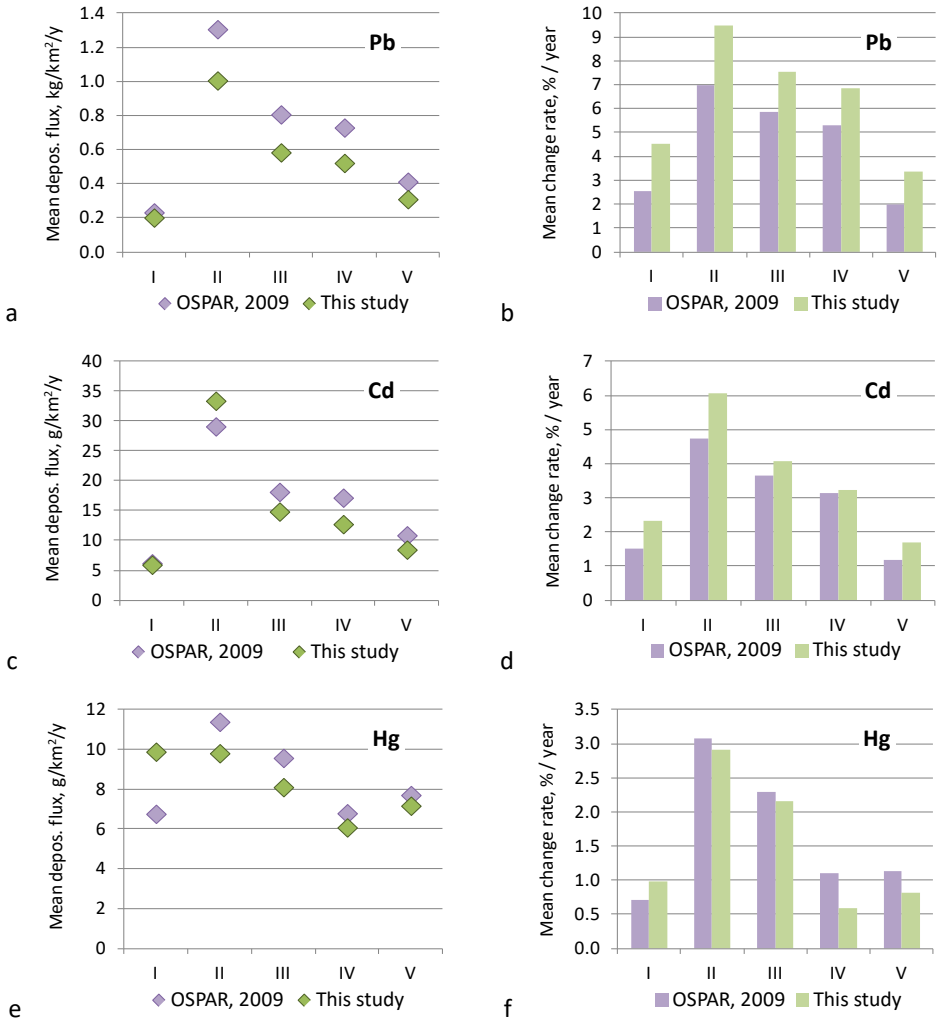

Figure 34. *Mean modelled deposition flux of Pb (a), Cd(c) and Hg (e) and mean rate of long-term change of Pb(b), Cd(d) and Hg(f) deposition to the OSPAR regions for the period from 1990 to 2006 presented in [OSPAR, 2009] and calculated in this study.*

7. Conclusions

Model assessment of heavy metal atmospheric input to the OSPAR maritime area was carried out for the period from 1990 to 2019. Long-term changes of national emissions of the OSPAR Contracting Parties and deposition of Pb, Cd and Hg to the five OSPAR maritime regions were estimated for the whole period. Contributions of national emissions of the OSPAR countries to total deposition were calculated for 1995, 2005 and 2015. The modelling results were evaluated against measurement data and compared with results of a previous study. The main findings of the research are summarized below.

- Emissions of Pb, Cd and Hg in the OSPAR Contracting Parties were reduced over the period 1990-2019 by 96%, 73%, and 83%, respectively. The most significant emissions reduction occurred in the first third of the period. Among the OSPAR Contracting Parties the largest reduction of Pb emissions took place in France (98%), Sweden (98%) and the United Kingdom (97%), whereas Pb emissions in Iceland increased by 77%. The strongest decline of Cd emissions occurred in Finland (88%) followed by France (87%). Mercury emissions the most significantly decreased in Denmark (93%) and the United Kingdom (90%).

- Deposition of the considered heavy metals to the OSPAR maritime area considerably decreased in the period from 1990 to 2019, following the emission reduction. The largest deposition decline was found for (Greater North Sea), where the deposition decreased by 87%, 80% and 45% for Pb, Cd and Hg, respectively. The lowest deposition reduction of heavy metals was estimated for the Arctic Waters and the Wider Atlantic, where deposition decline amounted to about 55 – 60% for Pb, about 35 – 40% for Cd, and below 25% for Hg. The decline of deposition to the OSPAR regions is lower than the emission reduction because of the effect of secondary and global sources.

- The largest contribution of the OSPAR Contracting Parties to atmospheric deposition of heavy metals is estimated for the Greater North Sea (Region II), while the lowest – to the Arctic Waters (Region I) and the Wider Atlantic (Region V). The major contributors to the Regions I, II, III are the United Kingdom, France and Germany, whereas the Regions IV and V are mostly affected by Spain, Portugal, France and the United Kingdom. Due to reduction of anthropogenic emissions contribution of the total deposition declined markedly from 1995 to 2005, and insignificantly decreased from 2005 to 2015.

- Modelled air concentrations and wet deposition Pb and Cd agree with observations from the CAMP monitoring programme within a factor of two at most of monitoring stations. However the model tends to somewhat underestimate wet deposition fluxes. Most of the modelled and observed wet deposition fluxes of Hg agree within ±40%. Higher discrepancies between the modelled and observed Pb, Cd, and Hg values for the first third (1990-2000) of the period are likely caused by uncertainties of measurements. At most of stations with a long monitoring period both modelled and observed air concentrations and wet deposition fluxes demonstrate declining trend.

- Heavy metal deposition to the OSPAR maritime area produced in this study was compared with the results of the previous OSPAR assessment covering period from 1990 to 2006 [*OSPAR*, 2009]. The model estimates were revised due re-calculation of national emissions by the EMEP countries, updates of meteorological and other input data as well as refinement of the model parameterizations. The new modelling results show 10-30% lower average deposition of all three heavy metals to most of the OSPAR regions. The new results also demonstrate somewhat higher reduction rates for Pb and Cd deposition, whereas the slopes of Hg deposition trends changed insignificantly.

References

Aas W. (ed) [2006] Data quality 2004, quality assurance, and field comparisons. EMEP/CCC-Report 4/2006, 95 p.

AMAP [2010] Updating Historical Global Inventories of Anthropogenic Mercury Emissions to Air. AMAP Technical Report No. 3. Arctic Monitoring and Assessment Programme (https://oaarchive.arctic-council.org/handle/11374/741).

AMAP [2011]. AMAP Assessment 2011: Mercury in the Arctic. Arctic Monitoring and Assessment Programme (AMAP), Oslo, Norway. xiv + 193 pp. (https://www.amap.no/documents/doc/amap-assessment-2011-mercury-in-the-arctic/90).

AMAP/UNEP [2013] Technical Background Report for the Global Mercury Assessment 2013. Arctic Monitoring and Assessment Programme, Oslo, Norway / UNEP Chemicals Branch, Geneva, Switzerland. vi + 263 pp. (http://www.amap.no/documents/download/1265).

AMAP/UN Environment [2019] Technical Background Report for the Global Mercury Assessment 2018. Arctic Monitoring and Assessment Programme, Oslo, Norway/UN Environment Programme, Chemicals and Health Branch, Geneva, Switzerland. viii + 426 pp including E-Annexes.

Bain L., Engelhardt M. [1992] Introduction to probability and mathematical statistics. 2nd ed., Duxbury.

CCC [2021] EMEP laboratory intercomparison. Heavy metals in precipitation 2020 - % deviation from expected value. https://projects.nilu.no/ccc/intercomparison/index.html. Site visited 09.06.2021.

Colette A., Aas W., Banin L., Braban C.F., Ferm M., González Ortiz A., Ilyin I., Mar K., Pandolfi M., Putaud J.-P., Shatalov V., Solberg S., Spindler G., Tarasova O., Vana M., Adani M., Almodovar P., Berton E., Bessagnet B., Bohlin-Nizzetto P., Boruvkova J., Breivik K., Briganti G., Cappelletti A., Cuvelier K., Derwent R., D'Isidoro M., Fagerli H., Funk C., Garcia Vivanco M., González Ortiz A., Haeuber R., Hueglin C., Jenkins S., Kerr J., de Leeuw F., Lynch J., Manders A., Mircea M., Pay M.T., Pritula D., Putaud J.-P., Querol X., RaffortV., Reiss I., Roustan Y., Sauvage S., Scavo K., Simpson D., Smith R.I., Tang Y.S., Theobald M., Tørseth K., Tsyro S., van Pul A., Vidic S., Wallasch M., Wind P. [2016]. Air pollution trends in the EMEP region between 1990 and 2012. Joint Report of the EMEP Task Force on Measurements and Modelling (TFMM), Chemical Co-ordinating Centre (CCC), Meteorological Synthesizing Centre-East (MSC-E), Meteorological Synthesizing Centre-West (MSC-W) EMEP: CCC-Report 1/2016. 105 p. Available at https://projects.nilu.no/ccc/reports.html.

Crippa M., Solazzo E., Huang G., Guizzardi D., Koffi E., Muntean M., Schieberle C., Friedrich R. and Janssens-Maenhout G. [2019]. High resolution temporal profiles in the Emissions Database for Global Atmospheric Research. Scientific Data, (2020) 7:121, https://doi.org/10.1038/s41597-020-0462-2.

ECMWF [2021] Operational archive. https://www.ecmwf.int/en/forecasts/dataset/operational-archive. Accessed 13.07.2021

EDGAR [2021]. Emissions Database for Global Atmospheric Research. https://edgar.jrc.ec.europa.eu/emissions_data_and_maps. Visited 06.10.2021.

Emmons L.K., Walters S., Hess P.G., Lamarque J.-F., Pfister G.G., Fillmore D., Granier C., Guenther A., Kinnison D., Laepple T., Orlando J., Tie X., Tyndall G., Wiedinmyer C., Baughcum S.L., and Kloster S. [2010] Description and evaluation of the Model for Ozone and Related chemical Tracers, version 4 (MOZART-4), *Geosci. Model Dev.*, 3, 43–67, doi:10.5194/gmd-3-43-2010.

Ferrari C. P. et al. [2008] Atmospheric mercury depletion event study in Ny-Alesund (Svalbard) in spring 2005. Deposition and transformation of Hg in surface snow during springtime. Sci. Total Environ. 397, 167–177.

Grell G., Dudhia J. and Stauffer D. [1995] A Description of the Fifth Generation Penn State/NCAR Mesoscale Model (MM5). NCAR Tech. Note, TN-398+STR, p.117.

Gusev A., I. Ilyin, V. Shatalov, O. Travnikov, N. Batrakova, O. Rozovskaya, I. Strijkina, K.Brevik, Nizzetto P.B., W. Aas, K. Mareckova, S. Poupa, C. Sosa, M. Tista, R. Wankmueller, F. Couvidat [2019] Assessment of transboundary pollution by toxic substances: Heavy metals and POPs. EMEP Status Report 2/2019.

Gusev A., Ilyin I., Mantseva L., Rozovskaya O., Shatalov V. and Travnikov O. [2006]. Progress in further development of MSCE-HM and MSCE-POP models (implementation of the model review recommendations). EMEP/MSC-E Technical Report 4/2006.

Gusev A., Ilyin I., Petersen G., van Pul A. and Syrakov D. [2000] Long-range transport model intercomparison studies. Model intercomparison study for cadmium. EMEP/ESC-E Report 2/2000, Meteorological Synthesizing Centre – East, Moscow, Russia. (http://www.msceast.org/reports/2_2000.pdf)

Gusev A., O.Rozovskaya, V. Shatalov [2007] Modelling POP long-range transport and contamination levels by MSCE-POP model. EMEP/MSC-E Technical Report 1/2007.

Ilyin I., Rozovskaya O., Travnikov O. and Aas W. [2017] Assessment of heavy metal transboundary pollution on regional and national scales, transition to the new EMEP grid. EMEP Status Report 2/2017, 95 p.

Ilyin I., Rozovskaya O., Travnikov O., Aas W. and Pfaffhuber K.A. [2018] Assessment of heavy metal transboundary pollution on global, regional and national scales. EMEP Status Report 2/2018. 70 p.

Ilyin I., Travnikov O., Schütze G., Feigenspan S. and Uhse K. [2020]. Country-scale assessment of heavy metal pollution: A case study for Germany. MSC-E Technical Report 1/2020. 119 p.

Johnson K. P., Blum J. D., Keeler G. J. and Douglas T. A. [2008] Investigation of the deposition and emission of mercury in arctic snow during an atmospheric mercury depletion event. J. Geophys. Res. Atmos. 113, D17304.

Kirk J. L., St Louis V. L. and Sharp M. J., [2006] Rapid reduction and reemission of mercury deposited into snowpacks during atmospheric mercury depletion events at Churchill, Manitoba, Canada. Environ. Sci. Technol. 40, 7590–7596.

Moore C.W. et al. [2014] Convective forcing of mercury and ozone in the Arctic boundary layer induced by leads in sea ice. Nature 506, 81-84.

OSPAR [2009] Trends in atmospheric concentrations and deposition of nitrogen and selected hazardous substances to the OSPAR maritime area. Monitoring and Assessment Series. OSPAR Commission. Available at https://www.ospar.org/about/publications/page21.

OSPAR [2017] Intermediate Assessment 2017. Available at: https://oap.ospar.org/en/ospar-assessments/intermediate-assessment-2017.

Pacyna J. M., Scholtz M. T. and Y.-F. Li [1995]. Global Budgets of Trace Metal Sources, Environmental Reviews, 3, 145-159.

Richardson G.M., Garret R., Mitchell I., Mah-Paulson M. and T.Hackbarth [2001] Critical Review of natural global and regional emissions of six trace metals to the atmosphere. Final Report. Risklogic Scientific Services, Inc, 52p.+tables.

Ryaboshapko A., Artz R., Bullock R., Christensen J., Cohen M., Draxler R., Ilyin I., Munthe J., Pacyna J., Petersen G., Syrakov D., and Travnikov O. [2005] Itercopmparison study of numerical models for long-range atmospheric transport of mercury. Stage III. Comparison of modelling results with long-term observations and comparison of calculated itens of regional balances. EMEP/MSC-E Technical Report 1/2005, Meteorological Synthesizing Centre – East, Moscow, Russia. (http://www.msceast.org/reports/1_2005.pdf)

Ryaboshapko A., Ilyin I., Bullock R., Ebinghaus R., Lohman K., Munthe J., Petersen G., Seigneur C., Wangberg I. [2001] Intercomparison study of numerical models for long-range atmospheric transport of mercury. Stage I: Comparison of chemical modules for mercury transformations in a cloud/fog environment. EMEP/MSC-E Technical report 2/2001, Meteorological Synthesizing Centre – East, Moscow, Russia. (http://www.msceast.org/reports/2_2001.pdf)

Salminen R. (Chief-editor) [2005]. Geochemical Atlas of Europe. Part 1 - Background Information, Methodology and Maps. A contribution to IUGS/IAGC Global Geochemical Baselines. ISBN 951-690-913-2 (electronic version). http://weppi.gtk.fi/publ/foregsatlas/index.php.

Shatalov V., Ilyin I., Gusev A., Rozovskaya O., Sokovykh V., Travnikov O. EMEP/MSC-E [2013] Heavy Metals and Persistent Organic Pollutants: Model Assessment of Pollution and Research Activities. Technical report 1/2013.

Skamarock W.C., Klemp J.B., Dudhia J., Gill D.O., Barker D.M., Duda M.G., Huang X-Y., Wang W. and Powers J.G. [2008]. A Description of the Advanced Research WRF Version 3. NCAR/TN–475+STR NCAR TECHNICAL NOTE.

Skamarock W.C., Klemp J.B., Dudhia J., Gill D.O., Barker D.M., Duda M.G., Huang X-Y., Wang W. and Powers J.G. [2008]. A Description of the Advanced Research WRF Version 3. NCAR/TN–475+STR NCAR TECHNICAL NOTE.

Steffen A. et al. [2008] A synthesis of atmospheric mercury depletion event chemistry in the atmosphere and snow. Atmos. Chem. Phys. 8, 1445-1482.

Strahler A., Muchoney D., Borak J., Friedl, M., Gopal S., Lambin E. and Moody A. [1999]. MODIS Land Cover Product. Algorithm Theoretical Basis Document (ATBD) Version 5.0. MODIS Land Cover and Land-Cover Change. Center for Remote Sensing, Department of Geography, Boston University, Boston, MA, 66 p.

Tian H. Z., Zhu C. Y., Gao J. J., Cheng K., Hao J. M., Wang K., Hua S. B., Wang Y. and Zhou J. R. [2015]. Quantitative assessment of atmospheric emissions of toxic heavy metals from anthropogenic sources in China: historical trend, spatial distribution, uncertainties, and control policies. Atmos. Chem. Phys., 15, 10127–10147.

Tista M., Matthews B. and R.Wankmueller [2019] Methodologies applied to the CEIP GNFR gap-filling 2019. Part II: Heavy Metals (Pb, Cd, Hg) of the year 2017. Technical report CEIP 2/2019.

Travnikov O. [2000] Uncertainty analysis of heavy metals long-range transport modelling. EMEP/MSC-E Technical note 9/2000, Meteorological Synthesizing Centre - East, Moscow, Russia. (http://www.msceast.org/reports/9_2000.pdf).

Travnikov O. and Ilyin I. [2009] "The EMEP/MSC-E mercury modeling system" in Mercury Fate and Transport in the Global Atmosphere, R. Mason, N. Pirrone, Eds. (Springer, Boston, MA, 2009), pp. 571–587.

Travnikov O. and Ilyin I. [2005] Regional Model MSCE-HM of Heavy Metal Transboundary Air Pollution in Europe. EMEP/MSC-E Technical Report 6/2005. (http://www.msceast.org/reports/6_2005.pdf).

Travnikov O. and J. E. Jonson (Eds.). [2011] Global scale modelling within EMEP: Progress report. EMEP/MSC-E Technical report 1/2011.

Travnikov O., J.E. Jonson, A.S Andersen, M. Gauss, A. Gusev, O. Rozovskaya, D. Simpson, V. Sokovyh, S. Valiyaveetil and P. Wind [2009] Development of the EMEP global modelling framework: Progress report. Joint MSC-E/MSC-W Report. EMEP/MSC-E Technical Report 7/2009.

Travnikov O. and Jonson J. E. (Eds.). [2011] Global scale modelling within EMEP: Progress report. EMEP/MSC-E Technical Report 1/2011.

Travnikov O., Angot H., Artaxo P., Bencardino M., Bieser J., D'Amore F., Dastoor A., De Simone F., Diéguez M. D. C., Dommergue A., Ebinghaus R., Feng X. B., Gencarelli C. N., Hedgecock I. M., Magand O., Martin L., Matthias V., Mashyanov N., Pirrone N., Ramachandran R., Read K. A., Ryjkov A., Selin N. E., Sena F., Song S., Sprovieri F., Wip D., Wängberg I., and Yang X. [2017] Multi-model study of mercury dispersion in the atmosphere: atmospheric processes and model evaluation, Atmos. Chem. Phys., 17, 5271-5295, doi:10.5194/acp-17-5271-2017.

Travnikov O., M.Kleimenov, A.Gusev [2001] Co-operative activities on Hg and POP pollution assessment within TF HTAP. Progress report. MSC-E Technical Report 1/2021.

UNECE [2012] 1998 Protocol on Heavy Metals, as amended on 13 December 2012. Executive Body for the Convention on Long-range Transboundary Air Pollution. 2012, http://www.unece.org/fileadmin/DAM/env/documents/2012/EB/ECE.EB.AIR.115_ENG.pdf.

UNEP [2010a]. Final review of scientific information on lead. UNITED NATIONS ENVIRONMENT PROGRAMME. Chemicals Branch, DTIE. 255 p. + annexes.

UNEP [2010b]. Final review of scientific information on cadmium. UNITED NATIONS ENVIRONMENT PROGRAMME. Chemicals Branch, DTIE. 201 p.+ annexes.

Wang S. et al. [2019] Direct detection of atmospheric atomic bromine leading to mercury and ozone depletion. PNAS 116, 14479.

Yang X., Cox R., Warwick N., Pyle J., Carver G., O'Connor F., and Savage N. [2005] Tropospheric bromine chemistry and its impacts on ozone: A model study, *J. Geophys. Res.,* 110, D23311, doi:10.1029/2005JD006244.

Yang X., Pyle J.A., Cox R.A., Theys N., and Van Roozendael M. [2010] Snow-sourced bromine and its implications for polar tropospheric ozone, *Atmos. Chem. Phys*., 10, 7763–7773, doi:10.5194/acp-10-7763-2010.

Zhu C., Tian H. and Hao J. [2020]. Global anthropogenic atmospheric emission inventory of twelve typical hazardous trace elements, 1995–2012. Atmospheric Environment 220 (2020) 117061.

Annex A. Assessment Elements

Table A.1. *Time-series of heavy metal depositions to all five OSPAR Regions*

#	**Work-plan elements**
1.	Preparatory work: adapting of software required for evaluation of deposition to the OSPAR region
2.	Preparation of time-series of total annual atmospheric deposition of Cd, Hg to the II, III, and IV OSPAR areas for the period from 1990-2018 (based on modelling made for HELCOM using standard EMEP grid, 0.4x0.4 degree resolution)
3.	Preparation of time-series of total annual atmospheric deposition of Cd, Hg to the I and V OSPAR areas for the period from 1990 -2018 (based on modelling made for HELCOM using global grid with 3x3 degree resolution)
4.	Calculation of time-series of total annual atmospheric deposition of Pb to the II, III, and IV OSPAR areas for the period 1990-2018 (modelling using standard EMEP grid, 0.4x0.4 degree resolution)
5.	Preparation of expert estimates of global Pb emissions for global modelling (1990-2018)
6.	Calculation of time-series of total annual atmospheric deposition of Pb to the I and V OSPAR areas for the period from 1990 -2018 (modelling using global grid with 3x3 degree resolution)
7.	Preparation of data on Cd, Hg and Pb deposition to all OSPAR areas for 2019 (based on regular EMEP modelling in 2021 on the standard EMEP grid, 0.4x0.4 degree resolution, and the global grid with 1x1 degree resolution)
8.	Time series of Total annual official emissions of Cd, Pb, and Hg from OSPAR countries for the period from 1990 to the latest available year (tables) – if necessary
9.	Producing EMEP report and supporting OSPAR's thematic report on inputs
	Due time (including S-R calculations described in Table 2)

Table A.2. *Evaluation of source-receptor (S-R) relationships*

#	**Work-plan elements for 3 years of data**
1.	Calculation of S-R matrices of Cd, Pb, Hg for the EMEP domain (0.4x0.4 degree) – for II, III, IV areas
2.	Calculation of S-R matrices of Cd, Pb, Hg for the global domain (3x3 degree) – for I and V areas
3.	Information on contributions (in %) of the OSPAR CPs to total annual depositions of Cd, Pb, and Hg to the 5 OSPAR areas

Annex B. Data Products

Table B.1. *Codes of countries used in this study*

Name	Code	Name	Code
Belgium	BE	**Netherlands**	NL
Denmark	DK	**Norway**	NO
Finland	FI	**Portugal**	PT
France	FR	**Spain**	ES
Germany	DE	**Sweden**	SE
Iceland	IS	**Switzerland**	CH
Ireland	IE	**United Kingdom**	GB
Luxembourg	LU		

Table B.2. *Annual **lead** emissions from the OSPAR Contracting Parties. Units: t/y .*

Pb, t	1990	1991	1992	1993	1994	1995	1996	1997	1998	1999	2000	2001	2002	2003	2004
Belgium	264	248	259	221	175	207	219	238	163	177	107	83.5	83.4	80.5	89.2
Denmark	130	109	100	58.8	26.4	26.0	24.9	23.0	25.0	31.6	19.6	18.7	18.1	19.1	21.1
Finland	321	237	165	105	73.9	72.7	49.2	31.8	37.2	34.8	30.6	30.4	30.7	24.9	26.5
France	4294	2887	2107	1852	1650	1476	1309	1159	1041	809	283	250	246	196	183
Germany	1919	1476	1150	967	776	716	578	451	403	393	401	362	341	310	298
Iceland	0.31	0.29	0.33	0.75	0.74	0.83	1.00	1.03	1.09	1.32	1.19	1.30	1.16	1.34	1.38
Ireland	158	142	150	130	113	98.4	82.8	87.1	59.1	34.8	14.2	12.7	11.7	11.7	11.9
Luxembourg	18.8	17.9	16.4	18.0	15.1	8.96	8.62	5.53	1.80	1.47	1.09	1.06	1.01	1.66	1.82
Netherlands	89.7	84.1	81.7	79.3	76.8	75.0	62.4	52.3	42.3	34	26.6	30.9	34.9	31.4	32.9
Norway	189	146	130	90.3	27.7	25.0	13.4	13.0	13.6	12.9	11.2	9.9	10.5	10.8	11.0
Portugal	575	631	708	751	775	796	327	335	347	351	43.7	41.8	42.1	42.0	42.8
Spain	2587	1711	1124	1017	1001	856	819	753	689	621	476	260	133	133	132
Sweden	354	309	288	138	46.5	32.2	27.9	28.2	27.2	25.1	21.9	20.3	17.4	17.4	16.5
Switzerland	379	350	320	263	232	169	145	131	89.3	52.9	30.8	28.1	24.9	22.1	21.6
United Kingdom	2921	2667	2446	2171	1872	1563	1327	1173	869	520	189	181	175	172	164
OSPAR	**14200**	**11015**	**9046**	**7863**	**6861**	**6123**	**4995**	**4482**	**3810**	**3101**	**1657**	**1331**	**1171**	**1073**	**1054**
Other	29072	25738	22347	21417	19297	17478	16101	14947	13878	12714	11192	9489	7863	7609	4290
EMEP	43272	36754	31393	29279	26158	23601	21097	19429	17688	15815	12848	10820	9033	8682	5344

Table B.2. (continued) *Annual **lead** emissions from the OSPAR Contracting Parties. Units: t/y .*

Pb, t	2005	2006	2007	2008	2009	2010	2011	2012	2013	2014	2015	2016	2017	2018	2019
Belgium	73.8	72.3	61.9	72.1	31.0	40.0	29.6	28.9	25.6	23.0	29.4	27.3	25.5	13.6	14.6
Denmark	17.4	16.3	13.9	14.0	13.1	12.8	12.5	12.1	12.2	11.6	11.9	12.1	12.1	12.5	12.0
Finland	21.4	24.9	21.8	19.8	16.8	20.4	19.2	16.3	16.0	16.6	14.7	15.7	15.6	15.4	13.2
France	179	171	167	152	126	138	127	128	124	120	114	114	115	114	84.8
Germany	269	257	241	214	188	212	207	202	200	201	209	203	211	207	161
Iceland	1.41	2.23	2.44	1.78	1.41	1.45	1.29	1.25	0.55	0.58	0.64	0.68	0.66	0.77	0.56
Ireland	8.05	7.60	7.47	7.39	6.60	6.24	5.76	5.67	5.74	5.47	5.51	5.36	5.06	5.10	4.80
Luxembourg	1.39	1.30	1.24	1.37	1.04	1.00	1.51	1.67	1.12	1.24	1.33	1.27	1.34	1.20	1.46
Netherlands	29.1	29.3	34.9	29.6	30.6	36.8	21.6	15.2	13.0	8.20	7.85	8.12	7.75	5.04	5.16

Norway	9.8	9.25	8.22	7.32	5.22	6.04	6.23	5.59	5.76	5.59	6.35	5.79	5.82	5.83	6.09
Portugal	42.5	43.4	44.0	43.7	40.4	40.5	40.6	40.5	40.0	40.4	39.9	39.5	40.1	43.0	25.3
Spain	130	131	132	126	112	117	96.4	88.0	94.6	95.4	94.2	90.0	86.6	89.9	98.5
Sweden	14.3	13.9	14.7	12.9	12.1	12.7	11.4	11.2	10.7	11.2	10.3	11.1	11.1	9.79	8.09
Switzerland	20.0	18.7	19.0	18.3	17.2	16.6	16.3	16.5	16.5	14.8	15.0	14.8	15.0	15.2	14.9
United Kingdom	155	136	124	115	101	102	101	105	98.9	107	106	96.5	95.6	92.8	92.6
OSPAR	**973**	**933**	**893**	**836**	**702**	**764**	**698**	**677**	**665**	**662**	**665**	**645**	**648**	**631**	**543**
Other	3913	3779	3706	3529	3081	3063	2838	2825	2678	2628	2564	2542	2577	2577	2394
EMEP	4886	4712	4600	4365	3783	3826	3536	3502	3343	3290	3230	3188	3225	3208	2937

Table B.3. *Annual* ***cadmium*** *emissions from the OSPAR Contracting Parties. Units: t/y.*

	1990	**1991**	**1992**	**1993**	**1994**	**1995**	**1996**	**1997**	**1998**	**1999**	**2000**	**2001**	**2002**	**2003**	**2004**	**2005**	**2006**
Belgium	6.25	6.03	6.78	5.60	4.09	5.10	4.18	4.35	2.41	2.36	2.78	2.49	2.35	2.45	2.87	2.15	2.32
Denmark	1.21	1.24	1.08	0.99	0.84	0.71	0.73	0.69	0.66	0.65	0.64	0.69	0.66	0.69	0.69	0.70	0.67
Finland	6.67	3.80	3.31	3.37	2.70	2.13	1.91	1.53	1.69	1.53	1.41	1.74	1.37	1.32	1.61	1.46	1.42
France	20.4	20.4	19.8	18.9	18.8	17.9	17.4	16.4	15.5	14.2	14.2	13.0	12.3	9.04	6.58	5.89	4.69
Germany	30.4	26.9	24.2	22.9	22.5	20.4	20.9	20.6	19.9	19.9	18.8	17.8	17.2	15.7	14.5	12.9	13.7
Iceland	0.01	0.01	0.01	0.02	0.02	0.03	0.03	0.03	0.03	0.03	0.03	0.03	0.03	0.03	0.03	0.03	0.05
Ireland	0.59	0.58	0.54	0.58	0.54	0.57	0.59	0.59	0.62	0.58	0.59	0.48	0.36	0.33	0.34	0.37	0.36
Luxembourg	0.09	0.09	0.09	0.09	0.09	0.07	0.08	0.07	0.06	0.06	0.06	0.06	0.07	0.07	0.14	0.08	0.08
Netherlands	2.08	1.78	1.60	1.42	1.23	1.06	0.94	1.03	1.12	0.93	0.92	1.60	2.17	2.32	1.73	1.67	1.93
Norway	1.66	1.53	1.40	1.54	1.52	1.30	1.40	1.34	1.40	1.32	1.05	0.97	0.94	0.90	0.83	0.78	0.82
Portugal	2.44	2.44	2.48	2.36	2.44	2.58	2.67	2.84	2.88	2.82	2.77	2.68	2.62	2.47	2.51	2.51	2.45
Spain	27.7	26.2	23.3	20.7	20.5	20.9	22.0	21.3	22.0	21.2	14.9	12.3	12.8	11.5	10.8	9.77	8.15
Sweden	2.31	1.74	1.37	1.08	0.77	0.75	0.71	0.71	0.63	0.54	0.52	0.60	0.52	0.52	0.54	0.54	0.56
Switzerland	3.68	3.47	3.30	3.09	2.85	2.49	2.37	2.19	1.92	1.65	1.47	1.32	1.14	1.03	1.03	1.04	1.05
United Kingdom	25.6	25.0	23.8	13.1	12.6	11.0	9.55	8.65	6.87	6.43	5.66	5.35	5.17	4.48	4.43	4.48	4.47
OSPAR	**131**	**121**	**113**	**95.8**	**91.5**	**86.9**	**85.4**	**82.4**	**77.7**	**74.2**	**65.8**	**61.1**	**59.7**	**52.9**	**48.6**	**44.4**	**42.7**
Other	277	252	244	223	216	213	200	195	187	181	175	172	161	197	171	180	178
EMEP	408	373	357	319	308	300	286	277	264	255	241	233	221	250	220	224	221

Table B.3. (continued) *Annual* ***cadmium*** *emissions from the OSPAR Contracting Parties. Units: t/y.*

	2007	**2008**	**2009**	**2010**	**2011**	**2012**	**2013**	**2014**	**2015**	**2016**	**2017**	**2018**	**2019**
Belgium	2.12	2.42	1.55	1.96	1.67	1.47	1.47	1.25	1.63	2.58	1.35	1.20	1.19
Denmark	0.75	0.73	0.70	0.72	0.68	0.66	0.68	0.67	0.74	0.76	0.78	0.80	0.71
Finland	1.26	1.21	1.16	1.29	1.22	1.17	1.08	0.92	0.89	0.94	0.96	0.88	0.79
France	4.33	4.37	3.31	3.34	3.10	2.95	3.03	3.18	2.94	3.39	3.11	2.64	2.62
Germany	13.2	12.1	10.9	13.3	13.3	13.0	13.0	12.7	13.1	12.8	13.1	12.7	10.8
Iceland	0.05	0.04	0.03	0.03	0.03	0.02	0.01	0.01	0.01	0.01	0.00	0.01	0.01
Ireland	0.34	0.33	0.31	0.30	0.28	0.29	0.28	0.30	0.31	0.30	0.30	0.28	0.25
Luxembourg	0.08	0.41	0.13	0.07	0.07	0.11	0.06	0.07	0.08	0.08	0.07	0.07	0.06
Netherlands	1.70	1.87	1.78	2.51	1.10	0.79	0.60	0.54	0.53	0.54	0.63	2.32	2.64
Norway	0.76	0.74	0.59	0.73	0.69	0.59	0.54	0.46	0.51	0.47	0.49	0.51	0.50
Portugal	2.36	2.33	2.17	2.14	2.21	2.12	2.04	2.03	2.07	1.99	2.04	2.04	1.83
Spain	6.78	6.17	5.30	5.31	5.92	5.01	5.03	4.79	5.02	4.75	4.86	4.90	7.36
Sweden	0.57	0.52	0.54	0.54	0.52	0.53	0.50	0.52	0.48	0.48	0.52	0.48	0.49
Switzerland	1.05	1.11	1.11	1.15	1.08	1.16	1.22	1.09	1.12	1.17	1.18	1.16	0.69
United Kingdom	3.68	3.59	3.43	3.77	3.93	3.53	3.66	4.10	3.92	3.68	3.88	4.05	5.59
OSPAR	**39.1**	**38.0**	**33.0**	**37.2**	**35.8**	**33.4**	**33.2**	**32.7**	**33.3**	**34.0**	**33.2**	**34.0**	**35.6**
Other	180	177.0	166.2	160.6	158.4	155.8	150.6	148.0	143.5	142.4	142.5	140.6	99.1
EMEP	219	214.9	199.2	197.8	194.3	189.1	183.8	180.6	176.9	176.4	175.7	174.7	134.7

Table B.4. *Annual* ***mercury*** *emissions from the OSPAR Contracting Parties. Units: t/y.*

	1990	1991	1992	1993	1994	1995	1996	1997	1998	1999	2000	2001	2002	2003	2004	2005	2006
Belgium	6.08	5.81	5.73	3.72	4.14	3.35	3.29	3.76	2.69	3.06	3.21	2.84	3.86	3.66	3.56	2.16	2.07
Denmark	3.16	3.28	3.00	2.93	2.54	2.32	2.46	1.98	1.68	1.48	1.00	0.87	0.84	0.87	0.73	0.69	0.61
Finland	1.08	0.93	0.89	0.76	0.80	0.80	0.86	0.80	0.69	0.63	0.60	0.68	0.67	0.82	0.75	0.89	1.03
France	25.6	26.1	24.8	22.8	22.3	21.1	20.1	15.9	14.3	12.8	12.3	10.9	9.93	7.29	6.94	7.25	7.07
Germany	35.4	29.9	25.3	22.6	21.3	20.2	19.7	19.4	19.0	18.2	18.2	17.6	16.6	15.9	15.2	14.0	13.4
Iceland	0.14	0.14	0.14	0.13	0.12	0.11	0.11	0.11	0.09	0.08	0.08	0.08	0.07	0.07	0.05	0.04	0.05
Ireland	0.83	0.81	0.73	0.74	0.68	0.67	0.70	0.66	0.46	0.41	0.44	0.44	0.42	0.43	0.43	0.45	0.43
Luxembourg	0.41	0.40	0.38	0.39	0.35	0.23	0.17	0.13	0.09	0.22	0.27	0.29	0.15	0.21	0.16	0.20	0.30
Netherlands	3.52	2.91	2.49	2.07	1.65	1.42	1.21	1.01	0.80	0.90	1.02	0.84	0.73	0.68	0.85	0.87	0.81
Norway	1.46	1.36	1.20	0.88	1.01	0.80	0.82	0.83	0.78	0.82	0.64	0.59	0.57	0.70	0.57	0.56	0.51
Portugal	2.20	2.24	2.26	2.21	2.32	2.46	2.55	2.82	2.63	2.58	2.37	2.08	2.02	1.91	1.96	1.84	1.83
Spain	10.6	10.8	11.6	10.2	10.4	12.8	10.6	9.80	10.3	10.9	8.83	7.82	8.72	7.42	7.31	7.31	6.49
Sweden	1.54	1.23	1.16	1.02	1.04	0.97	1.03	0.84	0.85	0.85	0.73	0.57	0.61	0.69	0.70	0.65	0.50
Switzerland	6.37	5.85	5.54	5.15	4.72	3.89	3.61	3.35	2.55	2.29	1.77	1.44	1.05	0.72	0.74	0.76	0.79
United Kingdom	38.2	38.4	36.6	22.1	20.8	20.2	14.9	11.6	10.7	8.36	8.33	8.17	7.24	7.58	6.81	7.51	7.55
OSPAR	**137**	**130**	**122**	**97.7**	**94.2**	**91.3**	**82.1**	**73.0**	**67.6**	**63.6**	**59.8**	**55.2**	**53.5**	**49.0**	**46.8**	**45.1**	**43.4**
Other	180	172	162	159	155	154	152	149	146	142	143	141	122	151	126	128	138
EMEP	317	302	284	256	249	245	234	222	213	206	202	197	176	200	173	173	182

Table B.4. (continued) *Annual* ***mercury*** *emissions from the OSPAR Contracting Parties. Units: t/y.*

	2007	2008	2009	2010	2011	2012	2013	2014	2015	2016	2017	2018	2019
Belgium	3.19	3.61	1.74	1.74	1.68	1.30	1.39	1.52	1.08	1.38	1.05	1.37	1.03
Denmark	0.59	0.59	0.45	0.43	0.38	0.29	0.33	0.32	0.28	0.33	0.28	0.27	0.23
Finland	0.87	0.82	0.76	0.89	0.75	0.74	0.76	0.71	0.62	0.59	0.58	0.68	0.59
France	5.41	4.77	4.47	4.78	4.92	4.38	4.30	4.62	4.00	3.48	3.30	3.19	3.00
Germany	12.6	11.1	10.3	11.1	10.5	10.2	9.78	9.63	9.44	8.63	8.55	8.25	7.21
Iceland	0.06	0.05	0.04	0.04	0.03	0.03	0.01	0.01	0.02	0.02	0.02	0.01	0.01
Ireland	0.42	0.41	0.38	0.36	0.34	0.36	0.35	0.34	0.35	0.35	0.34	0.30	0.33
Luxembourg	0.27	0.16	0.06	0.07	0.06	0.09	0.16	0.07	0.08	0.12	0.06	0.06	0.10
Netherlands	0.75	0.64	0.68	0.63	0.73	0.63	0.61	0.57	0.58	0.62	0.50	0.51	0.59
Norway	0.47	0.43	0.35	0.38	0.34	0.31	0.31	0.27	0.24	0.26	0.24	0.22	0.22
Portugal	1.81	1.74	1.70	1.67	1.51	1.46	1.40	1.38	1.44	1.41	1.48	1.43	1.27
Spain	5.81	4.95	4.29	4.19	4.29	4.59	4.00	4.15	4.34	4.37	4.30	4.06	3.08
Sweden	0.55	0.49	0.53	0.51	0.49	0.45	0.48	0.42	0.40	0.40	0.40	0.40	0.40
Switzerland	0.79	0.79	0.75	0.77	0.74	0.72	0.71	0.69	0.69	0.69	0.67	0.67	0.68
United Kingdom	7.08	6.94	6.41	6.47	5.95	5.74	6.03	5.36	4.76	4.04	4.03	3.95	4.01
OSPAR	**40.7**	**37.5**	**32.9**	**34.0**	**32.7**	**31.3**	**30.6**	**30.1**	**28.3**	**26.7**	**25.8**	**25.4**	**22.7**
Other	129	126	116	117	118	117	114	111	108	107	108	113	115
EMEP	170	164	149	151	150	148	144	141	136	133	134	139	138

Table B.5. *Annual modelled* ***lead*** *total depositions to the main regions of the OSPAR maritime area. Units: t/y.*

OSPAR region	I. Arctic Waters	II. Greater North Sea	III. Celtic Seas	IV. Bay of Biscay	V. Wider Atlantic
Area, km²	5480370	748586	381919	538114	6329170
1990	1487	1432	312	439	2333
1991	1479	1304	370	462	2243
1992	1516	1244	276	389	2660
1993	1353	1079	377	457	2447
1994	1363	1078	313	248	2032
1995	1322	985	302	361	2315
1996	1173	814	319	298	1823
1997	1068	857	280	272	2326
1998	1045	797	279	313	2280
1999	1051	676	159	290	1681
2000	1007	591	162	205	2046
2001	859	354	92.3	200	1488
2002	860	373	147	203	1928
2003	886	316	132	189	1504
2004	810	323	91.5	195	1461
2005	798	290	84.8	106	1236
2006	762	290	96.1	152	1569
2007	699	237	77.8	180	1373
2008	830	348	105	128	1614
2009	677	229	76.2	105	1287
2010	602	192	57.8	121	1089
2011	827	238	78.0	107	1249
2012	609	210	83.7	86.1	1037
2013	630	209	83.8	94.7	1334
2014	660	281	93.9	111	1316
2015	761	214	94.3	95.6	1280
2016	606	174	76.6	83.8	1222
2017	631	188	70.8	84.6	1079
2018	659	187	76.0	86.2	1225
2019	633	189	79.5	77.6	1197

Table B.6. *Annual modelled* ***cadmium*** *total depositions to the main regions of the OSPAR maritime area. Units: t/y.*

OSPAR region	I. Arctic Waters	II. Greater North Sea	III. Celtic Seas	IV. Bay of Biscay	V. Wider Atlantic
Area, km²	5480370	748586	381919	538114	6329170
1990	38.6	40.7	6.5	8.6	58.6
1991	38.3	34.4	7.5	8.9	57.9
1992	40.6	38.8	5.7	8.0	63.3
1993	37.5	30.9	7.5	9.0	60.1
1994	37.6	33.5	7.4	5.8	55.8
1995	36.4	30.0	6.7	7.4	55.3
1996	33.2	23.7	8.4	8.1	52.8
1997	30.5	24.0	6.6	6.6	59.8
1998	30.3	23.2	5.9	7.3	56.4
1999	30.6	23.7	4.6	7.0	49.2
2000	29.5	23.0	4.7	5.8	53.9
2001	27.5	16.3	3.7	6.4	47.8
2002	28.6	19.4	5.6	7.2	58.7
2003	29.6	15.5	4.9	5.9	49.2
2004	29.4	17.0	3.6	5.9	44.0
2005	28.0	15.7	3.3	3.7	40.4
2006	28.3	15.7	3.6	5.2	50.0
2007	26.4	12.5	3.0	5.2	44.7
2008	28.8	16.5	3.9	4.2	48.3
2009	24.7	11.4	3.1	3.6	43.0
2010	23.3	9.3	2.3	4.2	37.9
2011	30.0	13.1	3.1	3.6	43.1
2012	23.5	9.0	2.9	2.9	35.7
2013	24.1	9.5	3.1	3.5	47.2
2014	24.8	11.8	3.3	3.7	45.3
2015	28.9	10.0	3.4	3.2	44.4
2016	23.6	8.2	2.9	3.0	43.2
2017	24.8	8.7	2.7	3.0	38.7
2018	25.9	9.5	3.1	3.3	44.2
2019	21.8	7.0	2.8	2.7	39.6

Table B.7. *Annual modelled* ***mercury*** *total depositions to the main regions of the OSPAR maritime area. Units: t/y.*

OSPAR region	I. Arctic Waters	II. Greater North Sea	III. Celtic Seas	IV. Bay of Biscay	V. Wider Atlantic
Area, km²	5480370	748586	381919	538114	6329170
1990	59.64	9.68	3.38	3.11	50.70
1991	60.27	9.18	3.83	3.61	50.54
1992	56.77	9.67	3.54	3.30	47.38
1993	59.65	7.73	3.60	3.58	47.06
1994	55.26	8.30	3.63	3.18	46.30
1995	55.57	7.43	3.21	3.58	46.08
1996	53.00	6.92	3.27	3.32	43.36
1997	54.65	6.90	2.92	3.13	45.81
1998	50.05	7.48	3.32	3.07	44.75
1999	52.38	6.58	2.79	3.31	41.98
2000	56.34	7.26	2.74	3.48	42.61
2001	52.67	6.78	2.62	3.37	43.99
2002	49.21	6.52	3.06	3.47	45.59
2003	52.61	6.08	2.73	3.24	45.76
2004	48.68	5.86	2.54	3.02	40.69
2005	54.03	6.24	2.70	2.65	43.70
2006	50.90	6.32	2.77	3.25	45.94
2007	54.47	5.98	2.51	2.94	43.84
2008	52.48	5.86	2.67	2.97	42.98
2009	54.08	5.83	2.71	2.81	43.32
2010	47.88	5.53	2.36	3.13	41.47
2011	50.30	5.85	2.45	2.52	42.26
2012	46.91	6.01	2.85	2.93	39.38
2013	51.54	5.33	2.41	2.95	43.80
2014	47.40	5.92	2.44	3.04	40.29
2015	48.76	5.59	2.79	2.63	43.34
2016	43.70	4.89	2.57	2.71	43.01
2017	47.53	5.63	2.42	2.27	39.07
2018	46.17	5.07	2.20	2.46	39.47
2019	40.74	5.38	2.47	2.24	39.20

Table B.8. *Contribution of the OSPAR Contracting Parties to* ***lead*** *depositions to 5 regions of the OSPAR in 1995, 2005, 2015. (I. Arctic Waters, II. Greater North Sea, III. Celtic Seas, IV. Bay of Biscay, V. Wider Atlantic). Units: %*

	1995					2005					2015				
OSPAR region	I	II	III	IV	V	I	II	III	IV	V	I	II	III	IV	V
Belgium	0.46	2.28	1.20	0.71	0.30	0.33	3.12	1.05	0.57	0.18	0.18	1.75	0.37	0.28	0.07
Denmark	0.07	0.30	0.04	0.02	0.02	0.11	0.69	0.05	0.03	0.02	0.09	0.70	0.02	0.02	0.01
Finland	0.22	0.03	0.01	0.003	0.01	0.13	0.04	0.01	0.01	0.01	0.10	0.02	0.002	0.002	0.002
France	2.06	8.43	8.60	8.74	1.95	0.52	4.18	2.25	2.77	0.41	0.39	3.35	1.29	2.03	0.26
Germany	1.12	3.65	1.82	0.95	0.51	0.99	4.97	1.53	0.57	0.30	0.79	4.73	0.73	0.77	0.24
Ireland	0.03	0.001	0.001	0.00	0.01	0.08	0.01	0.01	0.003	0.02	0.04	0.003	0.01	0.001	0.01
Island	0.41	0.66	3.67	0.50	0.58	0.06	0.21	1.17	0.19	0.08	0.05	0.24	0.74	0.08	0.05
Luxembourg	0.01	0.05	0.04	0.02	0.01	0.004	0.03	0.01	0.01	0.002	0.01	0.03	0.01	0.01	0.002
Netherlands	0.21	1.23	0.36	0.17	0.10	0.15	1.75	0.35	0.14	0.06	0.05	0.63	0.08	0.05	0.02
Norway	0.32	0.15	0.02	0.01	0.02	0.24	0.19	0.02	0.01	0.01	0.18	0.17	0.01	0.01	0.004
Portugal	0.65	0.67	2.82	13.23	2.01	0.05	0.11	0.36	2.89	0.36	0.03	0.19	0.48	3.63	0.21
Spain	0.85	1.28	2.72	7.75	1.28	0.29	0.81	1.26	5.15	0.52	0.18	0.86	0.90	5.16	0.27
Sweden	0.14	0.07	0.01	0.01	0.01	0.12	0.09	0.01	0.01	0.01	0.10	0.09	0.01	0.004	0.003
Switzerland	0.14	0.39	0.27	0.15	0.07	0.04	0.14	0.07	0.05	0.01	0.03	0.12	0.02	0.03	0.01
UK	7.93	27.42	22.80	6.72	4.56	1.39	10.61	8.13	2.24	0.77	1.17	11.40	4.35	1.14	0.48
Other*	11.41	4.52	2.46	1.23	0.93	4.19	3.26	0.97	0.89	0.37	2.49	3.52	0.51	0.81	0.23
GLSE**	74.0	48.9	53.2	59.8	87.6	91.3	69.8	82.7	84.5	96.9	94.1	72.2	90.5	86.0	98.1

** Other (non-OSPAR) countries of the EMEP region (Europe and Central Asia)*

*** GLSE - Global and Secondary Sources*

Table B.9. *Contribution of the OSPAR Contracting Parties to* ***cadmium*** *depositions to 5 regions of the OSPAR in 1995, 2005, 2015. (I. Arctic Waters, II. Greater North Sea, III. Celtic Seas, IV. Bay of Biscay, V. Wider Atlantic). Units: %*

	1995					2005					2015				
OSPAR region	I	II	III	IV	V	I	II	III	IV	V	I	II	III	IV	V
Belgium	0.40	1.85	1.26	0.82	0.30	0.25	1.55	0.67	0.42	0.14	0.24	1.87	0.49	0.40	0.10
Denmark	0.07	0.29	0.05	0.02	0.02	0.11	0.55	0.05	0.04	0.02	0.12	0.93	0.02	0.03	0.01
Finland	0.23	0.02	0.01	0.004	0.01	0.23	0.04	0.02	0.01	0.01	0.14	0.02	0.003	0.003	0.003
France	0.92	3.68	4.08	4.26	0.93	0.45	2.37	1.59	2.19	0.36	0.24	1.76	0.80	1.36	0.17
Germany	1.12	3.40	2.23	1.25	0.61	1.30	4.24	1.73	0.79	0.43	1.28	6.18	1.27	1.40	0.43
Ireland	0.03	0.001	0.002	0.00	0.01	0.06	0.004	0.01	0.002	0.01	0.02	0.001	0.001	0.00	0.01
Island	0.09	0.14	1.05	0.15	0.15	0.08	0.19	1.46	0.25	0.11	0.08	0.28	1.22	0.14	0.07
Luxembourg	0.003	0.01	0.01	0.01	0.00	0.01	0.03	0.02	0.01	0.00	0.01	0.04	0.01	0.02	0.004
Netherlands	0.10	0.52	0.21	0.12	0.06	0.23	1.66	0.47	0.22	0.10	0.09	0.83	0.14	0.10	0.03
Norway	0.58	0.30	0.05	0.01	0.04	0.49	0.31	0.04	0.02	0.03	0.34	0.30	0.02	0.01	0.01
Portugal	0.08	0.07	0.37	2.74	0.55	0.11	0.10	0.47	4.87	1.03	0.04	0.17	0.60	5.20	0.42
Spain	0.71	1.05	3.16	13.30	1.54	0.58	1.02	2.14	11.47	1.22	0.21	0.75	1.09	6.88	0.38
Sweden	0.10	0.05	0.01	0.01	0.01	0.11	0.07	0.01	0.01	0.01	0.10	0.09	0.01	0.01	0.004
Switzerland	0.08	0.20	0.20	0.11	0.05	0.06	0.12	0.08	0.07	0.02	0.06	0.17	0.03	0.07	0.02
UK	1.99	6.61	8.48	2.26	1.42	1.07	5.54	6.06	1.91	0.66	1.01	8.67	5.06	1.27	0.48
Other*	5.69	1.47	1.04	0.44	0.49	6.84	1.88	0.74	0.79	0.43	5.55	2.94	0.52	0.73	0.36
GLSE**	87.8	80.4	77.8	74.5	93.8	88.0	80.3	84.4	76.9	95.4	90.5	75.0	88.7	82.4	97.5

** Other (non-OSPAR) countries of the EMEP region (Europe and Central Asia)*

*** GLSE - Global and Secondary Sources*

Table B.10. *Contribution of the OSPAR Contracting Parties to* ***mercury*** *depositions to 5 regions of the OSPAR in 1995, 2005, 2015. (I. Arctic Waters, II. Greater North Sea, III. Celtic Seas, IV. Bay of Biscay, V. Wider Atlantic). Units: %.*

	1995					2005					2015				
OSPAR region	I	II	III	IV	V	I	II	III	IV	V	I	II	III	IV	V
Belgium	0.10	1.53	0.47	0.39	0.14	0.07	1.09	0.22	0.23	0.09	0.05	0.69	0.15	0.18	0.06
Denmark	0.18	2.66	0.21	0.09	0.13	0.08	1.14	0.06	0.05	0.04	0.04	0.62	0.02	0.02	0.01
Finland	0.11	0.04	0.01	0.01	0.02	0.10	0.04	0.01	0.01	0.02	0.10	0.03	0.00	0.01	0.02
France	0.49	5.64	3.87	5.23	1.04	0.22	2.51	1.21	2.67	0.45	0.16	1.63	0.69	1.56	0.26
Germany	0.66	6.53	1.69	1.16	0.74	0.65	5.53	1.01	0.86	0.56	0.52	4.27	0.72	1.05	0.46
Ireland	0.12	0.03	0.05	0.02	0.07	0.05	0.02	0.02	0.01	0.02	0.03	0.01	0.01	0.004	0.01
Island	0.05	0.29	1.60	0.28	0.16	0.05	0.27	1.46	0.40	0.14	0.05	0.33	1.12	0.20	0.09
Luxembourg	0.004	0.03	0.02	0.02	0.01	0.004	0.04	0.02	0.02	0.01	0.003	0.02	0.01	0.01	0.003
Netherlands	0.05	1.52	0.18	0.11	0.05	0.05	1.01	0.11	0.10	0.04	0.04	0.82	0.09	0.08	0.03
Norway	0.24	0.62	0.05	0.02	0.04	0.19	0.50	0.04	0.02	0.03	0.13	0.27	0.01	0.01	0.01
Portugal	0.05	0.12	0.32	2.77	0.48	0.06	0.12	0.26	3.08	0.57	0.04	0.13	0.23	2.46	0.38
Spain	0.33	1.27	2.19	10.95	1.28	0.27	1.09	1.39	8.17	1.17	0.17	0.78	0.72	5.54	0.52
Sweden	0.11	0.21	0.02	0.01	0.03	0.08	0.16	0.02	0.01	0.02	0.06	0.12	0.01	0.01	0.01
Switzerland	0.07	0.33	0.22	0.16	0.10	0.02	0.08	0.04	0.05	0.02	0.02	0.09	0.02	0.06	0.03
UK	1.31	22.08	16.43	4.02	1.89	0.72	11.75	7.09	2.93	0.94	0.64	10.57	4.21	1.44	0.56
Other*	3.39	3.05	1.18	0.70	4.83	2.85	2.25	0.56	0.63	4.20	2.96	2.94	0.47	0.84	4.63
GLSE**	92.7	54.0	71.5	74.1	89.0	94.5	72.4	86.5	80.8	91.7	95.0	76.7	91.5	86.5	92.9

** Other (non-OSPAR) countries of the EMEP region (Europe and Central Asia)*

*** GLSE - Global and Secondary Sources*

Annex C. Comparison with Measurements

Lead, air concentrations, ng/m^3

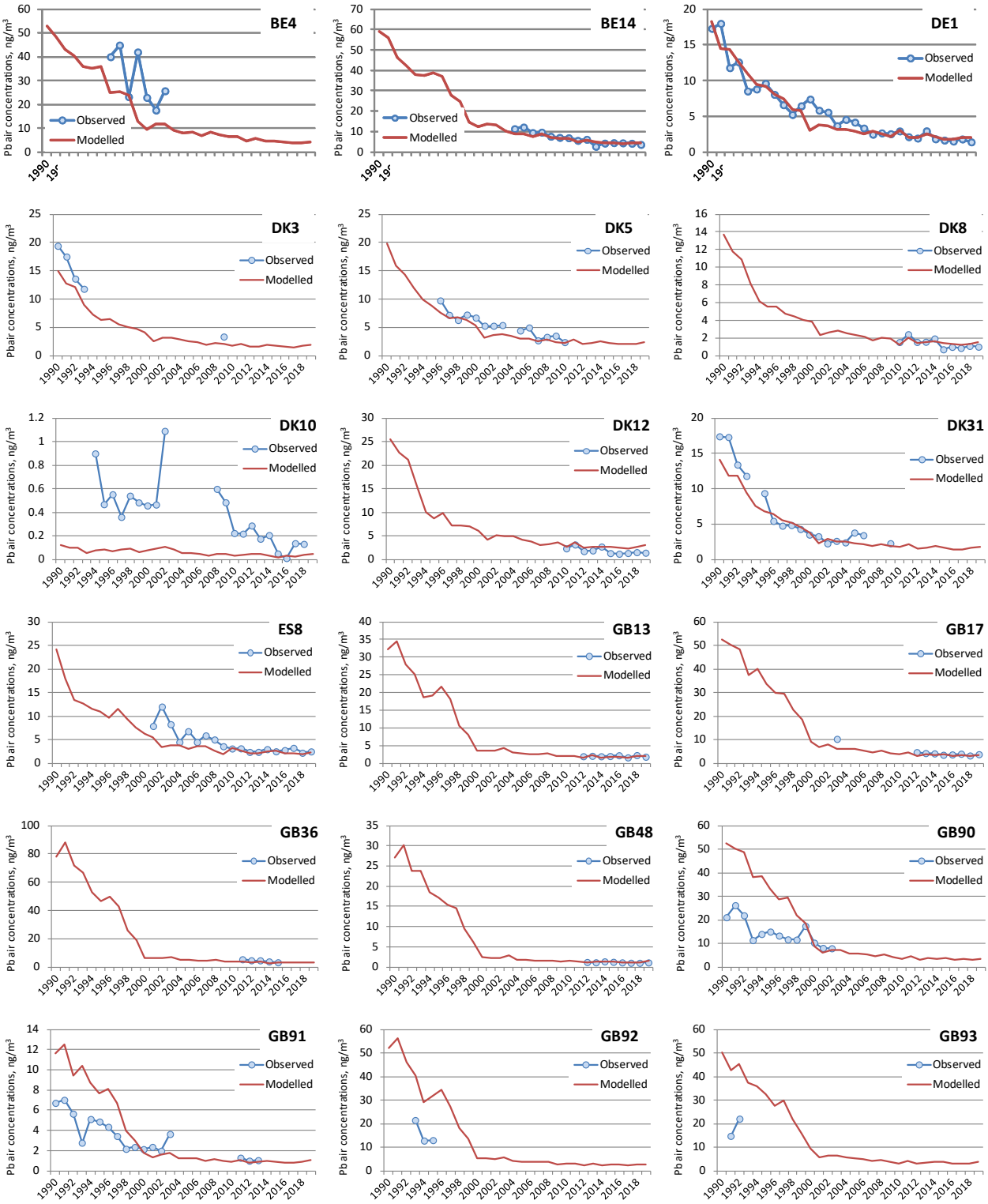

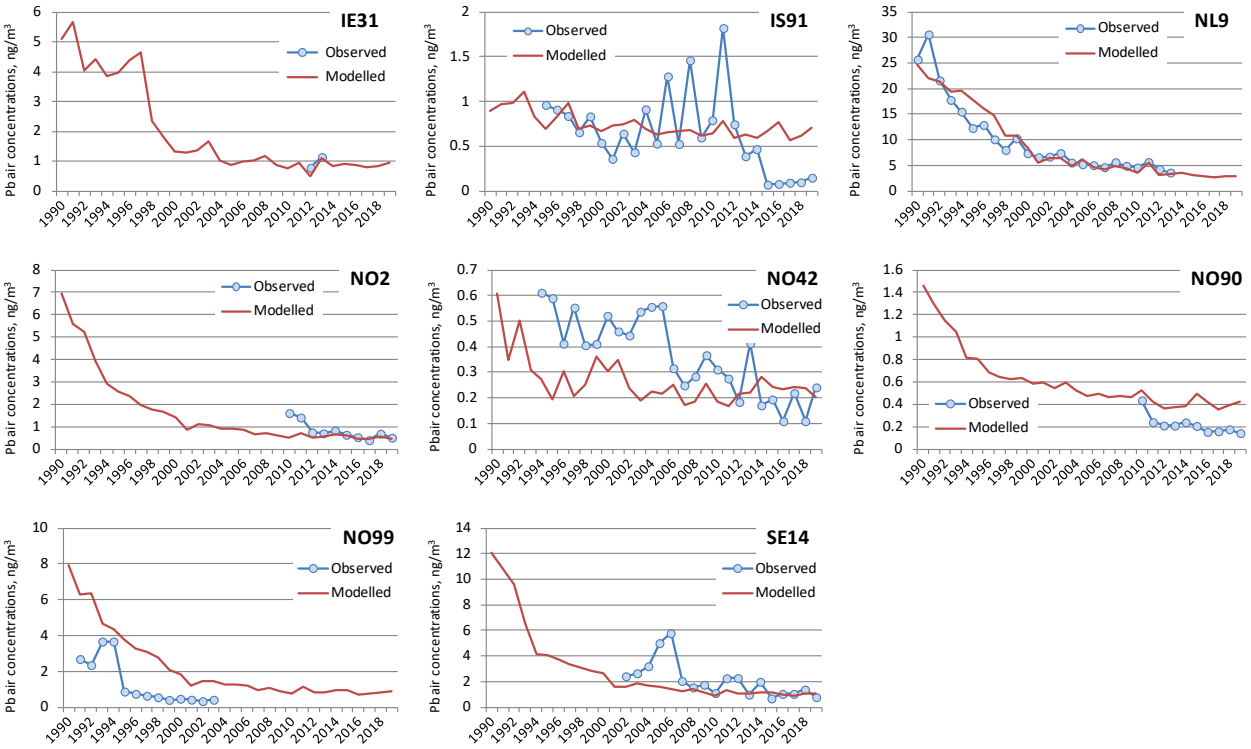

Lead, wet deposition, g/km^2/year

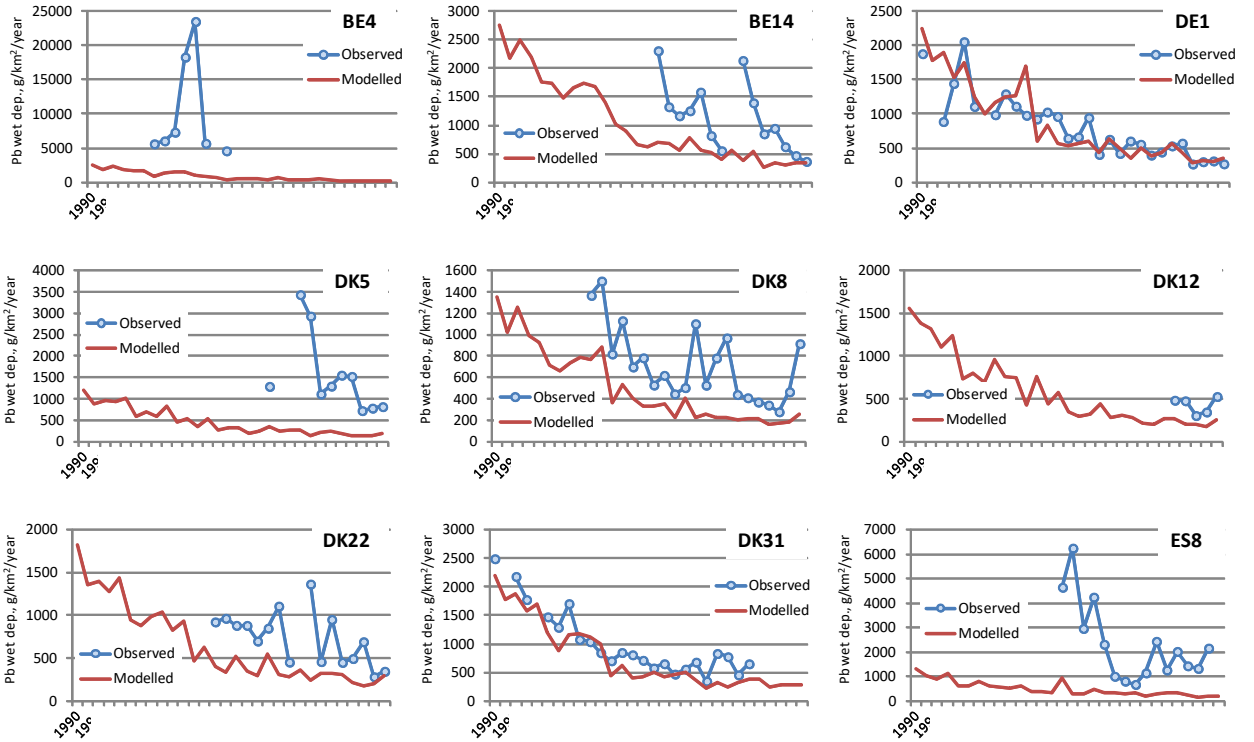

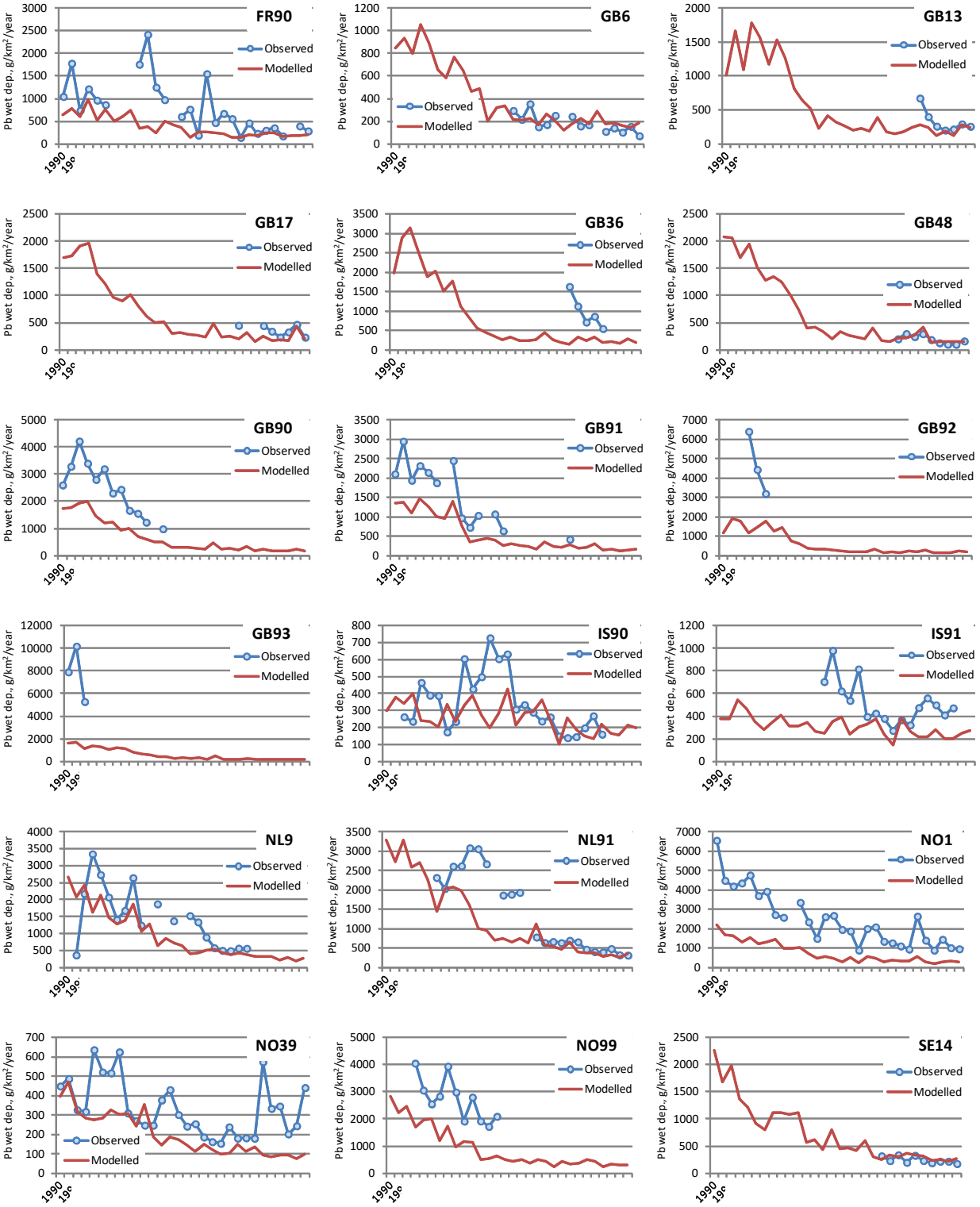
FR90
GB6
GB13
GB17
GB36
GB48
GB90
GB91
GB92
GB93
IS90
IS91
NL9
NL91
NO1
NO39
NO99
SE14
Observed
Modelled
Pb wet dep., g/km²/year
1990

Cadmium, air concentrations, ng/m^3

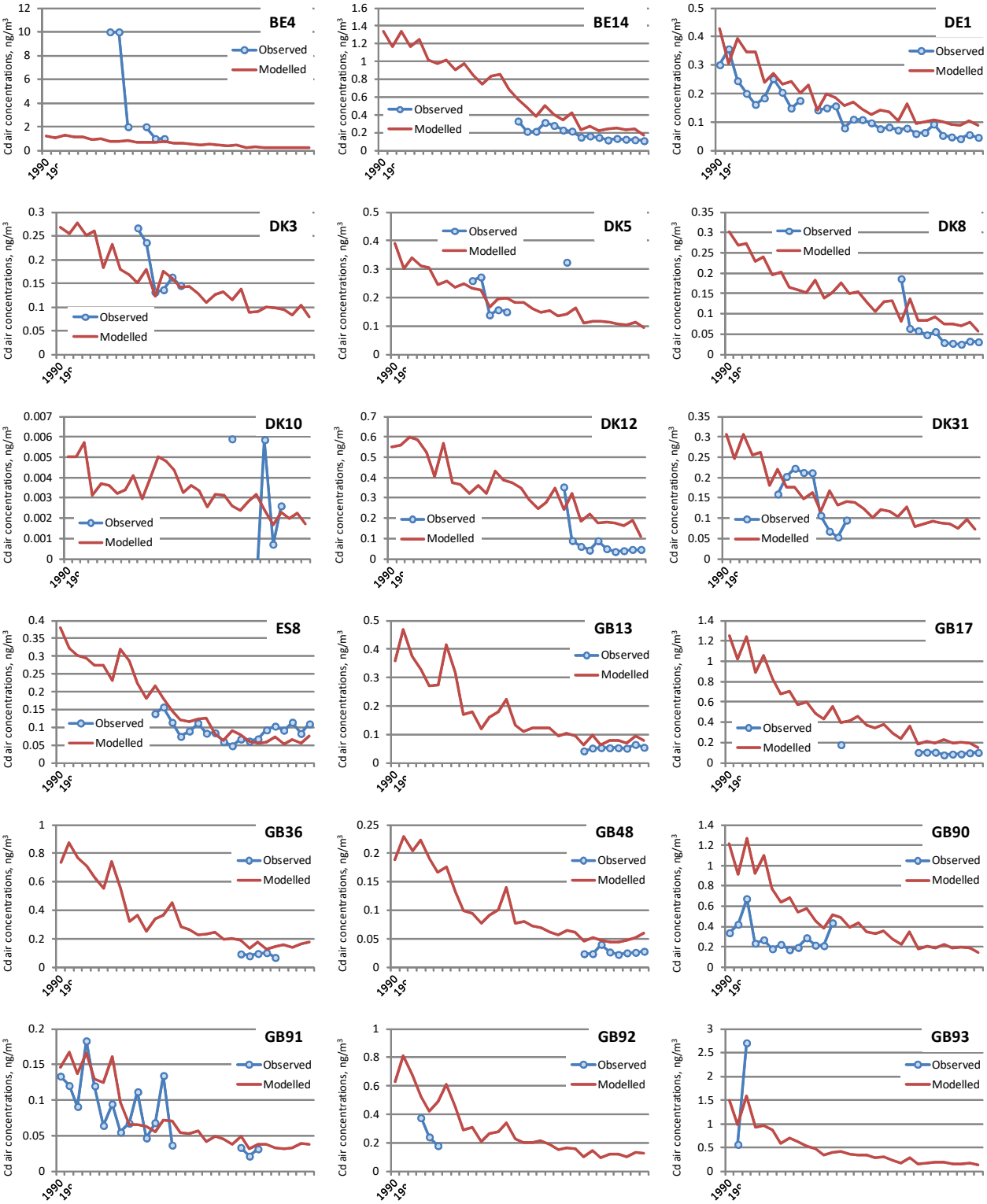

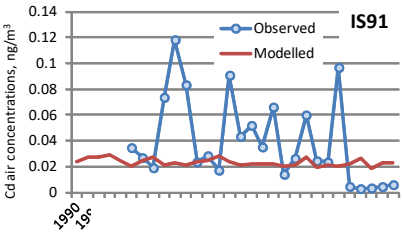

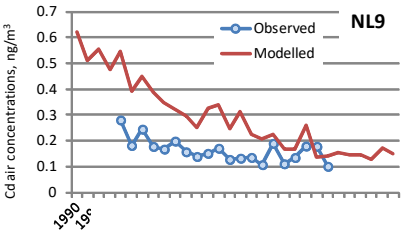

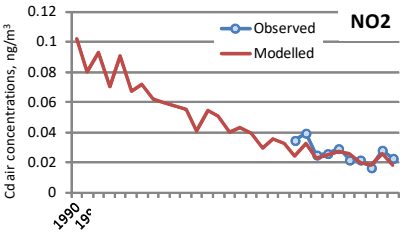

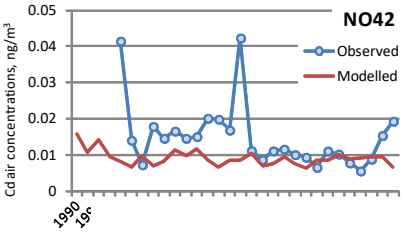

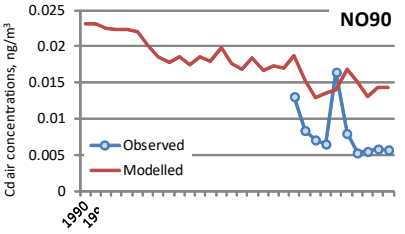

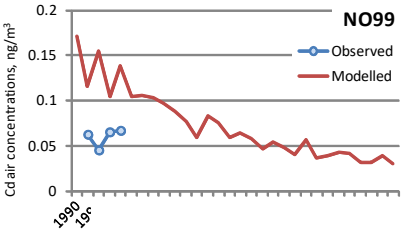

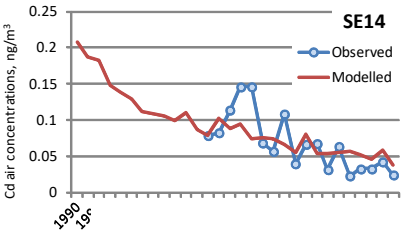

Cadmium, wet deposition, g/km^2/year

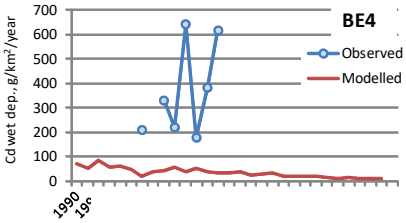

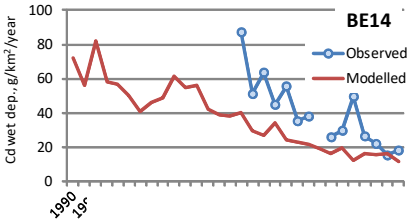

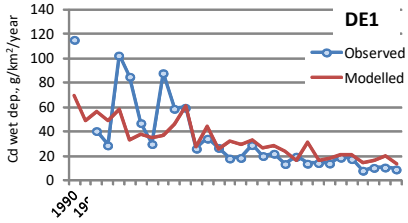

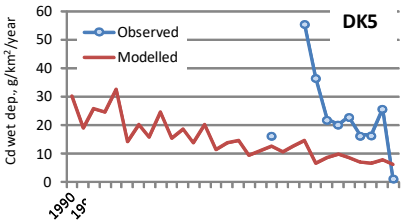

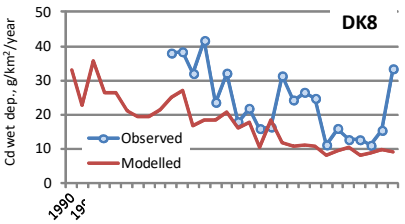

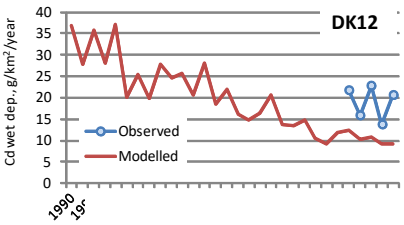

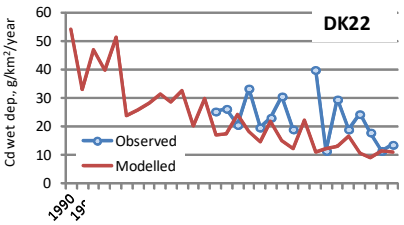

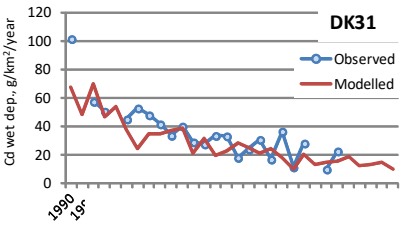

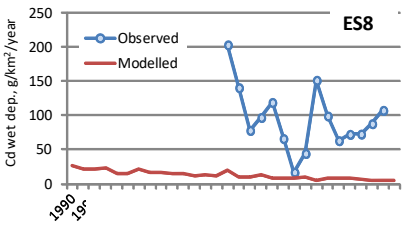

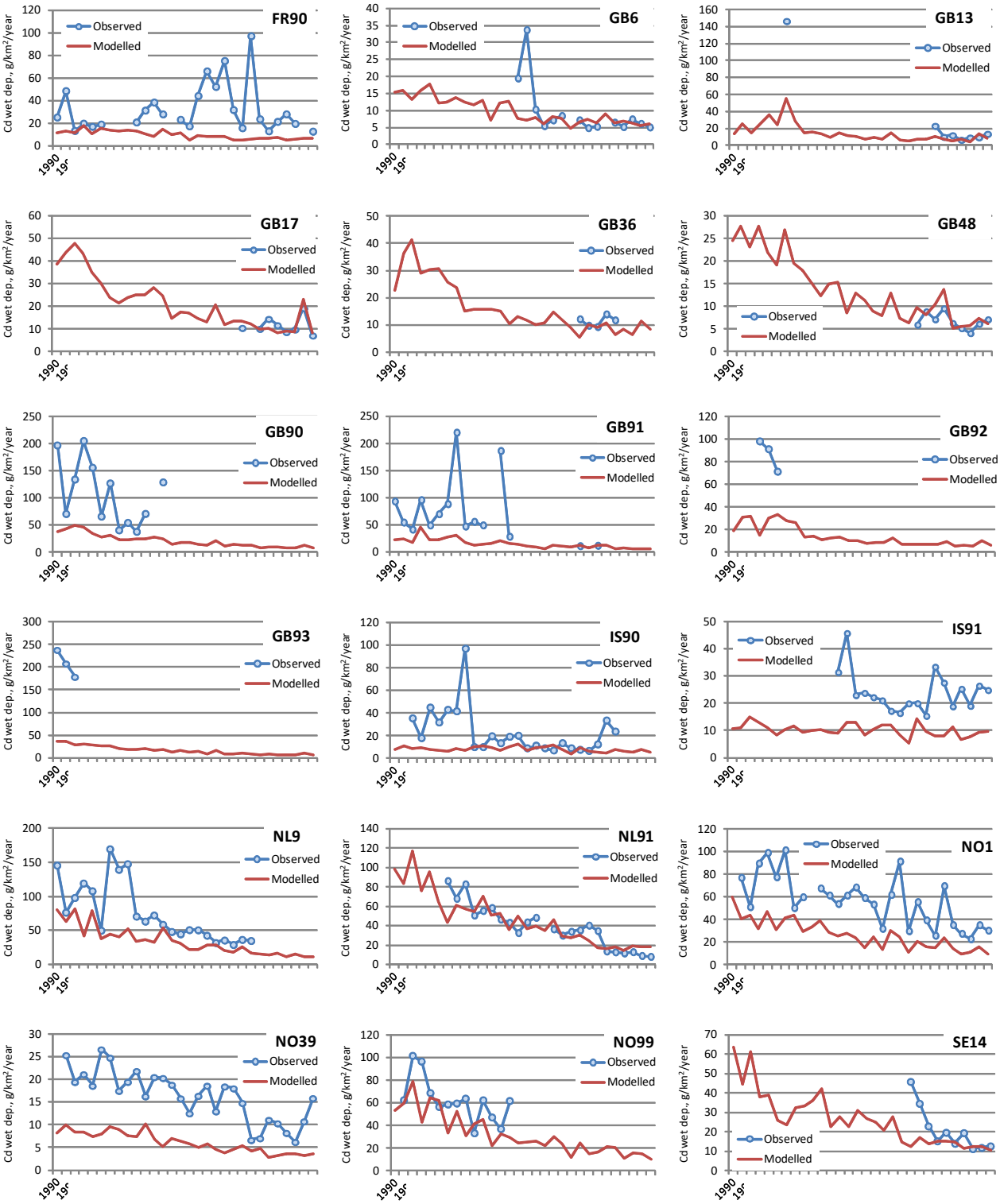
FR90
GB6
GB13
GB17
GB36
GB48
GB90
GB91
GB92
GB93
IS90
IS91
NL9
NL91
NO1
NO39
NO99
SE14
Observed
Modelled
Cd wet dep., g/km²/year

Mercury, air concentrations, ng/m^3

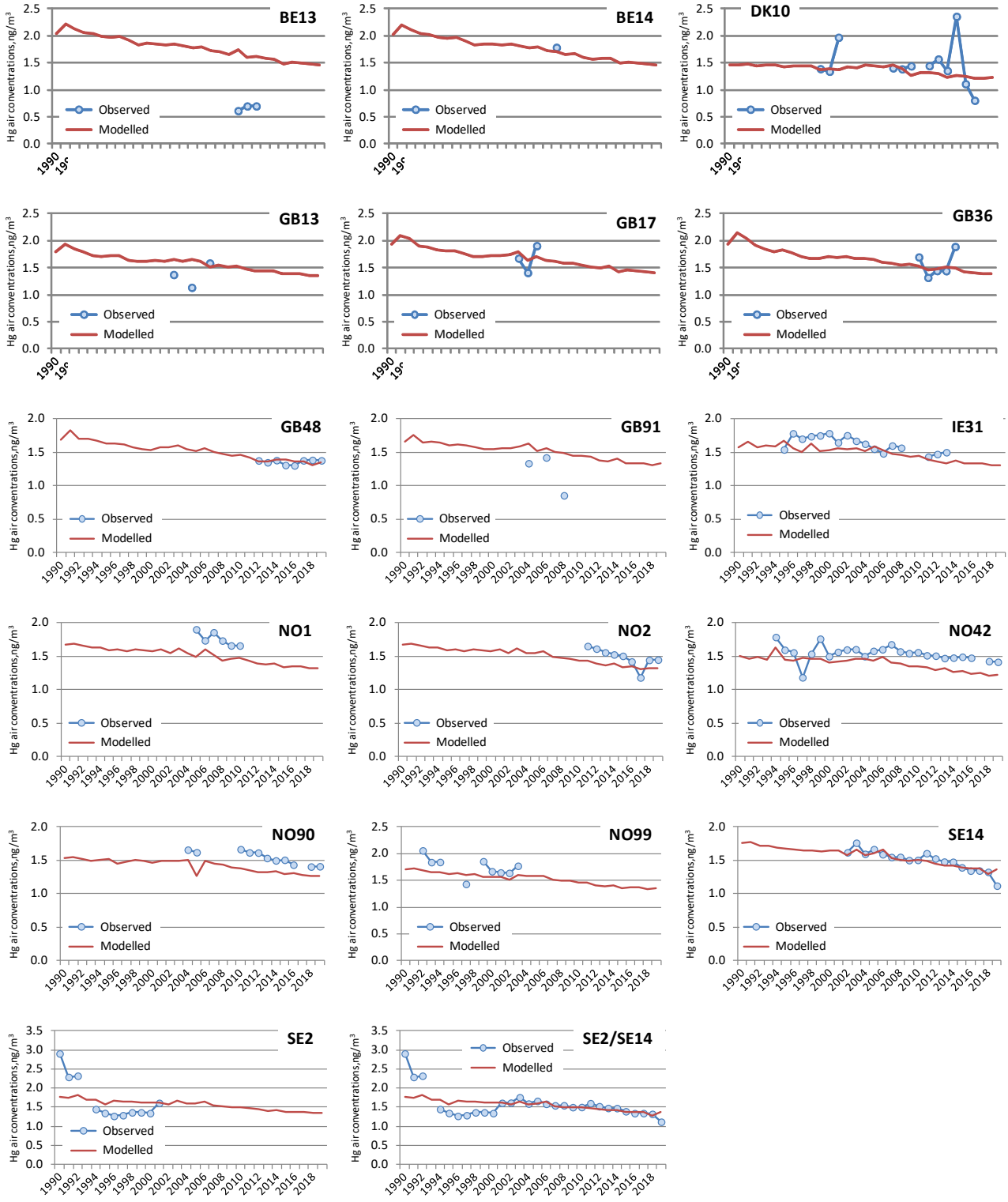

Mercury, wet deposition, g/km^2/year

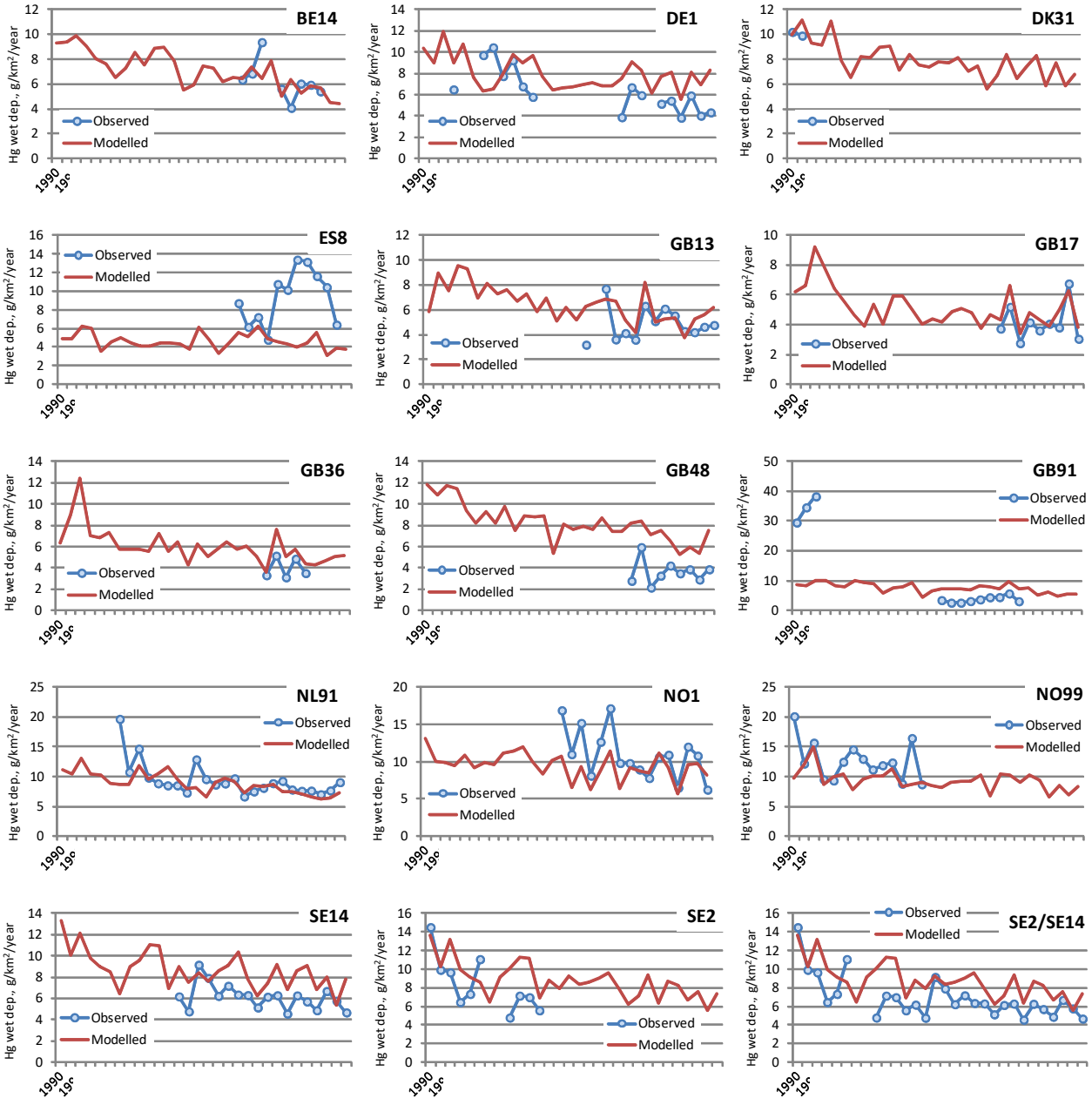

OSPAR Secretariat
The Aspect
12 Finsbury Square
London
EC2A 1AS
United Kingdom

t: +44 (0)20 7430 5200
f: +44 (0)20 7242 3737
e: secretariat@ospar.org
www.ospar.org

Our vision is a clean, healthy and biologically diverse North-East Atlantic Ocean, which is productive, used sustainably and resilient to climate change and ocean acidification.

Publication Number: 897/2022